2016

A Parametric Study of Meso-Scale Patterns for Auxetic Mechanical Behavior Optimization

Matthew C. Schuler
University of Central Florida

A PARAMETRIC STUDY OF MESO-SCALE PATTERNS FOR AUXETIC MECHANICAL BEHAVIOR OPTIMIZATION

by

MATTHEW C. SHULER

A thesis submitted in fulfillment of the requirements
for the Honors in the Major Program in Aerospace Engineering
in the College of Engineering and Computer Science
and the Burnett Honors College
at the University of Central Florida
Orlando, Florida

Spring Term, 2016

Thesis Chair: Dr. Ali P. Gordon

ABSTRACT

This thesis focuses on the development, parameterization and optimization of a novel meso-scale pattern used to induce auxetic behavior, i.e., negative Poisson's ratio, at the bulk scale. Currently, the majority of auxetic structures are too porous to be utilized in conventional load-bearing applications. For others, manufacturing methods have yet to realize the meso-scale pattern. Consequently, new auxetic structures must be developed in order to confer superior thermo-mechanical responses to structures at high temperature. Additionally, patterns that take into account manufacturing limitations, while maintaining the properties characteristically attached to negative Poisson's Ratio materials, are ideal in order to utilize the potential of auxetic structures. A novel auxetic pattern is developed, numerically analyzed, and optimized via design of experiments. The parameters of the meso-structure are varied, and the bulk response is studied using finite element analysis (FEA). Various attributes of the elasto-plastic responses of the bulk structure are used as objectives to guide the optimization process.

ACKNOWLEDGEMENTS

I would like to thank Dr. Ali. P Gordon for his commitment to the success of this research and many others. This would not have been possible without his continued guidance, advice, and enthusiasm. I would also like to thank the various members of the Mechanics of Materials Research Group that have been readily available to assist in the variety of skills required to ensure a successful study.

I would also like to thank the members of my committee, Dr. Jeffrey Kauffman and Dr. Kevin Mackie for their support and invested interest into furthering the study of auxetic structures.

TABLE OF CONTENTS

LIST OF FIGURES

LIST OF TABLES

CHAPTER 1. INTRODUCTION

1.1 Overview

By definition, auxetic materials have the unique property of Poisson's ratio, ν, being negative. Most solids have a positive Poisson's ratio ranging from values of zero for cork to about one-half for rubbers.

$$\nu = -\frac{\varepsilon_t}{\varepsilon_a} \tag{1}$$

Where ε_t and ε_a represent the transverse and axial strain, respectively. Under tensile loading, most materials will contract in the direction perpendicular to loading, resulting in the positive Poisson's ratio; however, for auxetic materials when the material is subjected to tension, both strains are positive. Figure 1 shows an unloaded and loaded auxetic structure. The structure has a hinge-like response where the individual links undergo rotation, but minimal amounts of compression.

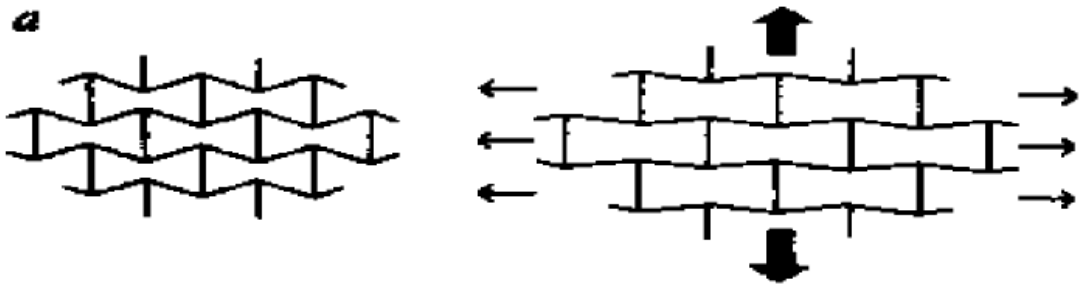

Figure 1: Effects of an auxetic material under tension [1].

There are a few natural auxetic materials, including bone tissue and graphene, but the majority are manufactured using specific meso-scale cellular patterns. Examples of manufactured auxetic

structures include, hinges, arrows, slits, and chirals. Each structure shares the common trait of having a specific hinge that reacts auxetically to loading. These structures and their hinge mechanics are shown in Figure 2. The cellular structure is repeated, mirrored, and rotated to confer an auxetic response on the bulk scale. Each structure represents a development towards more complex geometries to induce auxetic effects in materials.

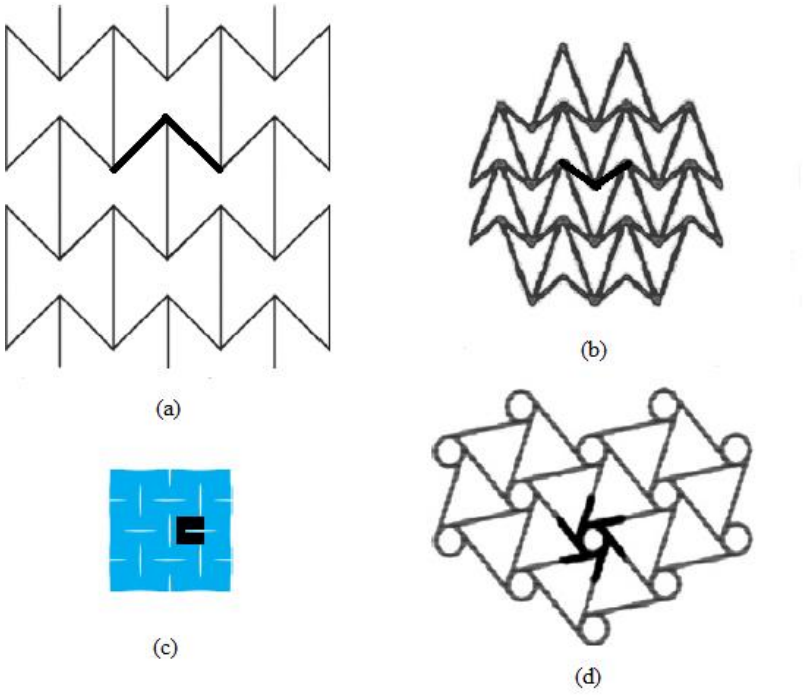

Figure 2: Examples of 2D auxetic structures with highlighted hinges: (a) re-entrant honeycomb (b) double arrowhead structure (c) rotating square units (d) chiral honeycombs [2-5].

1.2 Motivation

The primary focus of this study is the development of a new auxetic structure. There have been years of research and testing focused on basic auxetic structures where loading was relegated to the small strain region. The other deficiency in previous research is that most utilize

a linear elasticity. This research focuses on the development of a model experiencing elasto-plasticity. Auxetic materials have mechanical responses that can are extremely different from the bulk material from which they are made. Also, contemporary machines require next generation auxetic structures to fully realize their capabilities. Increases in strain rates, impacts of cyclical loading, and thermal and shock absorptivity are among the many characteristics that occur when fabricating a material, such as metal or plastic, to be auxetic [4,6]. These so-called meta-materials can have a major impact on the aerospace and mechanical industries allowing for improved quality of parts, along with the reduction of maintenance and repair costs. For example, auxetic materials can be used for padding during crashes and sports equipment, along with compressor casings [11-13]. Also, due to the advances in 3D printing and additive manufacturing, auxetic structures can be designed rapidly [14,15]; however, since material is being cut away to induce auxetic behavior, stress concentrations and locations for crack nucleation are introduced. This is the benefit of the capped spiral shape. The cap added to the previously researched spiral method, allows for reduced stress at the tips of the shape, and shields the tip of the crack from stress intensity. The meta-material obtains the hinged behavior and cellular structure from the spiral structure, while the cap allows for stress shielding.

The primary focus of this thesis is to characterize and optimize a novel auxeton, by parametrizing its shape into a group of eight distinct variables that include the length and rotation of the slit and cap, etc. In doing so, the key goal of the research is to demonstrate that a methodical approach to auxeton design is viable. A general-purpose finite element software, ANSYS, will be utilized during the first aspects of the research to parametrically simulate a large numbers of variations to find the Young's modulus, monotonic tensile strength, yield strength,

and Poisson's ratio for each value of the parameters. Due to the Poisson's ratio being a scale independent property, the meso-scale properties can be used to effectively model the macro-scale properties of the meta-material. The overall goal is to introduce an analytical model for the optimization of the curl shape based on a given set of parameters for a series of mechanical properties.

Chapter 2 contains a summary of relevant literature as well as the approach to the optimization of a new auxeton. The numerical modeling approach is provided in Chapter 3, which introduces the development of the constitutive model as well as the approach to post processing and data analysis. Chapter 4 presents the findings of the finite element analysis on a sample auxeton, and discusses the trends expected in the parameteric study. Finally, Chapter 5 develops the parametric study and optimization process utilized in order to reliably test new auxetons.

CHAPTER 2. BACKGROUND

2.1 Negative Poisson's Ratio

There has been attention geared towards both theoretical and experimental analysis of auxetic materials [2-4]. Consequently, it is necessary to summarize the works accomplished up to this point to determine knowledge gaps in this area. Synthetic auxetic materials were originally found by Lakes in the form of foams [**7**]. Nacre, the material found commonly in shells, has been proven an auxetic material [8]. For over a decade, most of the research conducted on auxetic materials was purely theoretical. In 2012, Prawoto focused on the structure and mechanical properties of negative Poisson's ratio materials [3]**.** The relations between Poisson's ratio and the three moduli, Young's, *E*, Shear, *G*, and Bulk, *K* were presented.

$$G = \frac{E}{2(1+\nu)} \tag{2}$$

$$K = \frac{E}{3(1-2\nu)} \tag{3}$$

For a conventional material, *K* must be greater than the *G*; however, for a material to have a negative Poisson's ratio, values of *K* must be much less than *G*. Auxetic materials display a much greater shear stiffness compared with conventional materials. Increased hardness and lower fatigue crack growth (FCG) have been reported to support this statement [3].

2.2 Forms of Meso-Scale NPR Structures

Since initial discovery, research has been conducted to develop and characterize innovative auxetic structures that further push previously found boundaries. Focus primarily

started with work on foams such as polytetrafluoroethylene and polyurethane [9-11]. Auxetic materials have been noted to have increased energy absorption and tensile strength. Although some materials are naturally auxetic. The vast majority of materials that exhibit a negative Poisson's ratio are manufactured with a given cellular meso-structure. Many 2D examples of this are shown in Figure 2. Where the primary focus was the hinged or honeycomb structure. This method was determined to be a successful way of altering a material to have a negative Poisson's ratio. Yang and coworkers, for example, created a honeycomb structure and acquired its Poisson's ratio [2]. A series of experiments were conducted on unit cells created by electron beam manufacturing. The unit cells are shown in Figure 3 along with the results attached to the experimental testing. The results for Poisson's ratio were found by measuring the displacement of the center layer. The focus was on the elastic response.

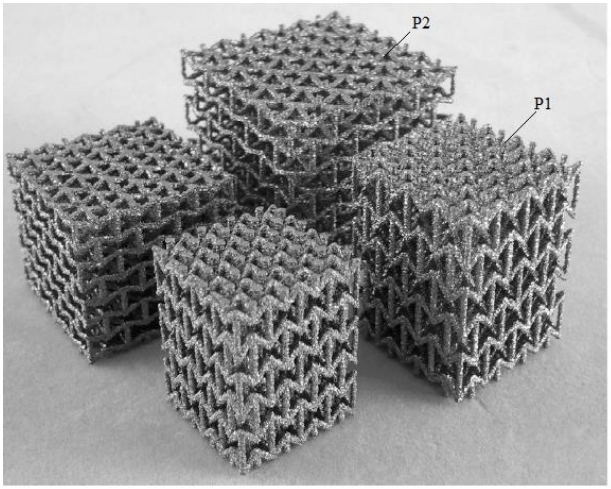

Poisson's ratio values of two designs.

Design	Measured values		
	ν_{zy}	ν_{yz}	ν_{yx}
P1	−0.14	−0.57	−0.23
P2	−0.37	−0.09	−0.31

Figure 3: Various auxetic structures and associated Poisson's ratios [2].

In all directions, the material is proven to be auxetic due to the three-dimensional form of the cellular structure. The expected variations in the effective modulus due to the change in

Poisson's ratio were encountered during testing. The values acquired from experimental testing for Young's modulus were within the theoretical limits produced,

$$\nu_{zx} = -\frac{2(\alpha - \cos\theta)\Delta x}{\sin\theta(2\Delta z_1 + \Delta z_2)} \tag{4}$$

where α and θ are dimensional properties of the cellular structure. In this equation, Δx and Δz represent the dimensional changes of the re-entrant strut.

The next stage in auxetic structures is porosity reduction. In previous models, the structure would lead to large porosity models, this was considered to be undesirable due to the lack of cooling performance and acoustic damping function [4]; therefore, Taylor and colleagues researched the slit method, created through laser etching, to look for a required porosity of 2 to 10 percent. They investigated a possible solution of creating a series of alternating perpendicular ellipses, and finding the point at which the aspect ratio would cause a test sample to become auxetic. Various sized ellipses, were studied via FEA, from aspect ratio of 1, a circle, to aspect ratio of 40. The Poisson's ratio was measured for various porosities as well. The results are shown in Figure 4 for the given porosities, ψ. The graph represents that the Poisson's ratio decrease linearly as the aspect ratio of the ellipse increases, and begins to show an auxetic effect at an aspect ratio of 15. Also, it is shown that the Poisson's ratio becomes more negative as the porosity of the sample increases. With results like this, a designer can pick the porosity and the desired Poisson's ratio by manipulating the elliptical hole aspect ratio.

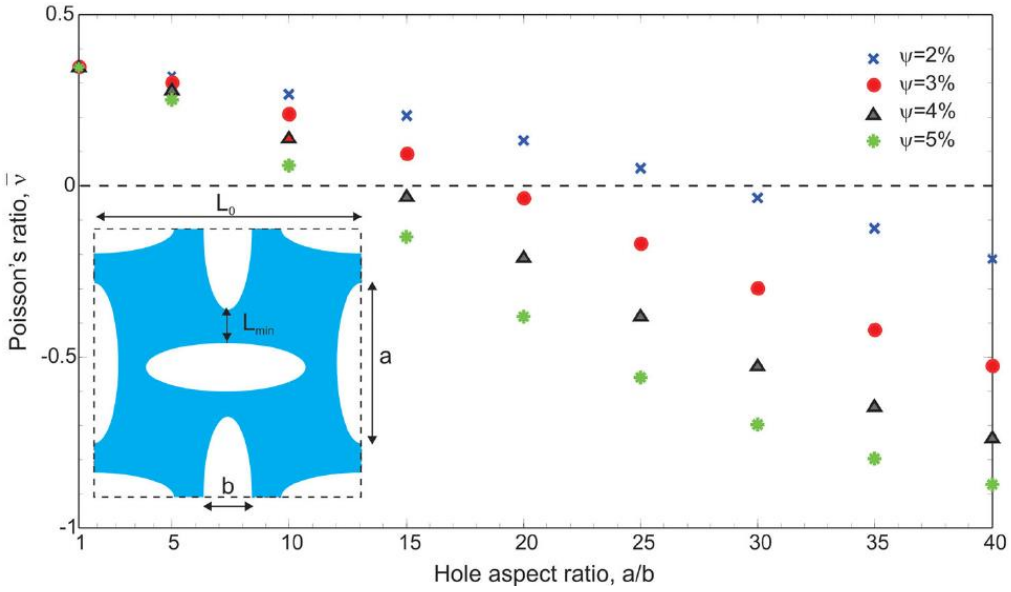

Figure 4: Poisson's ratio as a function of ellipse aspect ratio and porosity [4].

Once FEA was concluded, the von Mises stress caused by a specified displacement was determined. Two separate sample were used, the circle test sample along with the aspect ratio of 30 elliptical slit. Dogbone test samples were subjected to plane stress tension. The results were as hypothesized, the Poisson's ratios for the simulated and experimental results varied by less than 5%. The circular test sample displayed a much higher corresponding stress value than the elliptical slit section. The horizontal and vertical displacements were measured by testing the samples in an Instron biaxial testing machine with a 10kN load cell, while capturing the displacement using a Digital Image Correlation. Contour maps of each sample are provided in Figure 5. The apparent gray areas on the circular sample are plasticized regions.

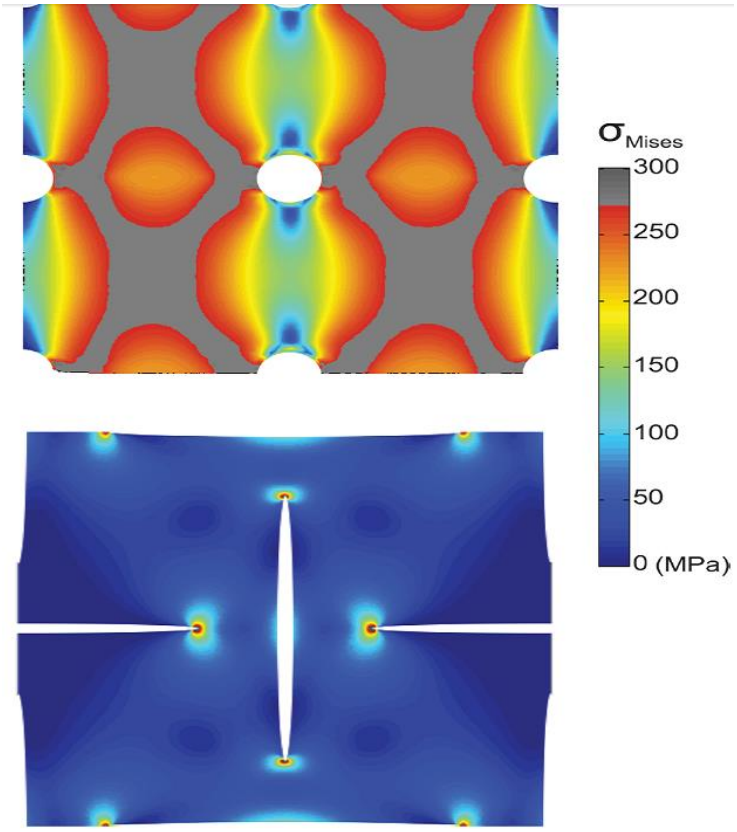

Figure 5: Stress contour plot [4].

Under specified boundary conditions, the elliptical slit test sample maintained a greater reduction in overall stress comparatively to the circular test sample. However, high stress concentrations occur at the points of the ellipses, causing concern for crack propagation.

2.3 Tensile Testing

The primary source of test data procured is obtained through the utilization of tensile testing. Tensile testing is a methodology that generate data regarding the stress-strain response of a given test sample under specified loading. The concept behind tensile testing is straightforward. The gauge section of the sample is the primary focus of tensile testing. Most commonly, researchers are looking to obtain the stress-strain curve for the provided test section,

that gives way to the mechanical properties of the material, such as Poisson's ratio, Young's modulus, yield strength, and ultimate tensile strength. Common responses for PLA applications in the textile industry look like the following.

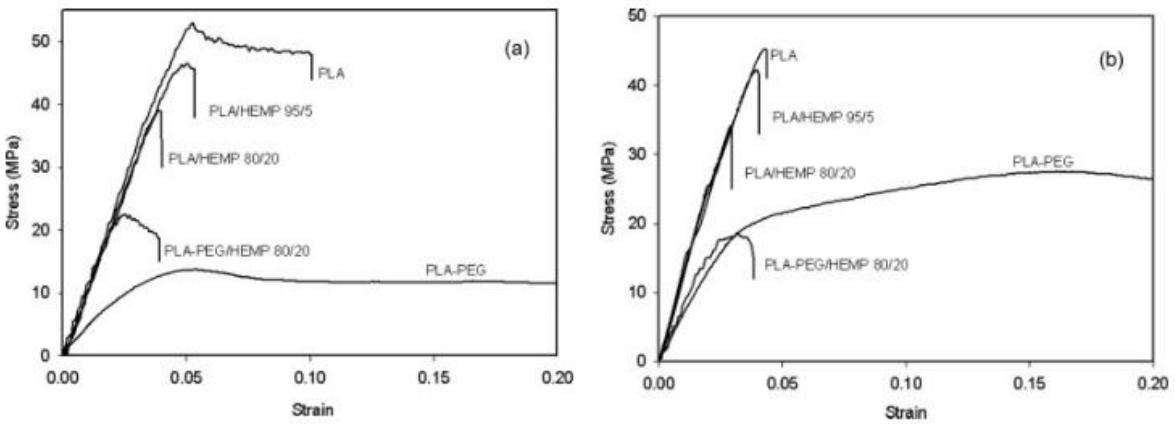

Figure 6: Tensile responses of common polymeric materials [5].

However, tensile testing expands past basic loading information. It can be utilized to realize the effects of heat addition on the test sample, as well as information regarding cyclical loading and fatigue analysis. For most cases, uniaxial loading is sufficient in order to map out the loading response of isotropic materials. In some cases, however, anisotropic materials, require the utilization of biaxial testing in order to effectively realize the full spectrum of mechanical properties. [5]

2.4 Optimization

Optimization is a process commonly employed in order to determine the most effective variation of a model for a given set of target parameters. Generally, a candidate model is constructed, and defined with a handful of variables in order to conduct a wide study for the purpose of optimization. Each parameter is assigned a range of values and simulations proceed to

find the optimal design for each target. The primary cause for concern of this is the large quantities of simulations or experiments that are required in order to justifiably state that a design can be considered optimal. A process called Design of Experiments (DoE) is deployed in order to drastically reduce the number of models required to find the optimal response and determine which parameters are the most influential on the design objective.

A DoE study attempts to reduce the bulk number of variations to a number that is practical to evaluate. For example, a design that induces 5 parameters and each parameter has 5 sublevels that allow the parameter to vary. The total amount of experiments required is 3125, an exceptionally high number for a relatively simplistic model. A common practice is to exploit the Taguchi Method developed by Genichi Taguchi to reduce the number of experiments in this case to a reasonable 25 [18].

This is accomplished through the use of orthogonal arrays put into practice by Taguchi based on his array selector. This table allows the user to see the required amount of experiments as well as the orientation of each of the sublevels, based solely on the number of parameters and the amount of sublevels for each parameter available in the parametric study, as shown in Table 1.

Table 1: Taguchi method array selector

	PARAMETERS											
LEVELS		2	3	4	5	6	7	8	9	10	11	12
	2	L4	L4	L8	L8	L8	L8	L12	L12	L12	L12	L16
	3	L9	L9	L9	L18	L18	L18	L18	L27	L27	L27	L27
	4	L16	L16	L16	L16	L32	L32	L32	L32	L32		
	5	L25	L25	L25	L25	L25	L50	L50	L50	L50	L50	L50

A 5 parameter, 5 level study would utilize a L25 array in order to be able to justifiably state reasonable conclusions based on the experimental or theoretical data obtained in the research.

Optimization is essential in manufacturing and design where many variables can influence the response of the outcome. Without the optimization process, one could not state that the constructed design is as effective as a slight dimensional adjustment. The primary reason for developing structures is to obtain the maximum possible results garnered by the structure, and to rank the influence of the parameters. Without proper optimization, primarily through parametric study, this goal would be unachievable.

CHAPTER 3. NUMERICAL MODELING APPROACH

3.1 Candidate Pattern

The candidate auxeton studied here is a modification based on the spiral "auxeton" presented by Blumenfeld [6]. The pattern consists of a comparatively large circle in the center with elliptical branches extending from the center at three specified angles, as seen in Figure 7. The design consists of a hollowed circle in the center of the auxeton, with three distinct curved arms protruding from the primary structure.

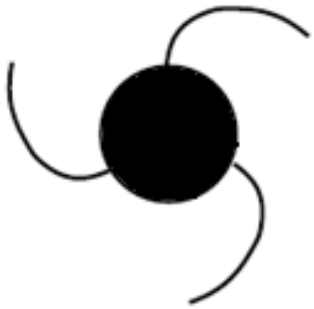

Figure 7: Base spiral pattern [17].

This design allows for the pattern to expand when placed under a load through rotational conventions. The modification of the Blumenfeld pattern, as shown in Figure 8, presented in the current study removes one the branches and attaches two circles at the end of each of the remaining branches.

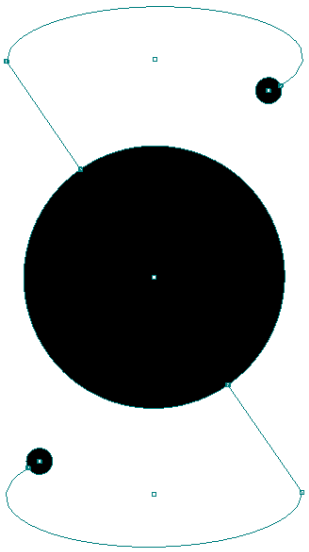

Figure 8: Blumenfeld-inspired bi-spiral auxeton.

The reduction of a branch is hypothesized to add a more rigid structure while still maintaining the desired auxetic effects, while the two small circles allows a location for stress to concentrate away from the primary structure of the pattern. Extensions, in order to relocate the caps from the main body, are added in order to add distance between the area of stress concentration and the primary structure. It is believed that this pattern will retain improved mechanical properties than the previously research spiral pattern, while creating a more stable structure.

3.2 Finite Element Modeling

Finite Element Analysis (FEA) is frequently used in order to procure data in order to gain understanding on the properties found by a given structure or material during loading. There are multitudes of software that allow the user too quickly and effectively perform FEA, but the software used in this research is ANSYS Workbench. It is an all-in-one program that gives the

user the ability to design models, setup the constitutive model that includes material properties, meshes, and boundary conditions, simulate the experiment, and contains a wide variety of post-processing options.

The process behind FEA consists of four major sections that are required in order to ensure that quality data is being produced by the simulations. First, the model must be created in order to actively proceed with the process. In this study, two dimensional behavior is assumed. Next the constitutive model needs to be prepared in order to obtain useful results after the simulation is performed. This includes setting up the material properties, such as a plasticity model, meshing the model in order to accurately capture results around key test areas, applying boundary conditions to obtain the desired effects during the simulation, simulating the experiment with a specified time step and targeted results, and finally, developing a procedure in order to take raw data and convert it into useful data about the structure, such as material properties.

3.3 Constitutive Model

The first component of the constitutive model is the setup of the material properties. The material that is utilized in this research is Polylactic Acid (PLA). The material properties that need to be established are the density, tensile yield and ultimate strengths. Also, two models, the isotropic elasticity, and the multilinear isotropic hardening, need to be developed in order to map out the elastic and plastic responses of the material. The major concern with the utilization of PLA in terms of simulation is that there are no specified values of mechanical properties for the material, only varied ranges. Therefore, specific values had to be selected in order to accurately

capture both the elastic and plastic responses of the material. A tabulated view of the material properties of PLA can be seen in **Table 2.**

Table 2: Mechanical properties of Polylactic Acid

Property	Bulk Modulus (GPa)	Young's Modulus (GPa)	Shear Modulus (GPa)	Poisson's Ratio	Yield Strength (MPa)	Ultimate Tensile Strength (MPa)
Value	3.9	3.5	1.3	.35	48	60

Most of the data was retrieved from experiments performed by Masirek [5]. The elastic model was developed from the Poisson's ratio and the Young's Modulus. Each value was checked to have a valid level through multiple sources [7-8]. The plastic response of the material is a much more strenuous model to prepare. The Ramberg-Osgood model was utilized to model the plasticity based on the equation below:

$$\varepsilon = \frac{\sigma}{E} + \left(\frac{\sigma}{K}\right)^{\frac{1}{n}} \quad (5)$$

In order to solve for the two constants, *h* and *n*, two points would be required to input into the equation into a mathematical solver. Yield stress and 0.2% yield stress were the selected points, and the following data was developed using the model above.

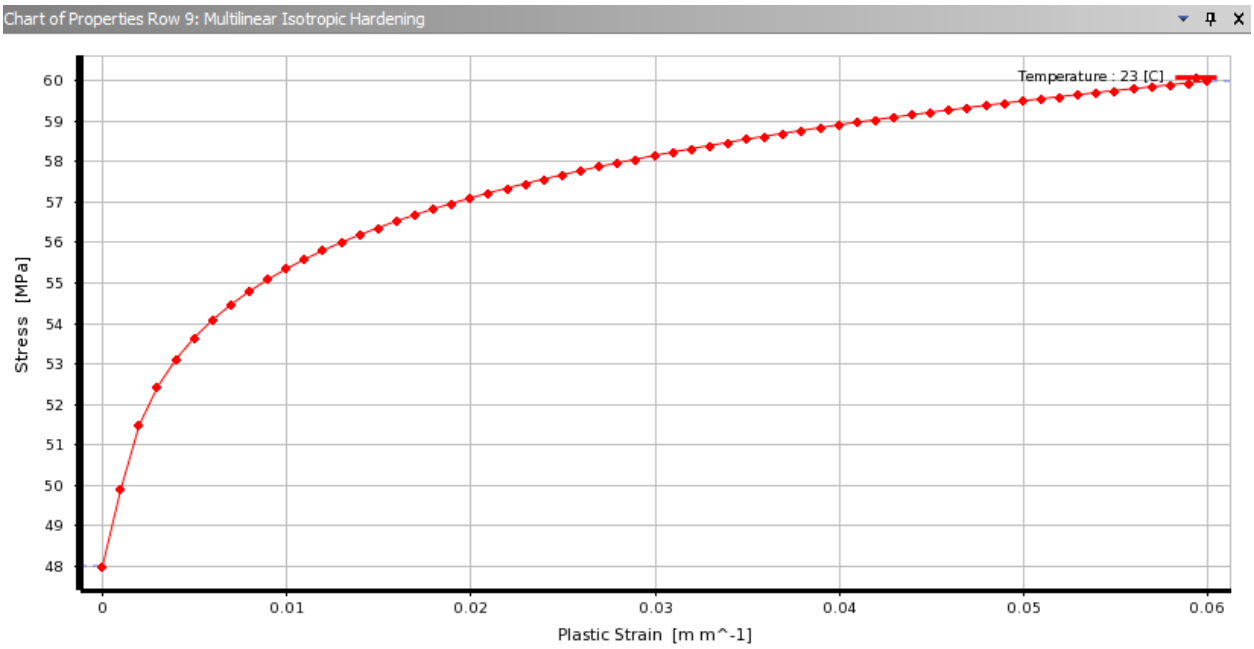

Figure 9: Multilinear isotropic hardening chart.

The next step is to ensure that the model focused on during the simulation is effectively portraying the desired results. The primary concern for this model is to ensure that every auxetic pattern is accurately placed so that the test specimen is uniform throughout the body. If the body is not considered to be uniform, the mechanical properties found through the simulations would not be applicable to anything other than the test subject. The other major concern with the model is the reduction in computing time required to complete the simulation. Due to the induction of a plasticity model, the computing time increased drastically per simulation. In order to reduce the overall time required to perform the simulations a couple of measures were put into place. First, the ends of the dog bone test sample were removed in order to only have the actual test section of the sample remaining. The second and much more effective measure, was to turn the simulation

into a 2D analysis rather than a 3D one. This had the benefit of drastically reducing the number of elements required for meshing by a multiples of 1000, and the overall computing time required for each simulation. An example of a finalized 52.07 x 19.05 x 1 millimeter test section can be seen below.

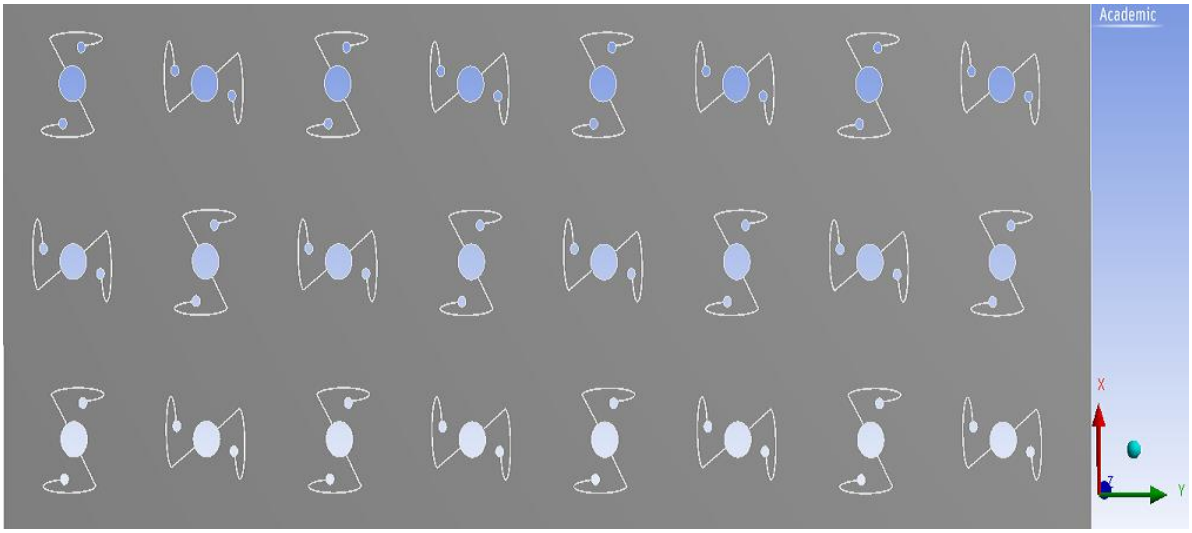

Figure 10: Example test section.

Appropriate Meshing is required in order to capture the appropriate data in the test section. The ANSYS Workbench automatic meshing tool was primarily utilized in order to properly mesh the body, with refinement being added in the areas surrounding the auxetic pattern when required. Extra elements needed to be added to these locations due to them being the primary focus of the research, as well as being the location of stress concentrations. Due to the reduction to a 2D analysis, the total amount of elements required to properly mesh the test section was approximately 30,000.

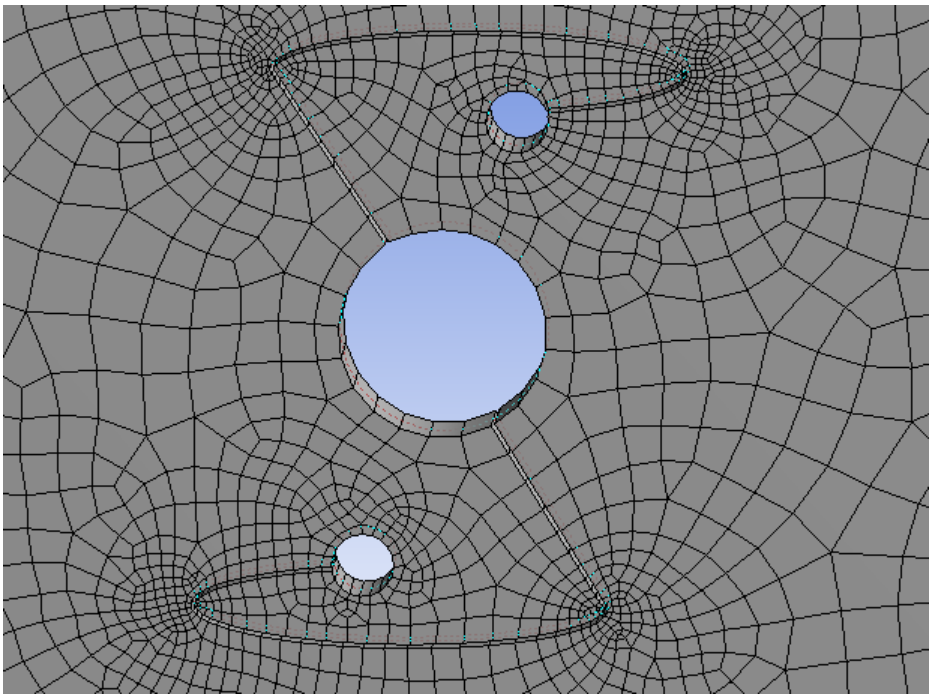

Figure 11: Example mesh of a given auxeton.

Finally, boundary conditions and targeted results can be setup in order to correctly assemble the simulation. Accurate representation of the experiment is required, so that meaningful data can be reproduced in a lab setting. The experiment is a simple tensile test, requiring one side to be fixed, and the other to undergo a specified displacement of 2 millimeters. ANSYS allows the user to easily apply these boundary conditions to the test sample. Below, it can be seen the fixed support attached on the left, and the displacement added onto the right side of the test subject.

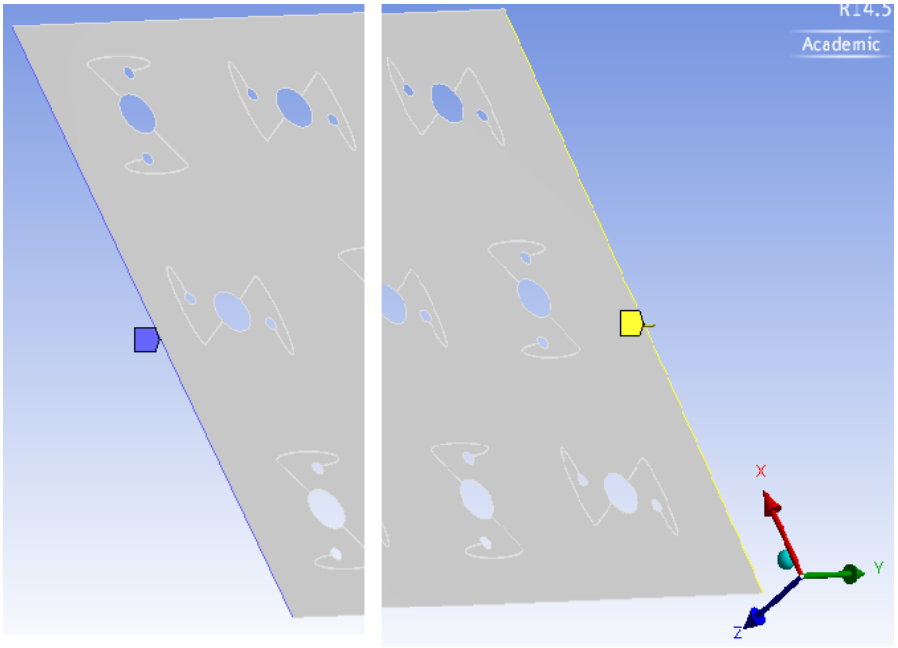

Figure 12: Boundary conditions: fixed support on the left and displacement on the right.

Once the boundary conditions are applied to the test sample, the targeted results of the simulation must be performed in order to find the appropriate data. The primary focus of the simulation is to find the average displacements along the outer perimeter of the test sample, along with the summation of the forces on the displaced edge. This is accomplished by grouping the nodes found along each of the edges and applying different displacement probes at each nodal group.

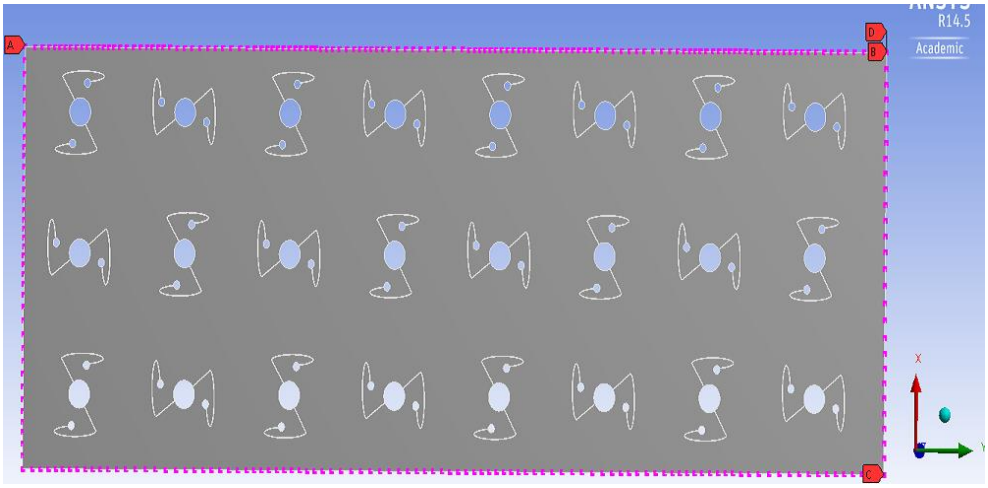

Figure 13: Nodal Selection.

Although the outer edges are the primary focus, an overall displacement gauge is added to the model in order to map out the displacement of each of the auxetic patterns. The final step of the constitutive model is to develop the analysis settings. The recommended settings were primarily utilized, but the total number of data points to be produced by the simulation was at 200 for each of the results. This was determined to be adequate to produce the appropriate stress-strain relations.

3.4 Post-Processing Approach

Once the results were gathered from the simulation, a post-processing approach had to be developed in order to turn the raw data into data that can be used to gather material properties. The simulation performed gathers force and displacement data that needs to be converted into stress and strain data. This process is primarily done in Microsoft Excel. The force-displacement data found through ANSYS Workbench was converted to stress and strain data through the use of two basic equations.

$$Stress = \sigma = \frac{Force_{Sum}}{A_{cross-section}} \quad (6)$$

$$Strain = \varepsilon = \frac{Displacement_{avg}}{Length} \quad (7)$$

The difference between the displacements along each of the two collaborating edges was normalized into a strain by dividing it by the original dimension of the test subject. The sum of the forces along the nodes on the displaced edge was normalized by the area of the cross section of the test subject. The new data was plotted against one another in the form of a stress-strain curve to depict the relations in both the transverse and axial directions, such as below.

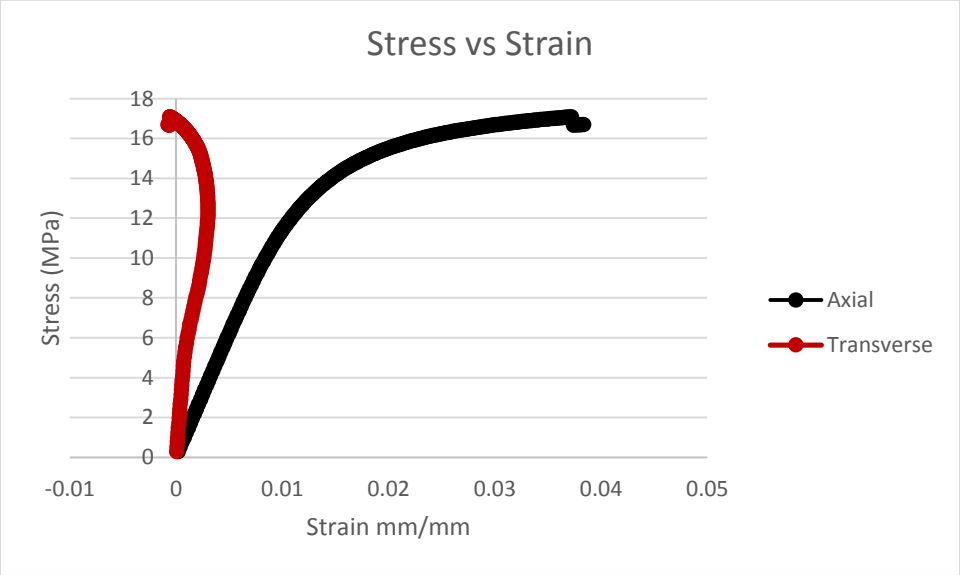

Figure 14: Example stress-strain relation for auxetic material.

The stress-strain curve is essential in order to calculate the appropriate mechanical properties focused on in the research.

3.5 Data Analysis Approach

Once the stress-strain curves were properly developed, a process must be created in order to determine the necessary mechanical properties. The primary focus of this research is to determine the Poisson's ratio, Young's modulus, ultimate tensile strength, and 0.2% yield strength. Each of these properties can be determined by looking at the relevant stress-strain data. The Poisson's ratio can be determined through the use of the equation 1, taking the negative of the ratio of transverse to axial strain. This value should remain constant throughout the elastic region of the stress-strain curve, but the values past that start to fluctuate when plasticity is included. To show this effect, a plot is created showing the relation between the axial strain and the Poisson's ratio.

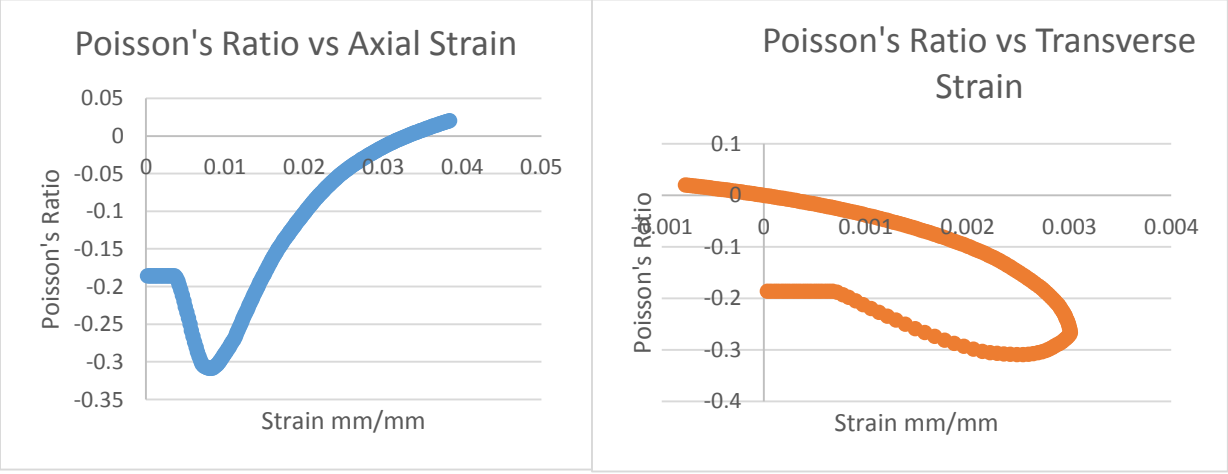

Figure 15: Poisson's ratio response for auxetic structure: axial on the left, transverse on the right.

It can be seen that the Poisson's ratio remains constant during the elastic region, however it will slowly increase in value then drastically once the model begins to plastically deform.

The next two materials properties to look for are the Young's modulus, and ultimate tensile strength. Both of these properties can be found on the stress-strain curve. The ultimate tensile strength is simply the highest value of stress seen by the model. The Young's modulus, can be calculated by looking at the slope of the axial strain versus stress curve's elastic region. The elastic region should be modeled linearly, and the slope easily determined by looking at the yield strength location.

The final material property of interest is the 0.2% yield strength. This value is determined by finding the intersection between the axial stress-strain curve, and the modified linearly elastic curve. The modified curve is replicated by placing the same sloped curve, developed by using the Young's modulus of the material, with an x-intercept of .002 strain. The intersection between the two curves is considered to be the 0.2% yield strength.

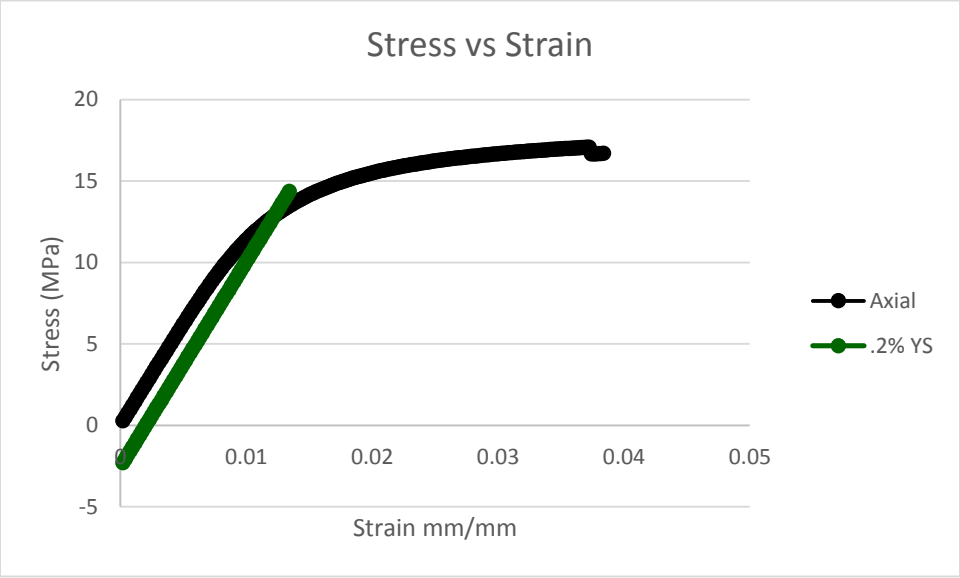

Figure 16: 0.2% yield strength intersection.

In order to expedite this process for future work during the optimization process. All relevant material properties will be stored in a separate spreadsheet that connects the properties to the specified model. Also, a macro will be developed in order to automatically perform the data analysis process. With these tools, the ability to effectively optimize the pattern developed will be exponentially simpler.

CHAPTER 4. SIMULATION RESULTS AND OBSERVATIONS

4.1 Tensile Responses

The primary focus of the preliminary research is to retrieve tensile responses for the candidate pattern in order to effectively characterize the mechanical properties of the meso-scale auxetic structure for application to the bulk scale. The motivation of the development of this particular auxetic meso-scale pattern is to orient a new design that reduces stress concentrations and allocates them further away from the primary structure. It can be seen below through the response of the test section that the pattern works as intended.

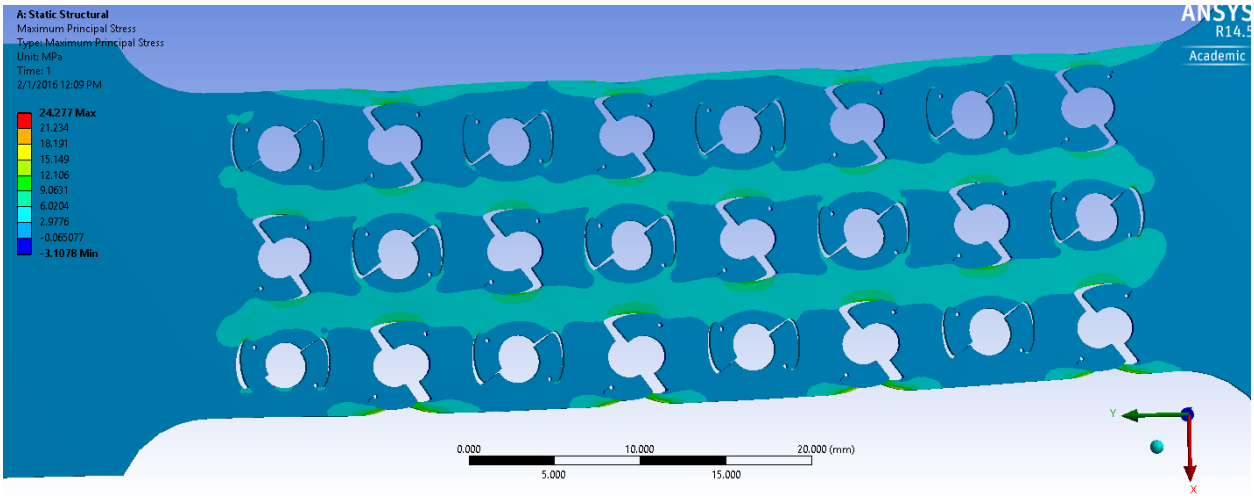

Figure 17: Stress response of candidate pattern.

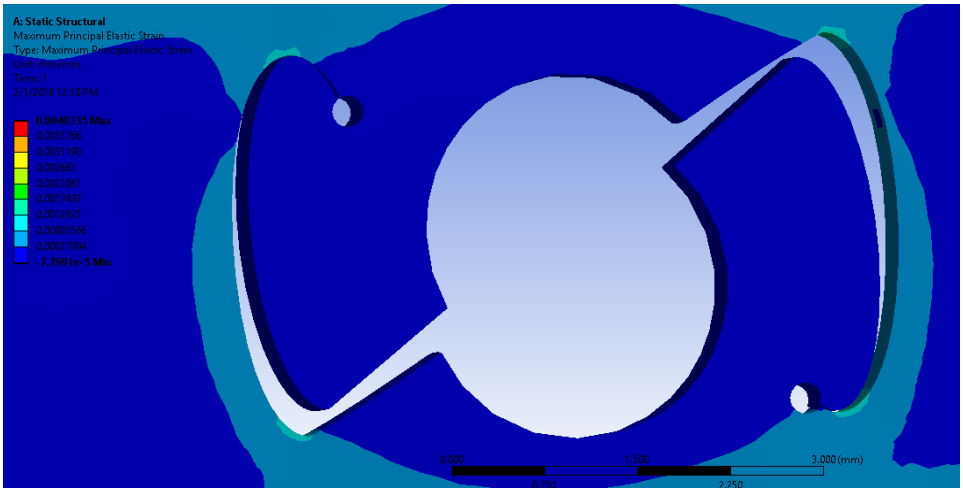

Figure 18: Zoomed strain response of the candidate pattern.

The primary concentration of stress is located along the cap, safely giving plenty of room for fatigue and cracks to propagate before severely damaging the structure. The major concern with this pattern is that deformation that occurs in the primary structure. The circle becomes misaligned, and with significant loading could become a permanent deformation. Although most of the stress is located away from the structure, after cyclical or continuous loading, this area could become a reason for major repairs or critical failure of the structure.

Once the pattern has been realized as successful as far as a design perspective, the demand is still prevalent to show that the meso-scale auxetic pattern improves any of the mechanical properties of the material it is embedded in. In order to do this, the tensile curve for the pattern had to be constructed so that the mechanical characterization could be retrieved. As seen previously, the tensile responses in the loading and transverse directions are as follows.

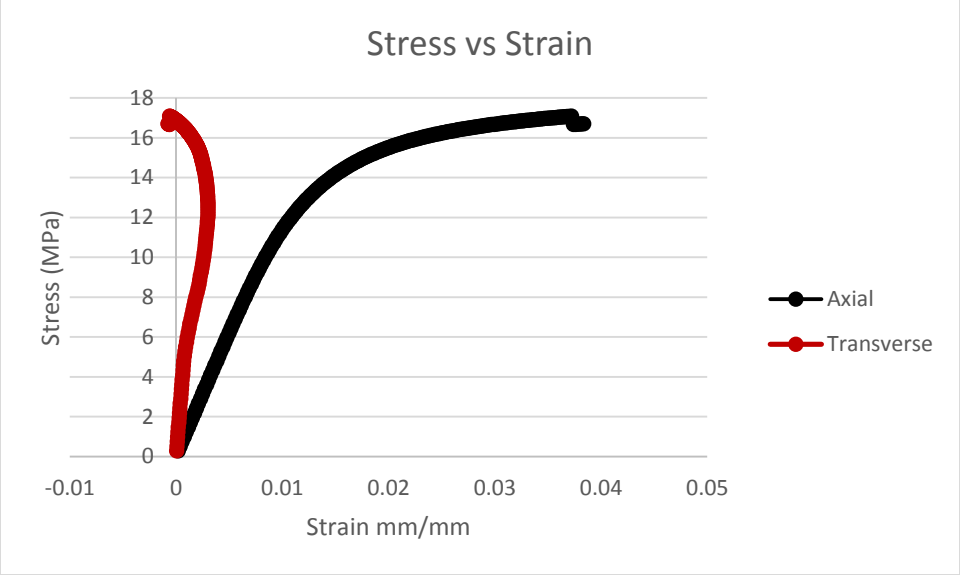

Figure 19: Candidate pattern tensile curve.

As expected, both of the directions experience elastic loading for the large portion of the stress contribution. The unique sense of a negative Poisson's ratio is the response of the strain in the transverse direction. Although the strain begins linearly in a positive manner, once plasticity is induced, the transverse strain begins to become more negative. With a significant enough loading, the auxetic structure has the possibility of plastically deforming into a non-auxetic or positive Poisson's ratio structure. This is a trend that has not been previously seen in research. Introduction of plasticity to an auxetic structure could potentially lead to devastating results. If the structure was deformed to the point of no longer maintaining a negative Poisson's ratio, all of the advantages that auxetic materials traditionally carry would be lost.

4.2 Poisson Ratio Trends

The main point of contention for the candidate pattern is to determine if the embedded pattern actually induces a negative Poisson's ratio, and how the Poisson's ratio shifts based on

the change from the linearly elastic region to the plastic region. It can be seen below that the Poisson's ratio remains a constant negative value until the structure is no longer linearly elastic.

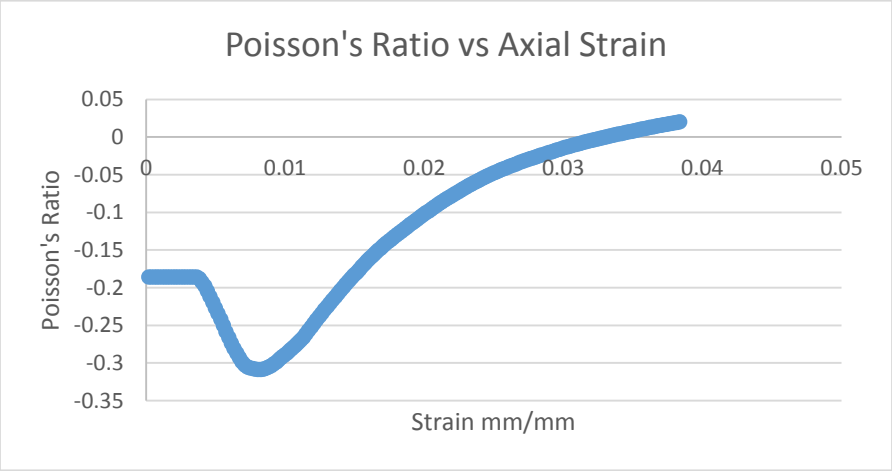

Figure 20: Poisson's ratio of the candidate pattern.

This depiction of the change in Poisson's ratio based on the axial strain can be compared to the tensile response in the same direction. As long as the material remains linearly elastic, until approximately 0.005 strain, the Poisson's ratio remains a constant -0.19. However, once the yield strength is passed, the Poisson's ratio decreases suddenly to above -0.3 and steadily increases into the positive region. It can be mentioned that a slight plasticity could be induced in the structure in order to significantly reduce the Poisson's ratio, if required by design. However, permanent deformation would occur to the structure and might be unable to sustain its auxetic property.

Also, it is worth noting the response of the Poisson's ratio in comparison to the strain in the transverse direction.

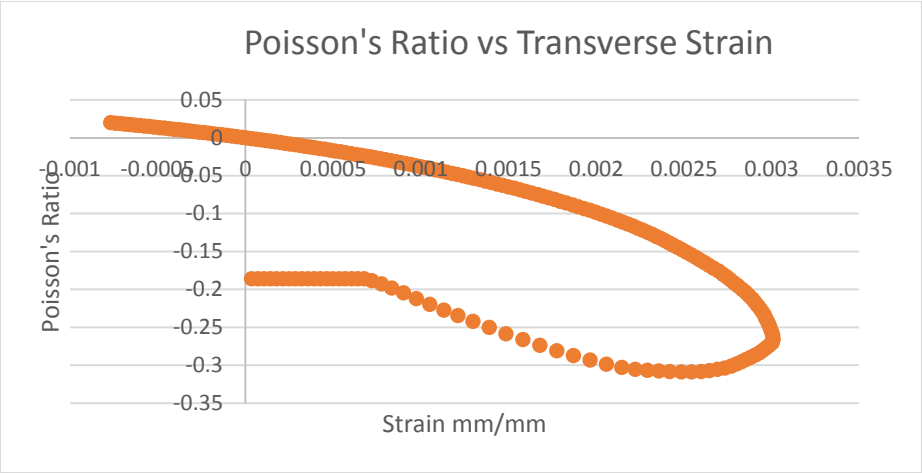

Figure 21: Poisson's ratio response in the transverse strain.

It can be seen that the response to the transverse strain is similar to that of the axial strain, but it has a unique parabolic shape to it. This relates to the response the strain has in relation to the induction of plasticity. While the loading direction responded as one would naturally expect, a slowly declining slope but still remaining positive, the transverse strain reverses direction and the sample begins to create a negative strain in that direction.

There are potential reasons as to why the Poisson's ratio behaves in such a manner when experiencing plasticity. There could be significant damage inflicted onto the primary structure after undergoing a significant loading experience that causes the pattern to no longer be auxetic. The Poisson's ratio could be unstable when undergoing plastic deformation, and once a particularly negative value is obtained it can no longer sustain the severe level of Poisson's ratio. This is an area where more research is certainly required to effectively explain the trend.

4.3 Macro-Scale Properties

A major focal point of this research is to mechanically characterize the candidate auxetic meso-scale pattern, and retrieve the mechanical properties gained by the test section and compare

the results to the bulk material properties of PLA. The material properties are ascertained by the procedures laid out in the previous section. For this particular candidate pattern, the material properties are as follows, as well as the bulk material properties of PLA for comparison.

Table 3: Left: auxetic pattern material properties. Right: non-auxetic bulk material properties.

Poisson's Ratio	-0.186
Young's Modulus (Megapascal)	1260
Ultimate Tensile Strength (Megapascal)	17
.2% Yield Strength (Megapascal)	13

Poisson's Ratio	0.35
Young's Modulus (Megapascal)	3500
Ultimate Tensile Strength (Megapascal)	60
.2% Yield Strength (Megapascal)	48

It can be seen that although the candidate pattern does indeed maintain the desired auxetic effect, the mechanical properties are severely reduced in the process. It is considered this the pattern would be infeasible for conventional application due to the relatively low strength properties, unless the only desired outcome is for the Poisson's ratio of the structure to be negative. Due to this development, it is necessary to optimize this design, so that the auxetic effect can be maintained, along with gaining increased mechanical properties.

CHAPTER 5. OPTIMIZATION

5.1 Parameterization

In order to optimize the candidate pattern to maximize the mechanical properties while maintaining the negative Poisson's ratio effect in the macro-scale, the pattern must be parameterized into a series of dimensions to fully characterize the auxetic pattern. The pattern is considered to be a mirror of itself, therefore the bottom half of the pattern is a replica of the top half. This allows for a significant reduction in the overall quantity of parameters. A collection of 8 parameters are employed to fully dimensionalize the candidate pattern and the test section as a whole. Six of the parameters pertained to the actual shape of the pattern, while two consisted of the vertical and horizontal spacing in the test section as a whole.

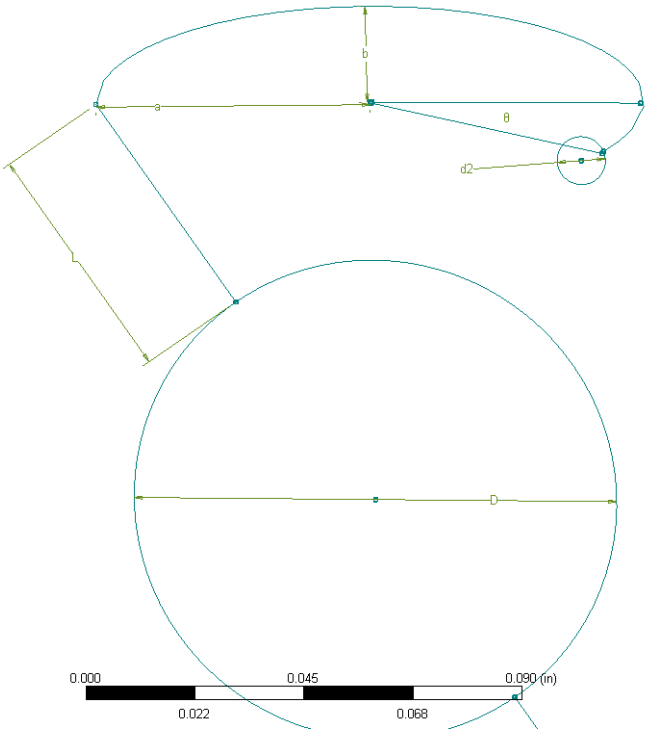

Figure 22: Parameterization of the auxetic candidate pattern.

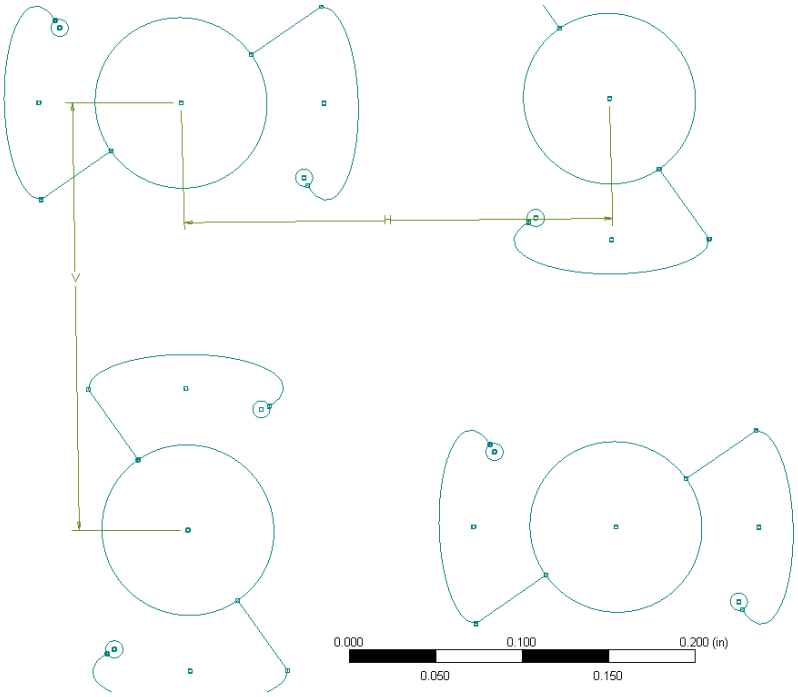

Figure 23: Parameterization of the test section.

The shape is parameterized to focus on the two diameters of the circles, major and minor, the major and minor axis of the cap, the length of the extension, and the continuation angle of the cap past 180 degrees. Also, the horizontal and vertical spacing between auxetic patterns on the test subject are varied. With the model properly parameterized, a design of experiments can be processed in order to begin the optimization process.

5.2 Design of Experiments

With the candidate pattern fully parameterized, a process needs to be developed in order to limit the values of the parameters, so that no models begin to have overlapping sections or other issues. Careful consideration is taken into account but the following values were selected and tested so that no complications will arise during the simulation process. The following levels

of each parameter is selected in order to give a significant spread in models, while maintaining consistency in the models.

Table 4: Selected parameter levels.

Levels	Vertical Spacing (in)	Minor Diameter (in)	slit length (in)	cap major axis (in)	cap minor axis (in)	continuation angle (degrees)	Major Diameter (in)	Horizontal spacing (in)
1	0.25	0.01	0.05	0.055	0.02	25	0.1	0.25
2	0.3	0.015	0.045	0.05	0.015	20	0.0625	0.275
3	0.15	0.02	0.04	0.045	0.01	15	0.075	0.325
4	0.3	0.025	0.055	0.06	0.025	30	0.0875	0.3
5	0.35	0.03	0.06	0.065	0.03	35	0.05	0.35

One of the primary concerns with this research was the abundant amount of simulations required in order to effectively optimize the auxetic pattern. Steps were already taken in the setup of the constitutive model in order to reduce individual computational time, however, there is no conceivable way to perform approximately 390,000 simulations in a timely manner. Therefore, a methodology had to be adapted in order to drastically reduce the amount of simulations required to produce meaningful results regarding the optimization of the candidate pattern.

5.3 Taguchi Method

The necessity to reduce the number of total simulations invokes the use of the Taguchi method. As discussed previously, the Taguchi method, through the use of orthogonal arrays, has the ability to reduce the number of simulations to anything below 50, a much more reasonable endeavor. The Taguchi method is dependent on only two things, the number of parameters selected for the parametric study and the amount of levels each parameter varies between. With these two values, the Taguchi array selector can be utilized to determine the orthogonal array required for a sufficiently expanse parametric study and optimization procedure. For convenience, the table is reproduced below.

Table 5: Taguchi method array selector.

	PARAMETERS											
LEVELS		2	3	4	5	6	7	8	9	10	11	12
	2	L4	L4	L8	L8	L8	L8	L12	L12	L12	L12	L16
	3	L9	L9	L9	L18	L18	L18	L18	L27	L27	L27	L27
	4	L16	L16	L16	L16	L32	L32	L32	L32	L32		
	5	L25	L25	L25	L25	L25	L50	L50	L50	L50	L50	L50

Given the fact that the parameterization of the candidate pattern lead to 8 different parameters, along with there being 5 levels of variation, an L50 array is required to be able to safely state that the parametric study produces meaningful results. The L50 array consists of 50 different models that will be simulated in order to find data trends for each mechanical property calculated relative to each of the parameters. A sample of the L50 array constructed is below.

Table 6: Sample L50 array.

Experiment	Vertical Spacing (in)	Minor Diameter (in)	Extension (in)	Cap Major Axis (in)	Cap Minor Axis (in)	Continuation angle (degrees)	Major Diameter (in)	Horizontal Spacing (in)
1	0.25	0.01	0.05	0.055	0.02	25	0.1	0.25
2	0.25	0.01	0.045	0.05	0.015	20	0.0625	0.275
3	0.25	0.01	0.04	0.045	0.01	15	0.075	0.35
.	.	.	.	.	.	.	.	.
50	0.3	0.03	0.06	0.06	0.02	25	0.0875	0.275

With the array developed, the simulations can proceed knowing that purposeful data will be procured by the simulations.

5.4 Results

Although developing and discovering the optimal variation of the original candidate pattern is a focus of the research, realizing how each parameter effects the mechanical characterization of the pattern is a much more prevalent reason to conduct a parametric study. Because of this, the results are displayed as a series of trend plots that describe the variation of each of the four mechanical properties, Poisson's ratio, ultimate tensile strength, Young's modulus, and 0.2% yield strength, with respect to each variation in the parameters. Once the trend lines are developed, it can be noted which parameters have the greatest effect on the mechanical properties of the induced auxetic bulk structure. Also, the optimal auxetic patterns can be selected based off their mechanical characterization.

The first parameter is the vertical spacing between the auxetic patterns in the test sample. The Taguchi method adapted for this research only allocated two levels of study for the first parameter. The following trend lines were found.

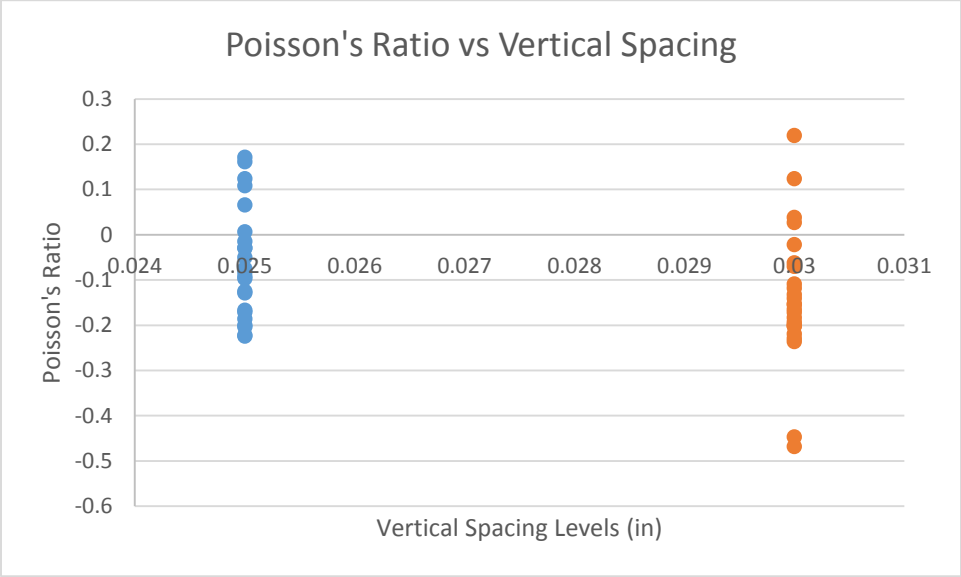

Figure 24: Vertical spacing trend: Poisson's ratio.

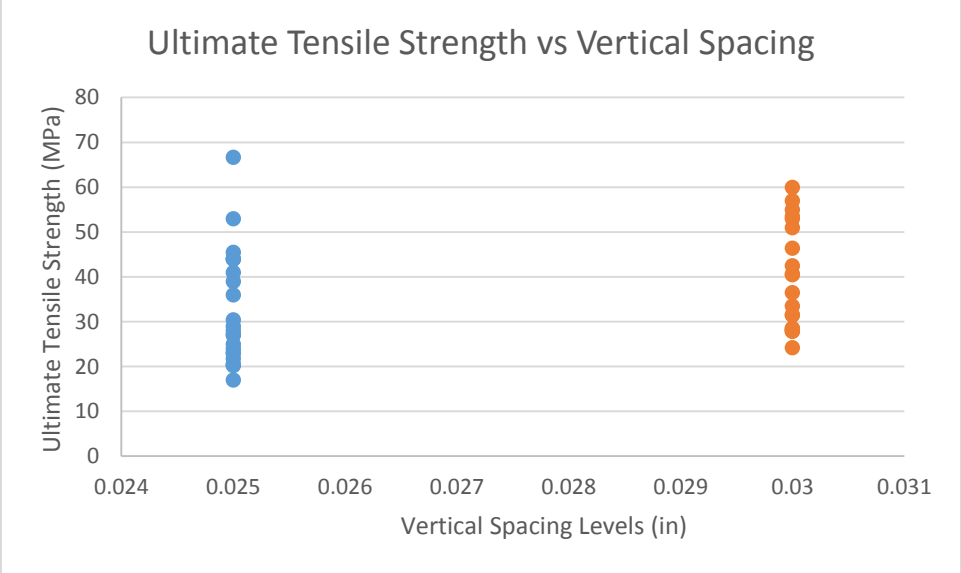

Figure 25: Vertical spacing trend: ultimate tensile strength.

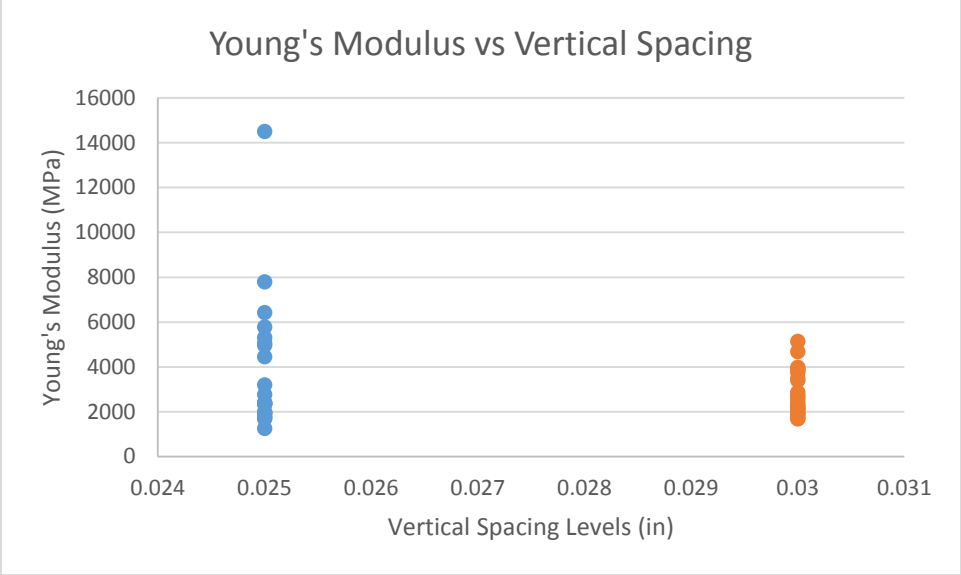

Figure 26: Vertical spacing trend: Young's modulus.

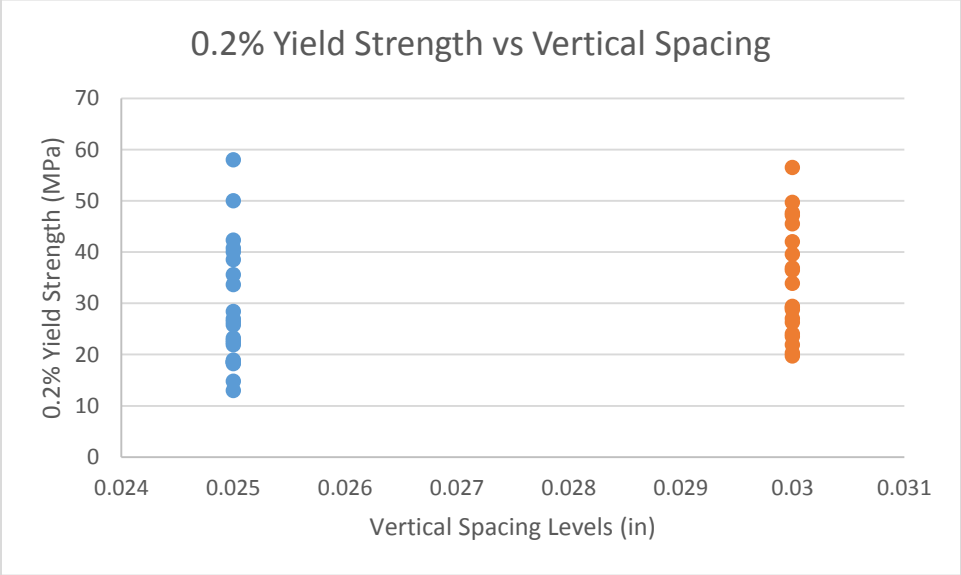

Figure 27: Vertical spacing trend: 0.2% yield strength vs.

At first glance, it can be seen that the majority of the models produced a negative Poisson's ratio which is significant. Also, there seems to be an outlier in one of the Young's modulus values that has a significantly higher value than any other at 14,500 MPa. As far as the trends go for vertical

spacing, there seems to be very little correlation between the vertical spacing and any of the material properties. It is worth noting the clustering found in **Figure 27** in level 2. It could signify that the vertical spacing of 0.3 inches does not allow for the other parameters to significantly affect the Young's modulus.

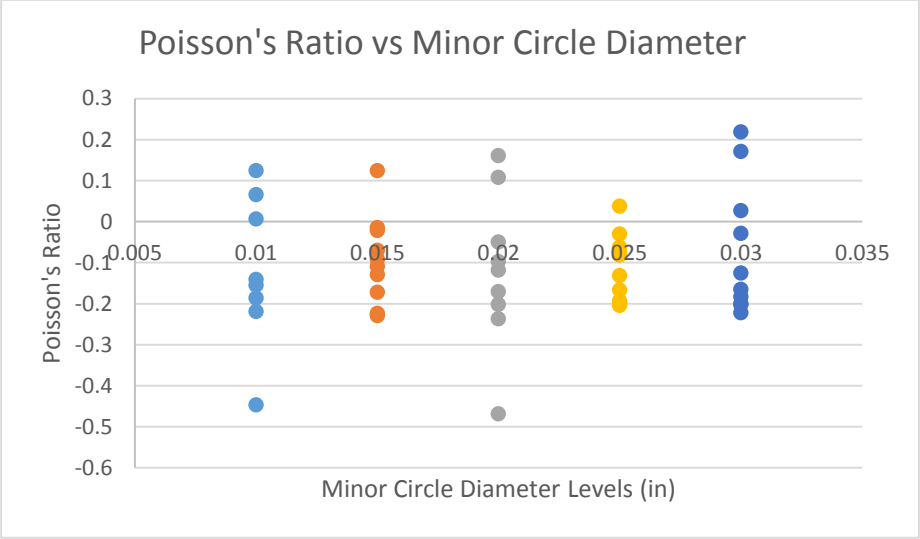

Figure 28: Minor diameter trend: Poisson's ratio.

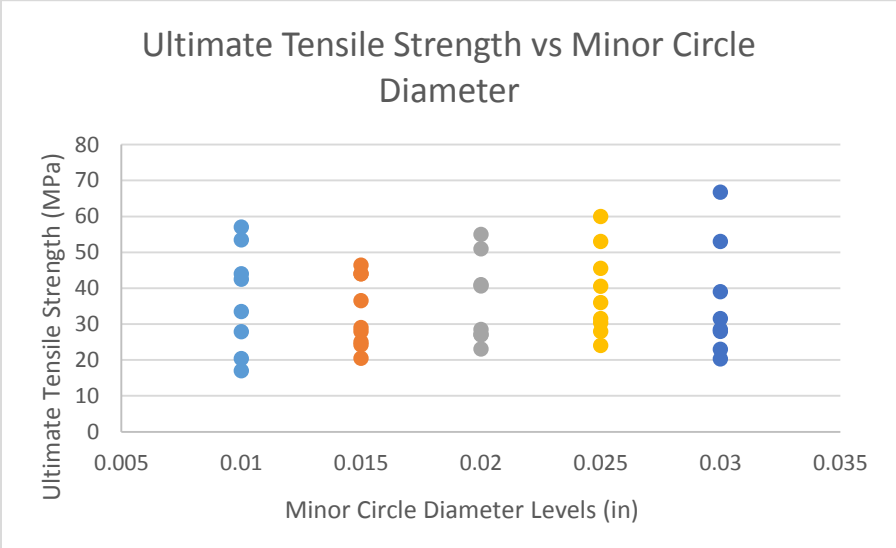

Figure 29: Minor diameter trend: ultimate tensile strength.

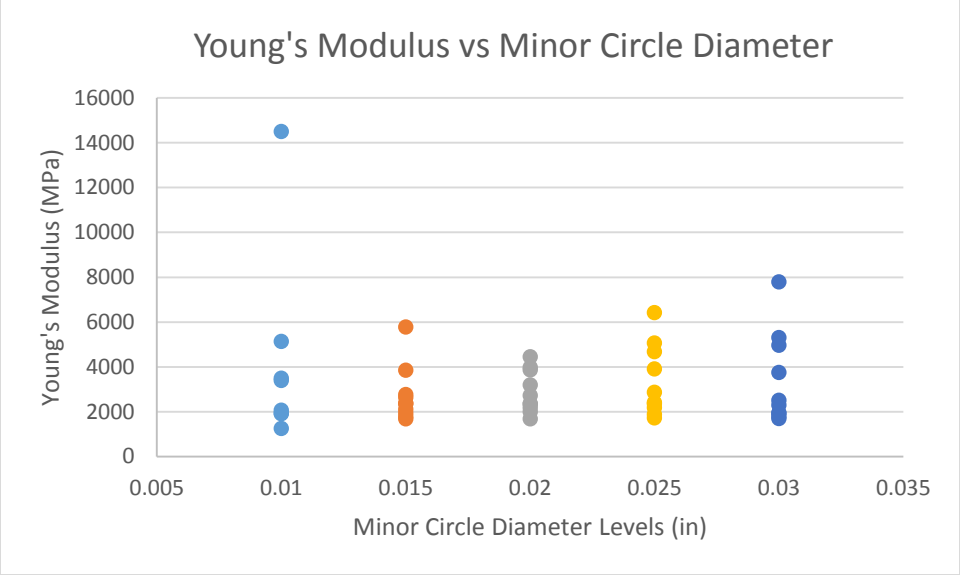

Figure 30: Minor diameter trend: Young's modulus.

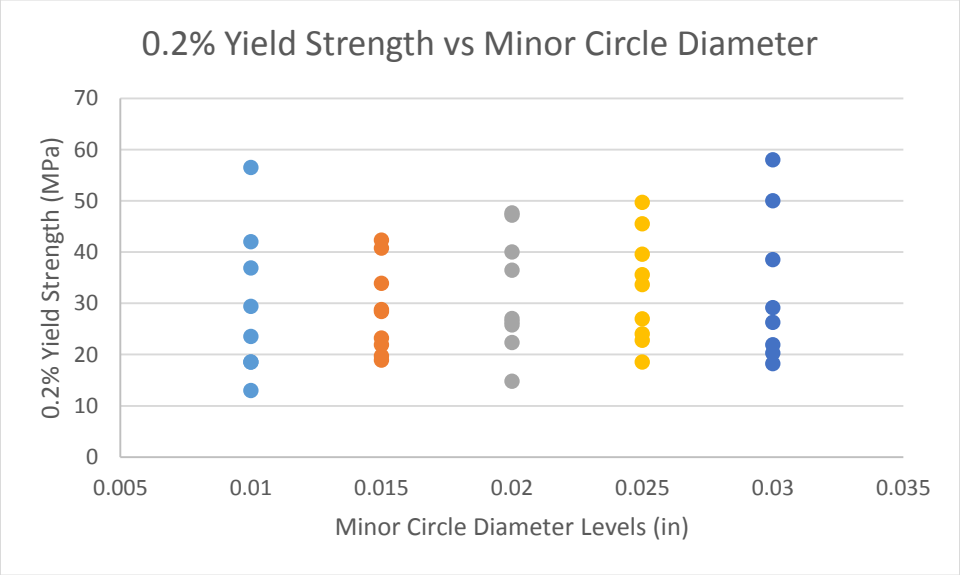

Figure 31: Minor diameter trend: 0.2% yield strength.

The minor diameter has a much more significant impact comparatively to the vertical spacing. Past the Poisson's ratio, each of the remaining mechanical properties has an almost parabolic trend line. The ultimate tensile strength and 0.2% yield strength have the most

significant impact, with level two being significantly lower while levels one and five have much higher values. Similarly to the vertical spacing, clustering can be found in level 3 and 4 of the Young's modulus and Poisson's ratio, respectively.

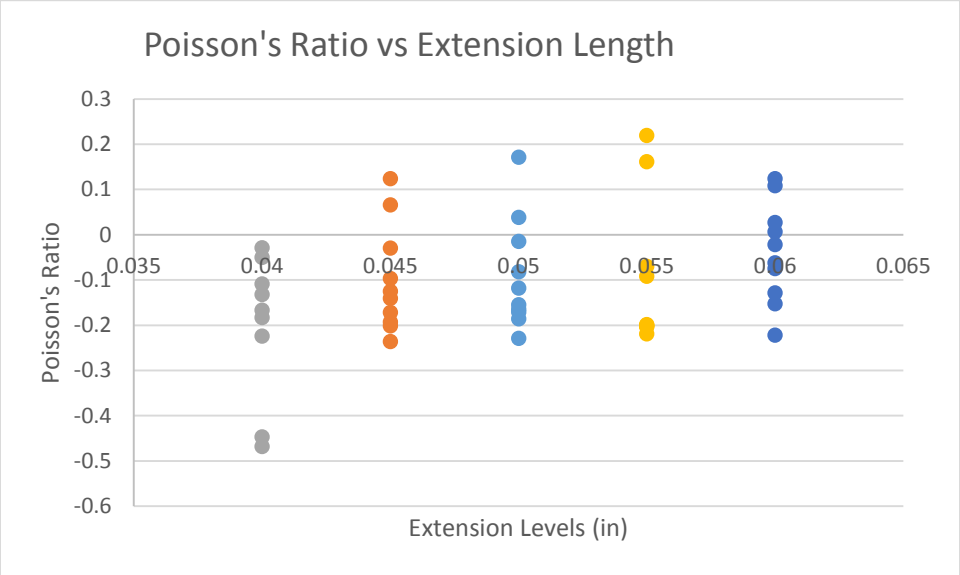

Figure 32: Extension length trend: Poisson's ratio.

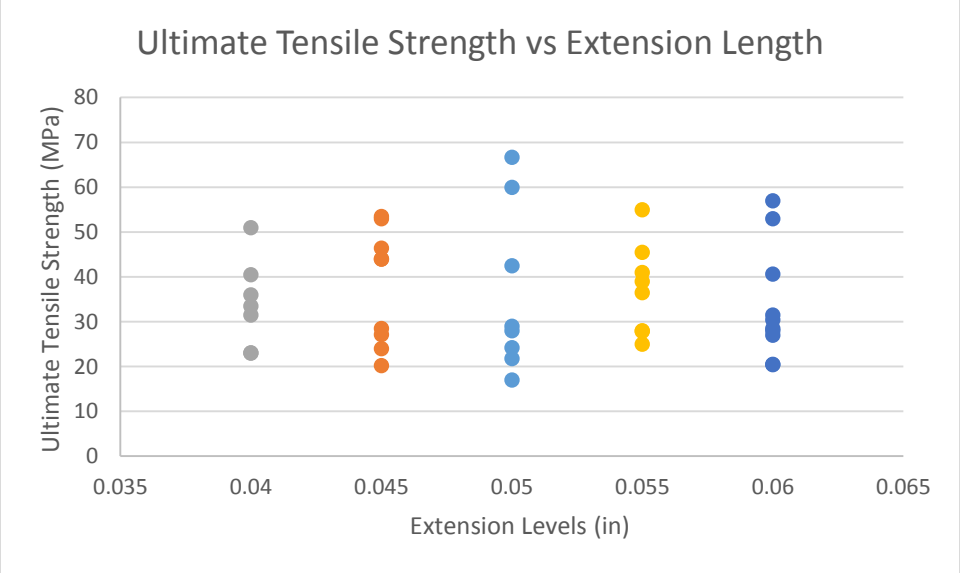

Figure 33: Extension length trend: ultimate tensile strength.

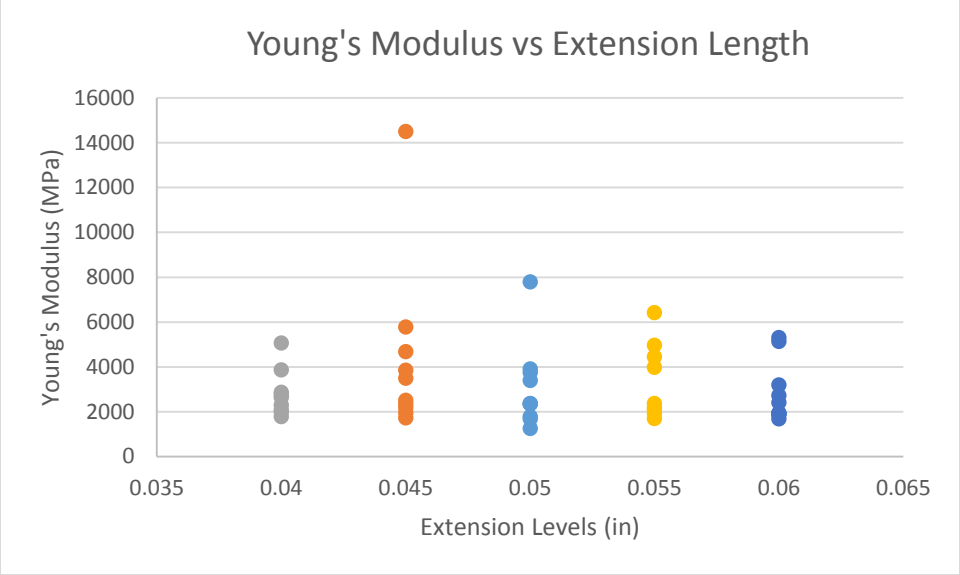

Figure 34: Extension length trend: Young's modulus.

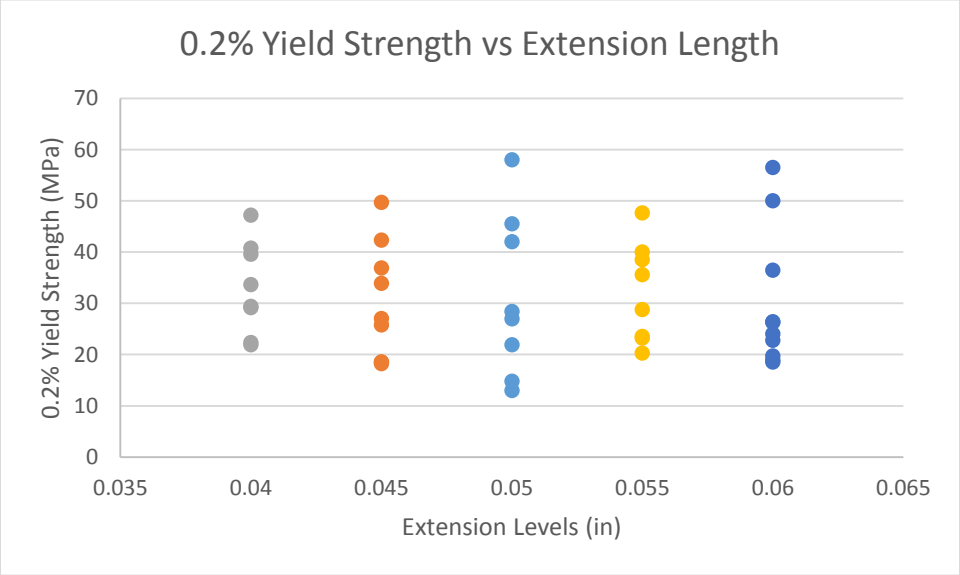

Figure 35: Extension length trend: 0.2% yield strength.

The extension length has a very apparent parabolic trend line focusing on the level 3 point. Each of the properties has a vertex on this level. Also, level 3 seems to be the least

resistant of the levels to change. It is exceptionally likely that the extension length of 0.04 inches leads to an optimal auxetic pattern.

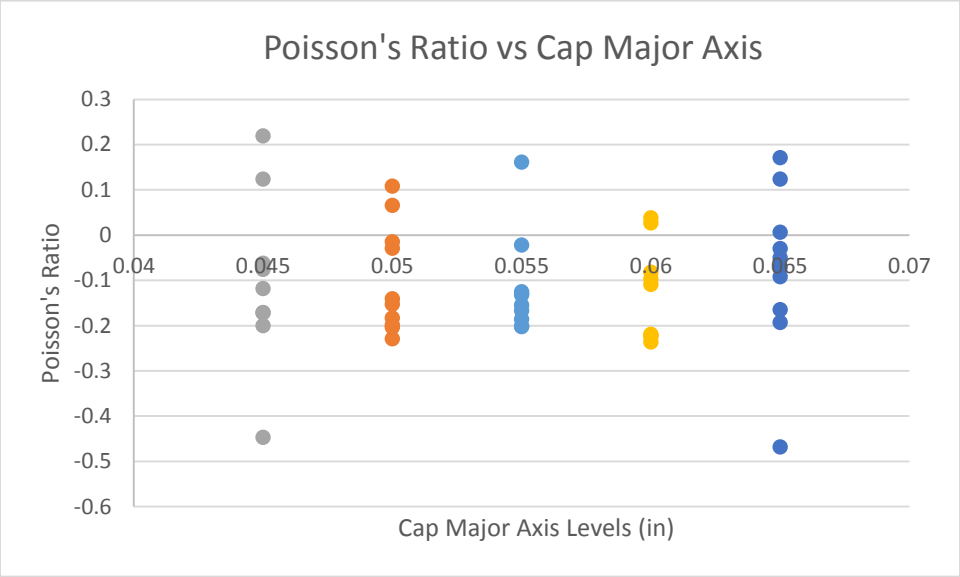

Figure 36: Cap major axis trend: Poisson's ratio.

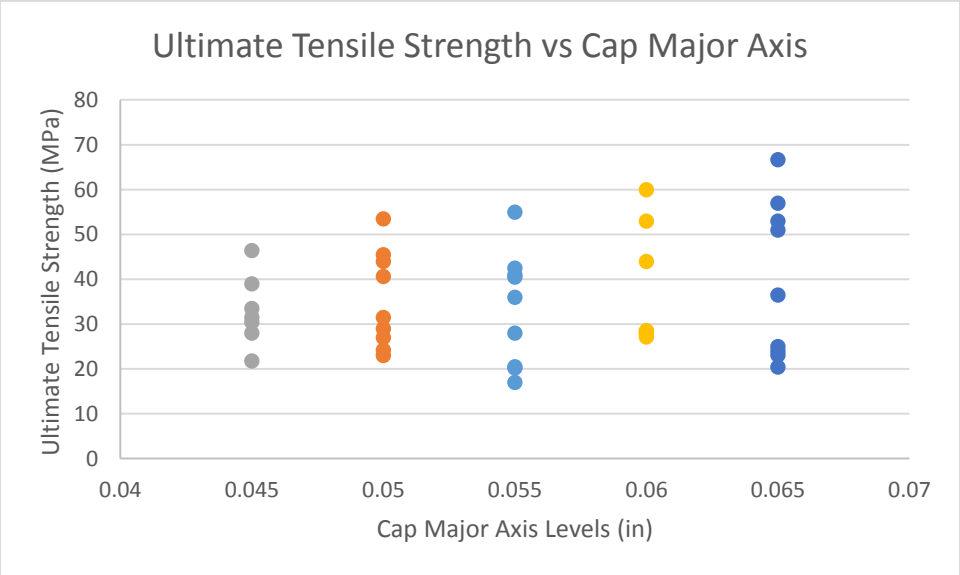

Figure 37: Cap major axis trend: ultimate tensile strength.

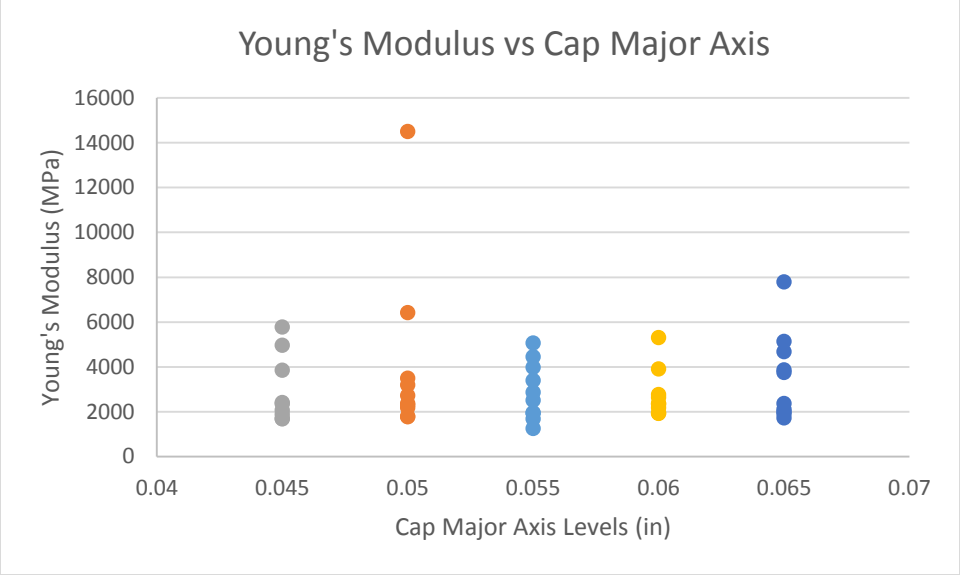

Figure 38: Cap major axis trend: Young's modulus.

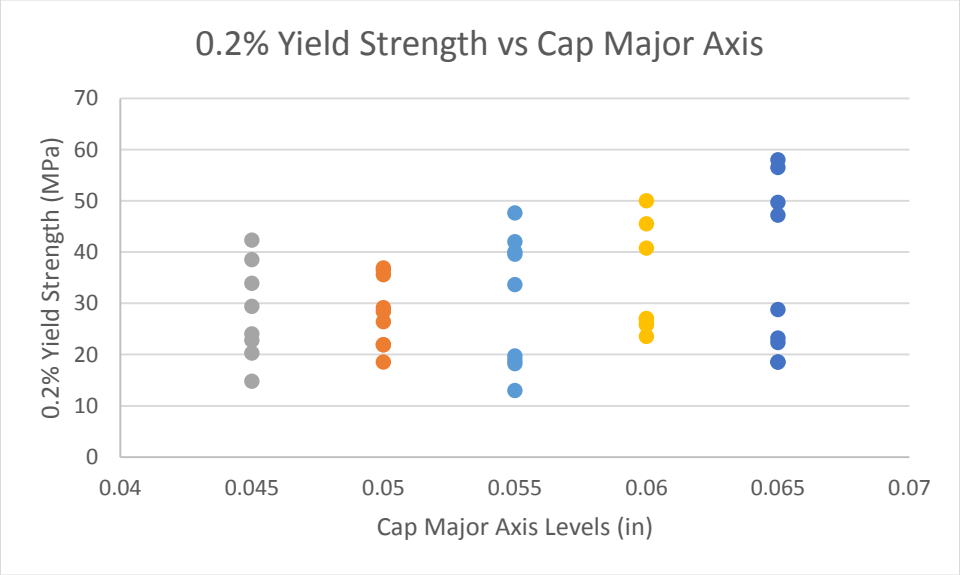

Figure 39: Cap major axis trend: 0.2% yield strength.

The cap major axis has a very unusual trend compared to the previous two. There is a definitive parabola in all the material properties outside of the Poisson's ratio, but they focus on different levels. The Young's modulus and 0.2% yield strength have a vertex on level two while

the ultimate tensile strength has a vertex at level three. Also, besides the outlier, it is apparent that the cap major axis does not allow for much change in the Young's modulus of the bulk structure.

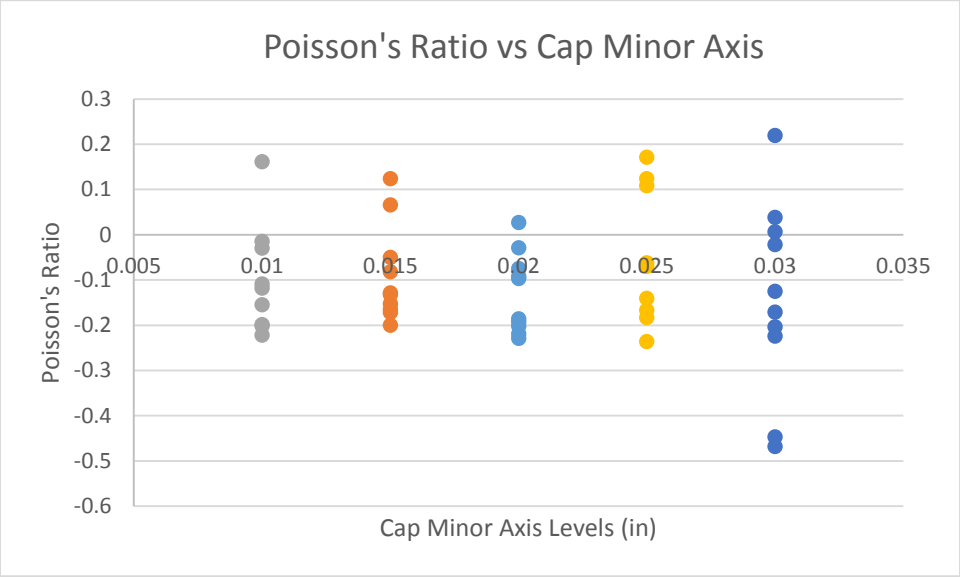

Figure 40: Cap minor axis trend: Poisson's ratio.

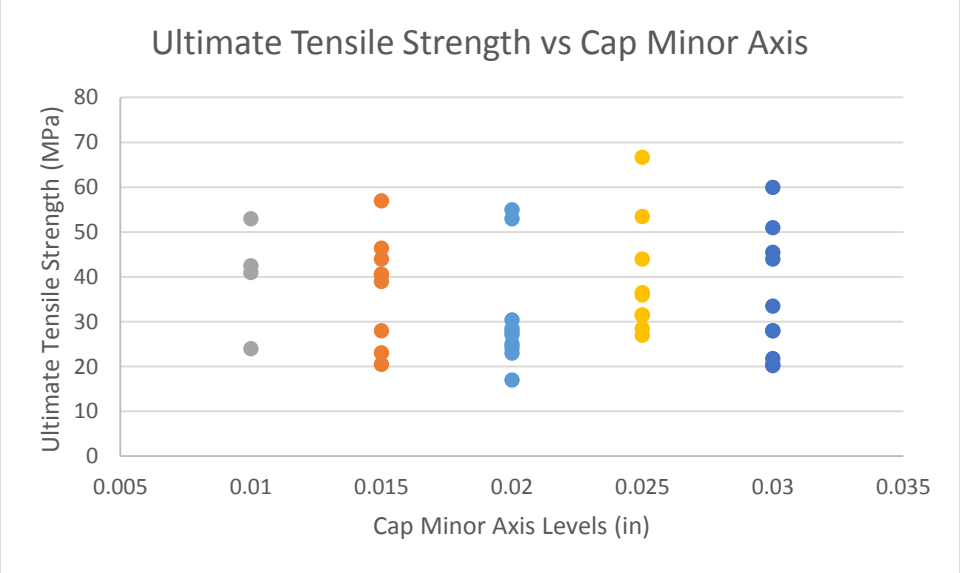

Figure 41: Cap minor axis: ultimate tensile strength.

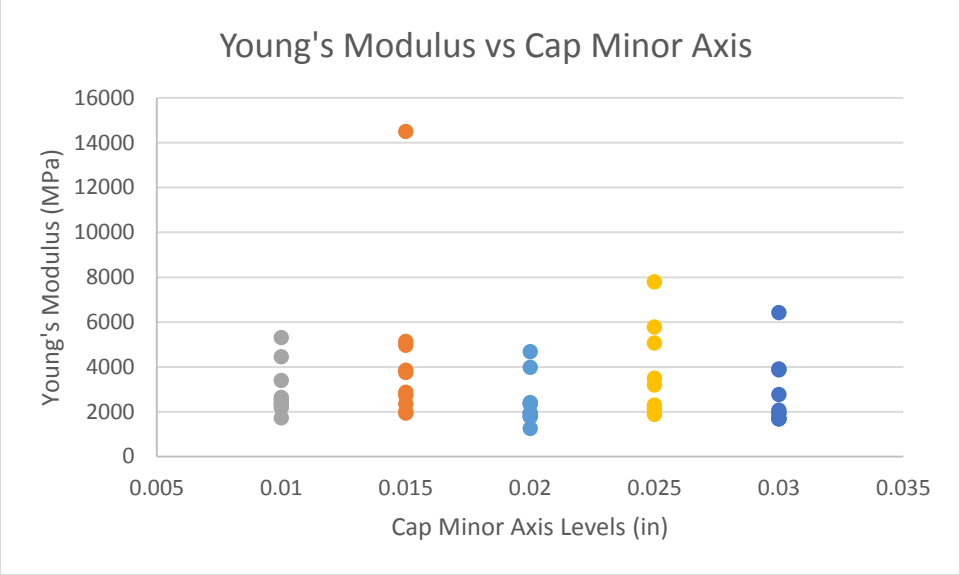

Figure 42: Cap minor axis trend: Young's modulus.

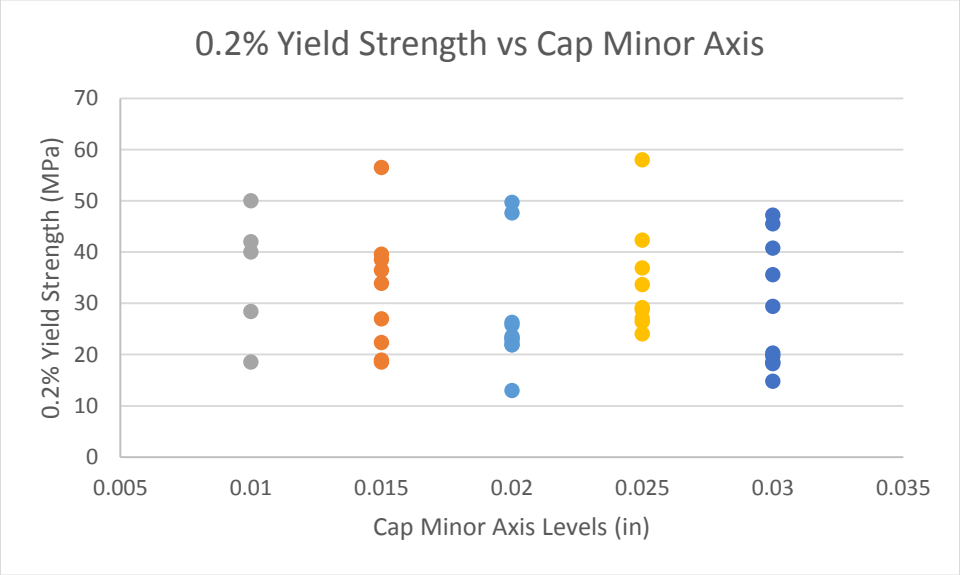

Figure 43: Cap minor axis trend: 0.2% yield strength.

There does not seem to be a significant trend between the mechanical properties of the macro-scale and the cap minor axis. Most of the data is not confined to one area or experience a particularly parabolic trend. Although, looking at the Young's modulus in correlation with the

Young's modulus trend line for the cap major axis. It seems very plausible that the cap utilized for stress shielding is the driving factor for the Young's modulus

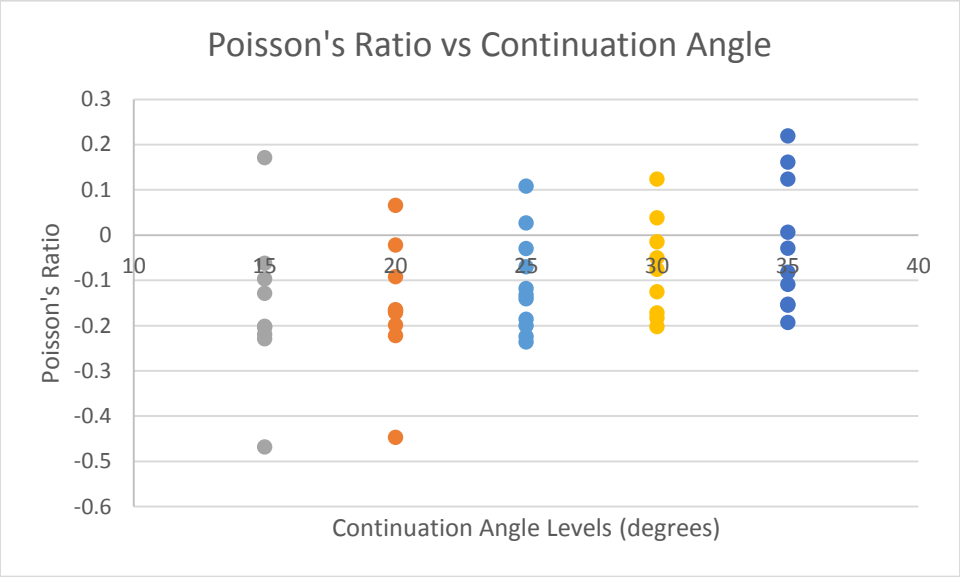

Figure 44: Continuation angle trend: Poisson's ratio.

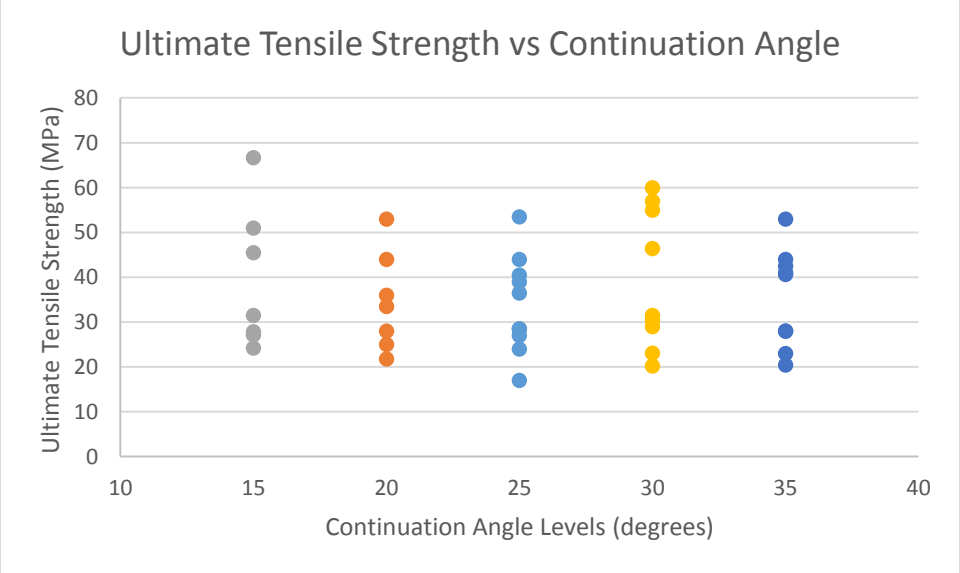

Figure 45: Continuation angle trend: ultimate tensile strength.

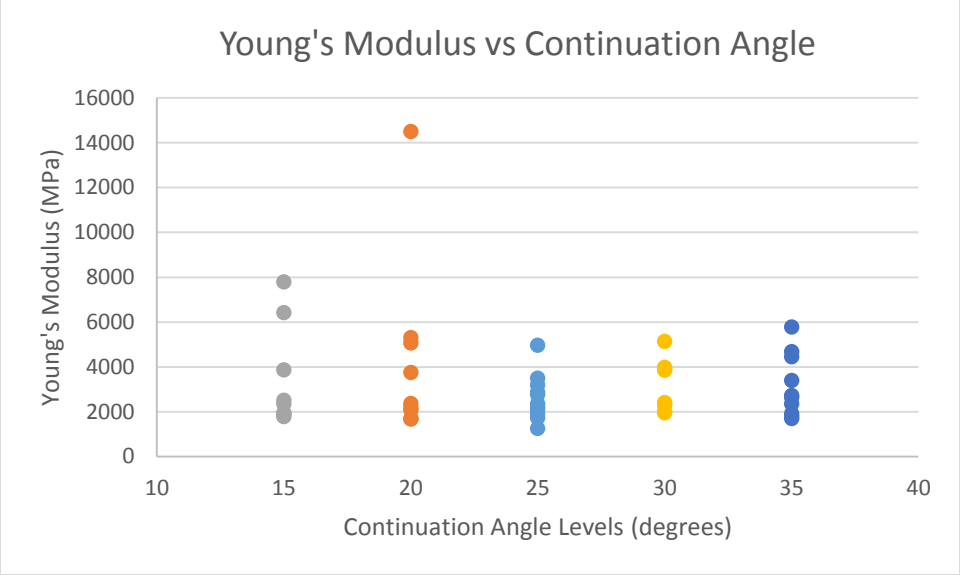

Figure 46: Continuation angle trend: Young's modulus.

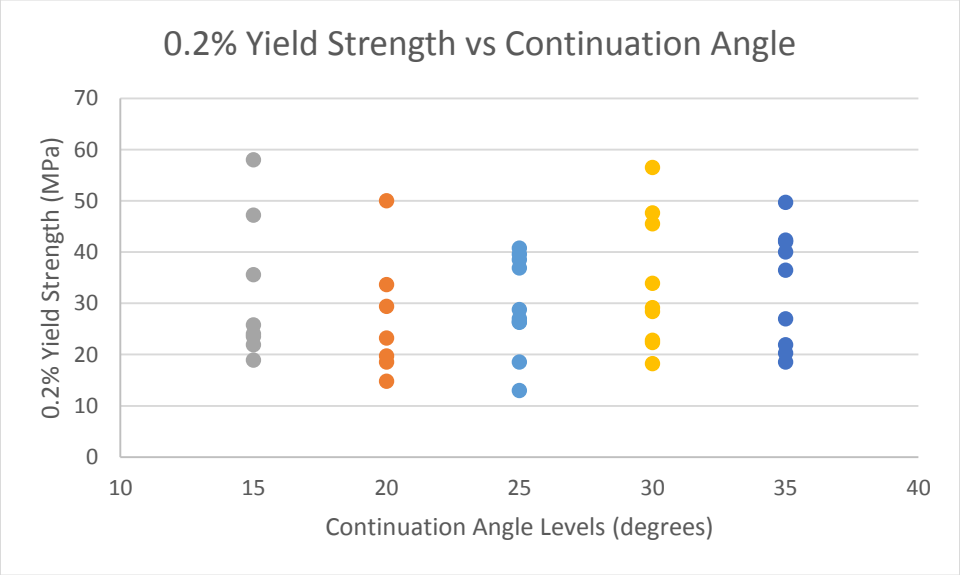

Figure 47: Continuation angle trend: 0.2% yield strength.

The continuation angle has a very unique trend line being the only one so far that expresses a negative parabola, with the maximum occurring at level 3 or 25 degrees. This leads to a great avenue to determine an optimal pattern, given that level 3 seems to surpass every other

case in terms of continuation angle. Also, considering the continuation angle is another parameter attached to the cap feature, it should not be a surprise that very little variation occurs within levels with regards to the Young's modulus.

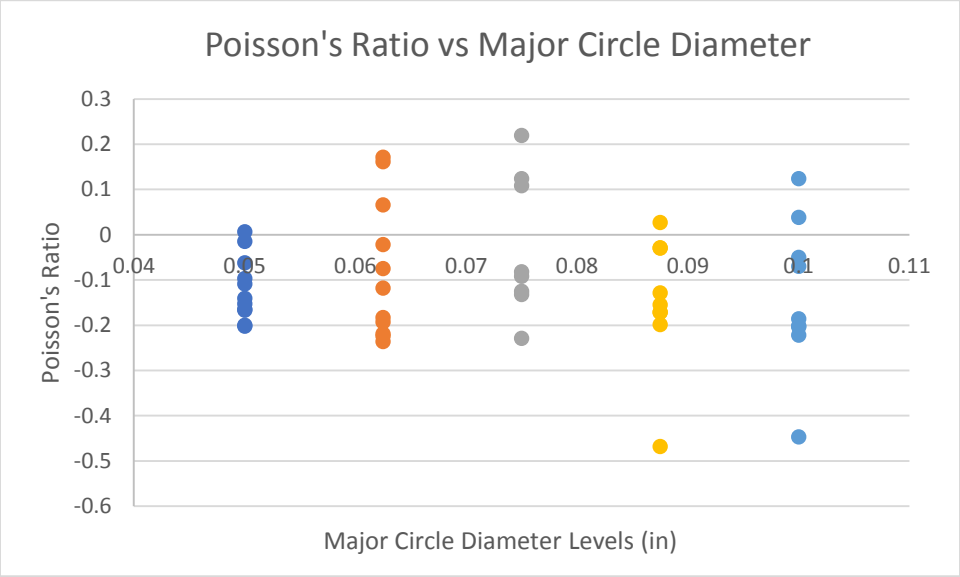

Figure 48: Major diameter trend: Poisson's ratio.

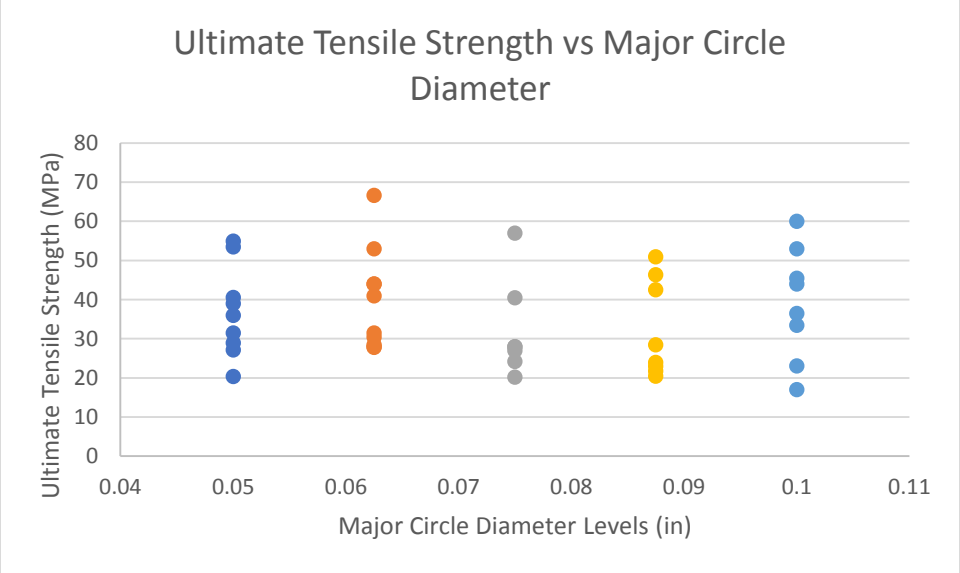

Figure 49: Major diameter trend: ultimate tensile strength.

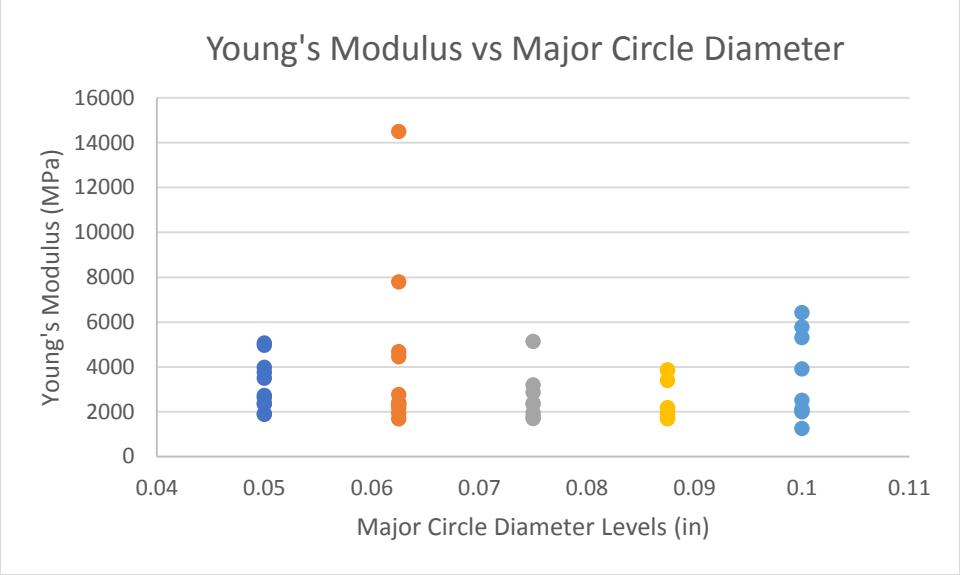

Figure 50: Major diameter trend: Young's modulus.

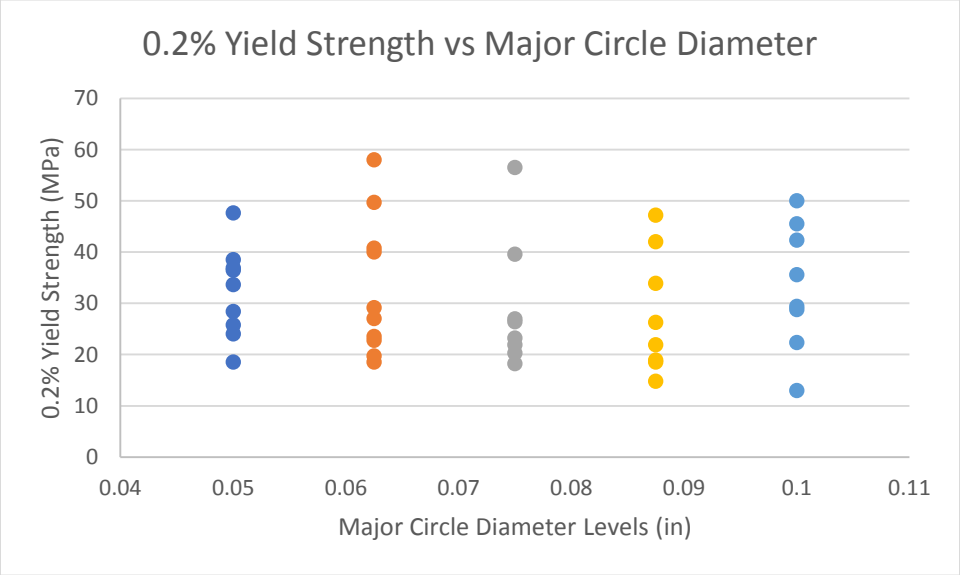

Figure 51: Major diameter trend: 0.2% yield strength.

Interestingly, the primary diameter does not seem to have a great impact on any of the mechanical properties, the most significant being the Poisson's ratio. There seems to be a very

slight cubic trend attached to a few of the properties, but overall there seems to be little variation based on the varying sizes.

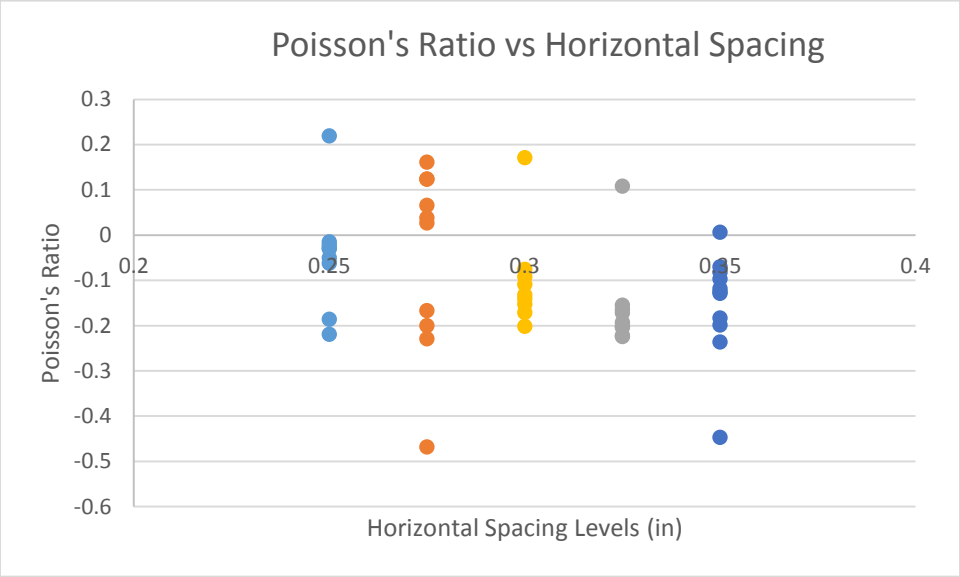

Figure 52: Horizontal spacing trend: Poisson's ratio.

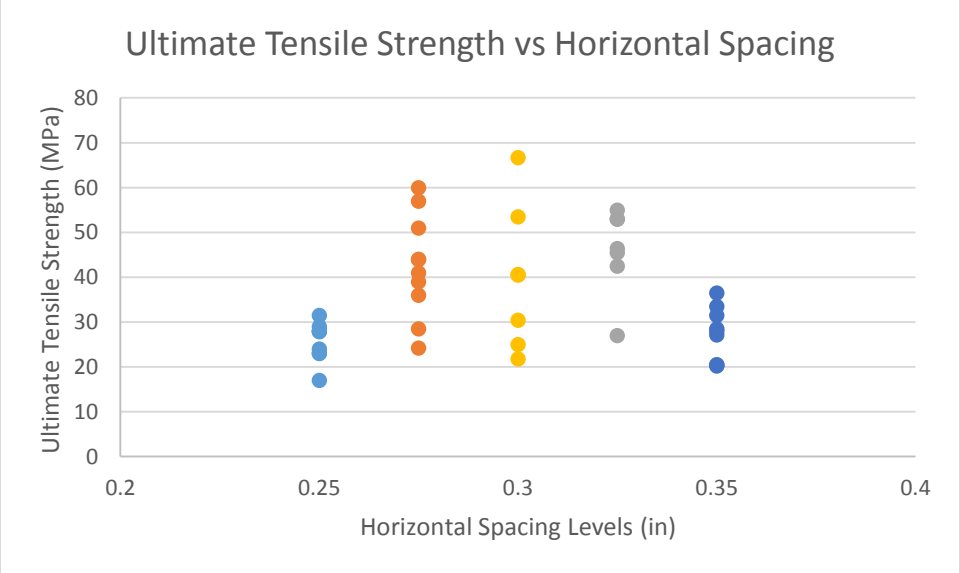

Figure 53: Horizontal spacing trend: ultimate tensile strength.

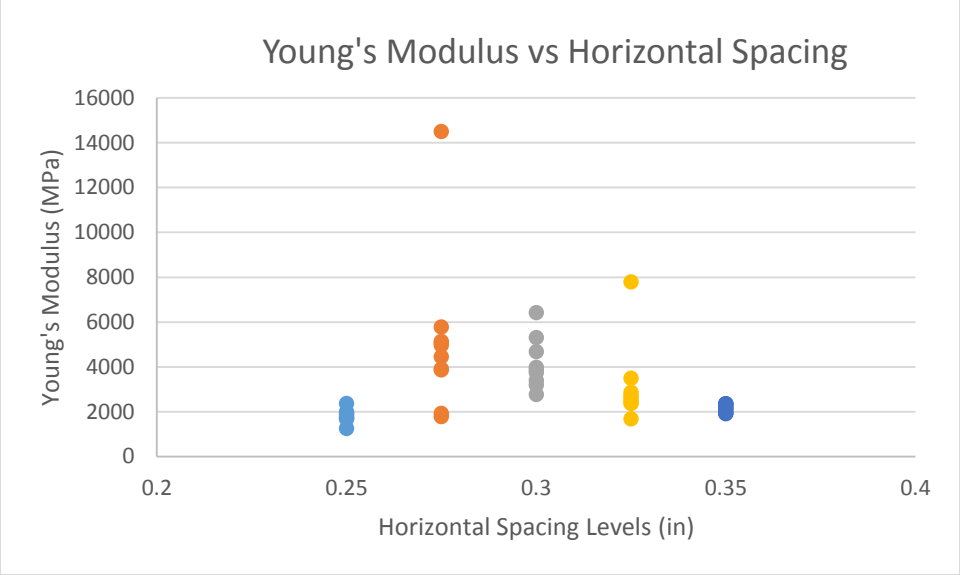

Figure 54: Horizontal spacing trend: Young's modulus.

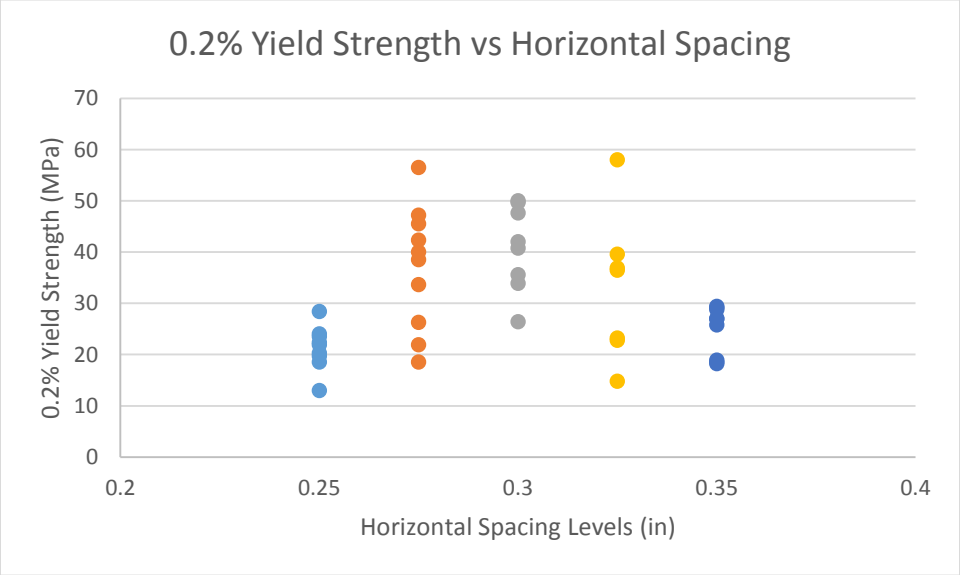

Figure 55: Horizontal spacing trend: 0.2% yield strength.

The final parameter that is varied is the horizontal spacing. The horizontal spacing seems to have a much more significant impact than its counterpart, the vertical spacing. Each of the four mechanical properties seem to have an almost quartic trend line attached to them, with each

of them being more consolidated in levels 1 and 5, the largest and smallest spacing. It is hard to comment on why this is without further expanding the bounds of the horizontal spacing, but it can be assumed that only certain values of the horizontal spacing obtain useful patterns, but which ones it is hard to clarify.

With all of the trend lines developed a few optimal patterns can be selected for their overall quality of mechanical properties. Each one should still maintain the essential property of a negative Poisson's ratio, in order to remain auxetic, but the other three properties are not constricted.

The model with the most negative Poisson's ratio is model 38 with a Poisson's ratio of -0.468. The stress response for the model can be seen below, it has a more pronounced response in the transverse direction than many of the other models, which leads to the high negative Poisson's ratio.

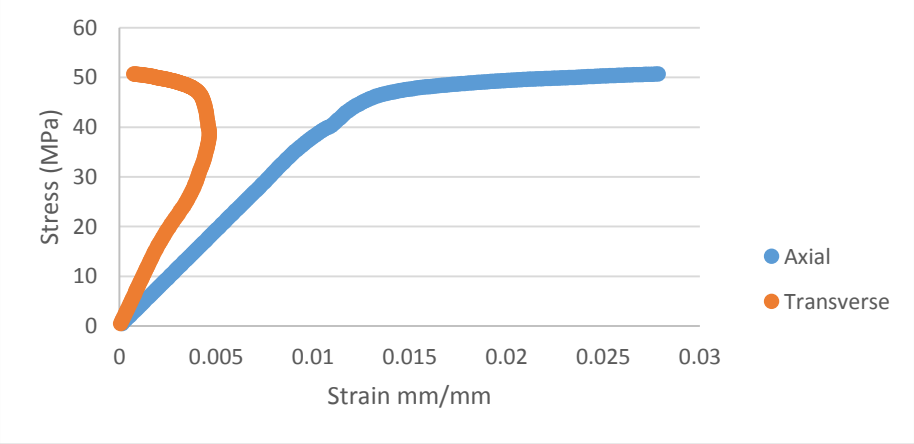

Figure 56: Model 38 (0.3, 0.02, 0.04, 0.065, 0.03, 15, 0.0875, 0.275) stress-strain curve.

The significant stress response in the transverse direction allocates the high valued negative Poisson's ratio. The response of the Poisson's ratio versus strain and material properties can be seen below.

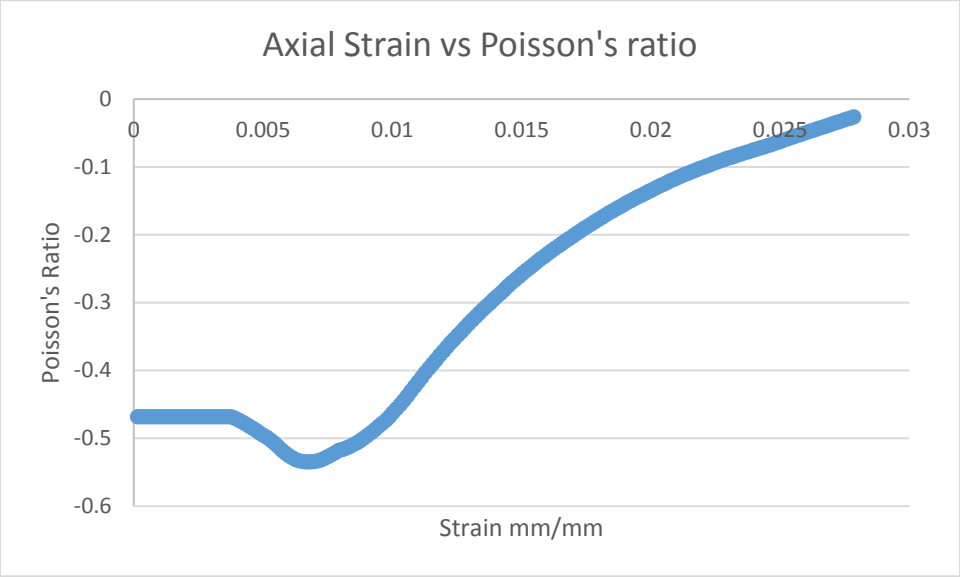

Figure 57: Model 38 (0.3, 0.02, 0.04, 0.065, 0.03, 15, 0.0875, 0.275) Poisson's ratio response.

Table 7: Model 38 (0.3, 0.02, 0.04, 0.065, 0.03, 15, 0.0875, 0.275) material properties.

Material Property	Value
Poisson's Ratio	-0.4685
Young's Modulus (MPa)	3868
Ultimate Tensile Strength (MPa)	51
0.2% Yield Strength (MPa)	47.17

Model 38 experiences a slight increase Young's modulus while compared to the bulk material and has similar values for both the ultimate tensile strength and 0.2% yield strength. The dimensions for the model and the auxeton follow.

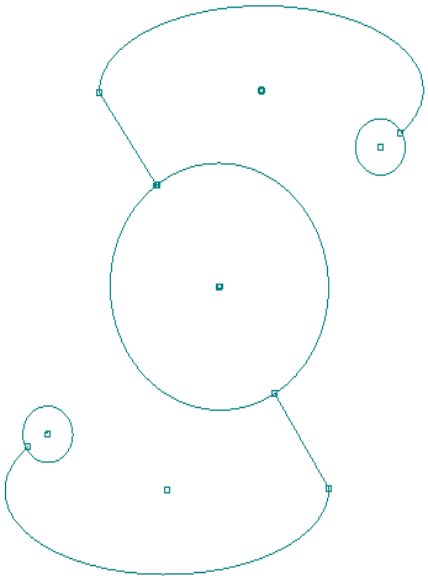

Parameter	Dimension
H	0.275 in
V	0.3 in
D	0.0875 in
d	0.02 in
a	0.065 in
b	0.03 in
L	0.04 in
θ	15 degrees

Figure 58: Model 38 dimensions and auxteon.

The model with the greatest value for ultimate tensile strength is model 39 with an ultimate tensile strength of 55 MPa. There were other models with greater values than this, but this was the highest that still maintained a negative Poisson's ratio. The model's responses and material properties can be seen below.

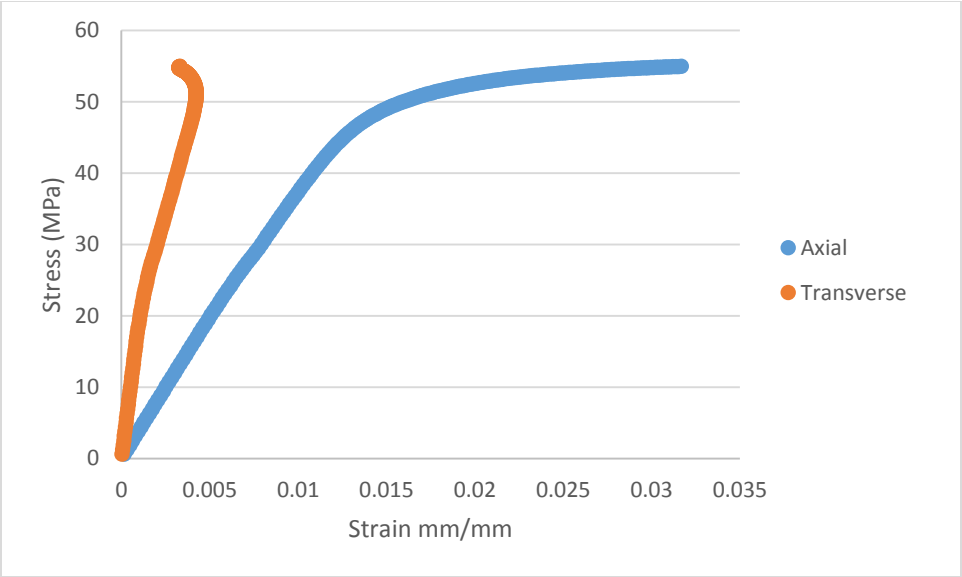

Figure 59: Model 39 (0.3, 0.02, 0.055, 0.055, 0.02, 30, 0.05, 0.325) stress-strain response.

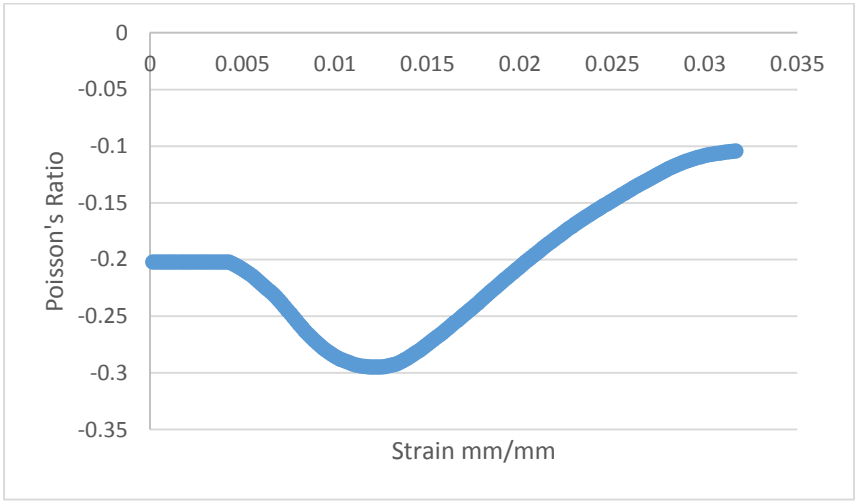

Figure 60: Model 39 (0.3, 0.02, 0.055, 0.055, 0.02, 30, 0.05, 0.325) Poisson's ratio response.

Table 8: Model 39 (0.3, 0.02, 0.055, 0.055, 0.02, 30, 0.05, 0.325) material properties.

Material Property	Value
Poisson's Ratio	-0.2022
Young's Modulus (MPa)	3988
Ultimate Tensile Strength (MPa)	55
0.2% Yield Strength (MPa)	47.64

This model has very similar results with model 38 with the exception of the exceptionally high negative Poisson's ratio. This can accounted for by the dimensions, especially the extension length, which is the most significant difference. Model 39's auxeton and parameter combinations follow.

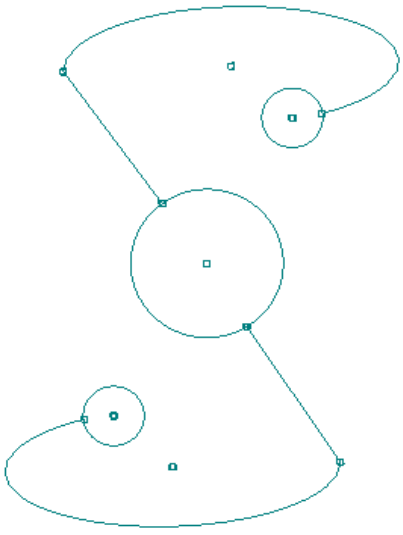

Figure 61: Model 39 auxeton dimensions.

Parameter	Value
H	0.325 in
V	0.3 in
D	0.05 in
d	0.02 in
a	0.055 in
b	0.02 in
L	0.055 in
θ	30 degrees

The optimal model in regards to Young's modulus is model 19 with a Young's modulus of 6419 MPa. The responses of the model can be seen below.

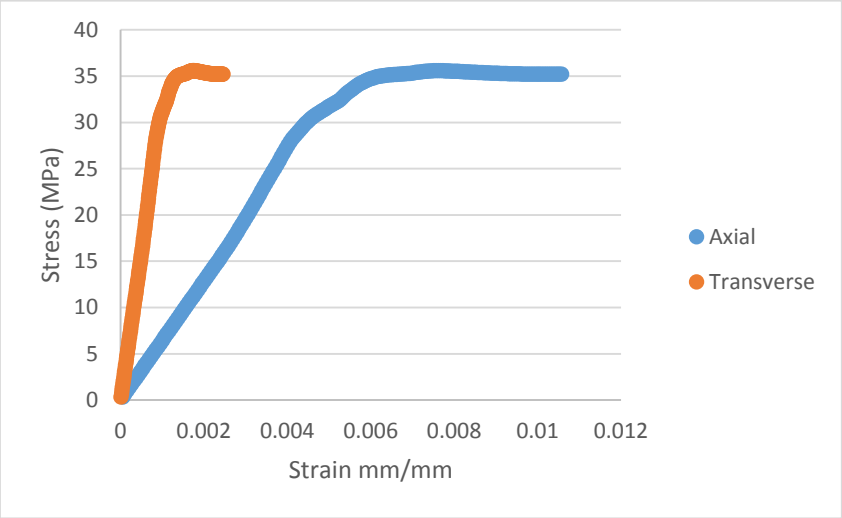

Figure 62: Model 19 (0.25, 0.025, 0.055, 0.05, 0.03, 15, 0.1, 0.325) stress-strain response

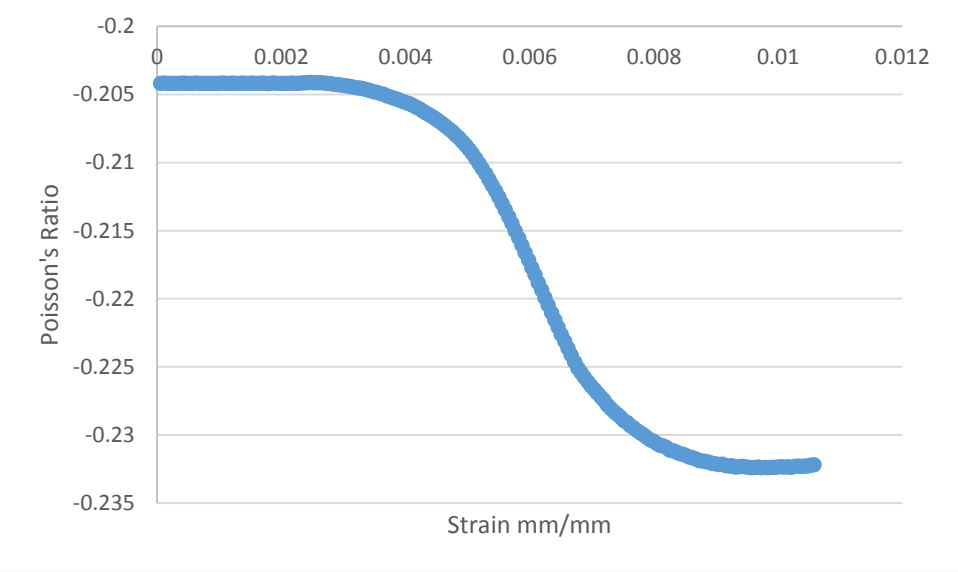

Figure 63: Model 19 (0.25, 0.025, 0.055, 0.05, 0.03, 15, 0.1, 0.325) Poisson's ratio response.

Table 9: Model 19 (0.25, 0.025, 0.055, 0.05, 0.03, 15, 0.1, 0.325) material properties.

Material Property	Value
Poisson's Ratio	-0.204
Young's Modulus (MPa)	6419
Ultimate Tensile Strength (MPa)	45.5
0.2% Yield Strength (MPa)	35.57

Model 19 has a unique response such that the axial and transverse strains both react in a similar manner. Both have a linear response then slowly taper off as plasticity is induced. This leads to the Poisson's ratio dipping to be slightly more negative, but the ratio never increases to a positive value, for these strain rates. This is explained by the auxeton characteristics seen below. Each of the values for the pattern lies within the fifth level of the parameterization, which results in the high Young's modulus and unique response.

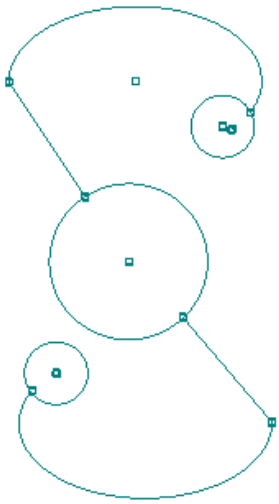

Parameter	Value
H	0.325 in
V	0.25 in
D	0.1 in
d	0.025 in
a	0.05 in
b	0.03 in
L	0.055 in
θ	15

Figure 64: Model 19 auxeton dimensions.

The optimal model with thought to the 0.2% yield strength is model 42, with a value of 50 MPa. The responses of model 42 can be seen below.

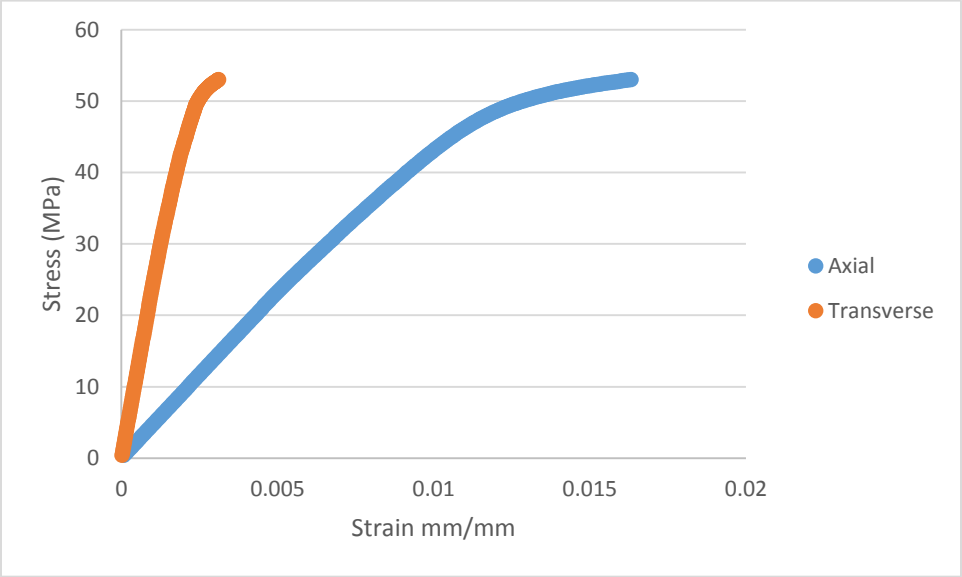

Figure 65: Model 42 (0.3, 0.025, 0.045, 0.065, 0.02, 35, 0.0625, 0.325) stress-strain response.

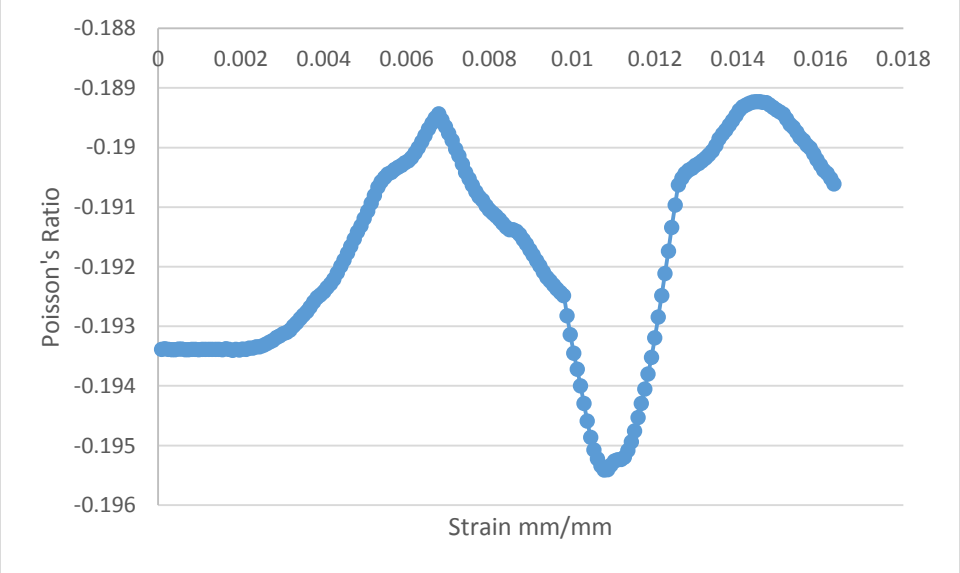

Figure 66: Model 42 (0.3, 0.025, 0.045, 0.065, 0.02, 35, 0.0625, 0.325) Poisson's ratio versus strain.

Table 10: Model 42 (0.3, 0.025, 0.045, 0.065, 0.02, 35, 0.0625, 0.325) material properties.

Material Property	Value
Poisson's Ratio	-0.193
Young's Modulus (MPa)	4675
Ultimate Tensile Strength (MPa)	53
0.2% Yield Strength (MPa)	50

Model 42 responses similarly to model 19 in the stress-strain response, however, it has an exceptionally different response in Poisson's ratio. The value almost remains constant throughout the simulation, with little variation between values at all strain levels. This can be seen through the dimensions of the auxeton, which are listed below. The high levels of horizontal and vertical spacing in combination with the small diameter ratio, cause the Poisson's ratio to remain relatively constant.

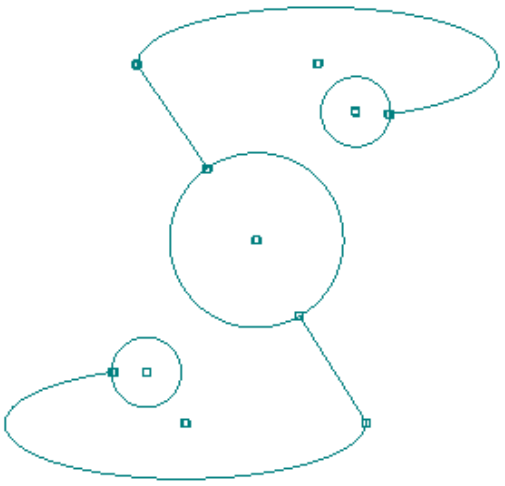

Figure 67: Model 42 auxeton dimensions.

Parameter	Value
H	0.325 in
V	0.3 in
D	0.0625 in
d	0.025 in
a	0.065 in
b	0.02 in
L	0.045 in
θ	35

Another objective of the parametric study is to determine the influence that is placed on each material by each of the varying parameters, and to rank them accordingly. This was completed through exploring the variance of each level of parameter related to the four principle mechanical properties, as well as the porosity of each of the samples. During this exercise, a table is developed that shows the decreasing impact each parameter has on the specific bulk material property. In order to properly due a statistical analysis of the test data, the one outlier representing the Young's modulus value of 14500 was removed.

Table 11: Influence rankings based on variance study.

Property	1	2	3	4	5	6	7	8
Poisson's	L	θ	H	D	V	b	d	a
Young's	H	b	D	d	a	θ	V	L
UTS	H	V	D	b	a	d	θ	L
0.2% YS	H	b	a	V	θ	D	d	L
Porosity	D	H	d	V	L	a	θ	b

According to the study, the horizontal spacing, H, had the most significant impact on the variance of the simulative data. The minor axis of the cap, b, as well as the primary diameter, D, and vertical spacing, V, seemed to contribute equally around the second highest amount. Extension length, L, was the least likely to influence the variance in data, being last in three of the five categories. For porosity, it would be expected that the two diameters would drastically

affect the data, however, horizontal and vertical spacing also contributed a major portion due to have varying numbers of rows and columns of auxetons embedded into the test sample.

CHAPTER 6. CONCLUSION

The focus of this research is to develop, parameterize, and optimize a novel auxetic pattern. The auxetic pattern proposed is a natural progression based on previous work that helps to shield the structure from stress concentrations as well as reduce the overall porosity that plagues many auxetic structures. This auxetic structure is simulated using the Ramberg-Osgood model for plasticity, in order to obtain a better understanding of the effects auxetic structures experience during plastic deformation. During optimization, the Taguchi method is utilized to drastically reduce the overall number of simulations required to produce meaningful results. Once all of the data is collected, trend plots are developed in order to properly map out the effects of each parameter on the characterized material properties, Poisson's ratio, Young's modulus, ultimate tensile strength, and 0.2% yield strength. Once the trends are found, optimal patterns can be found regarding each of the material properties found.

APPENDIX: INDIVIDUAL SIMULATION RESULTS

Model 1

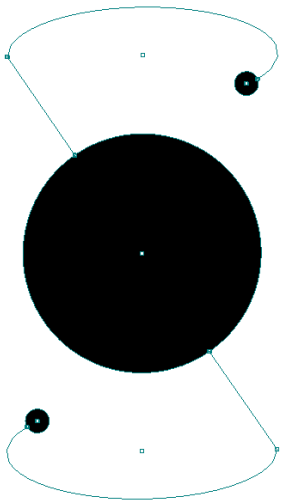

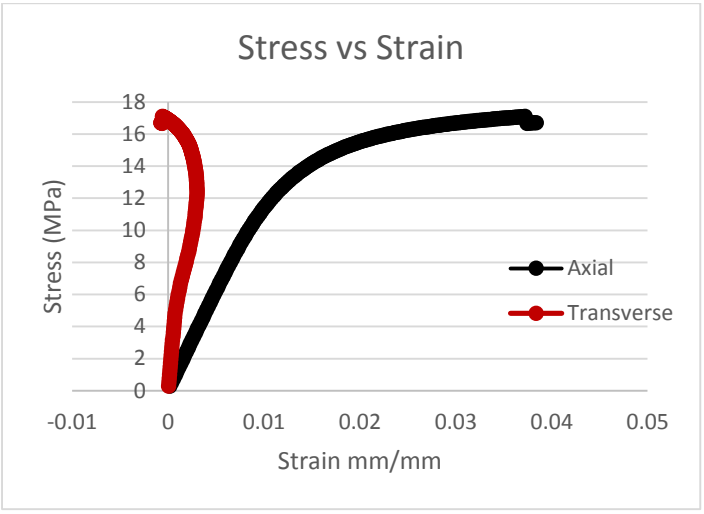

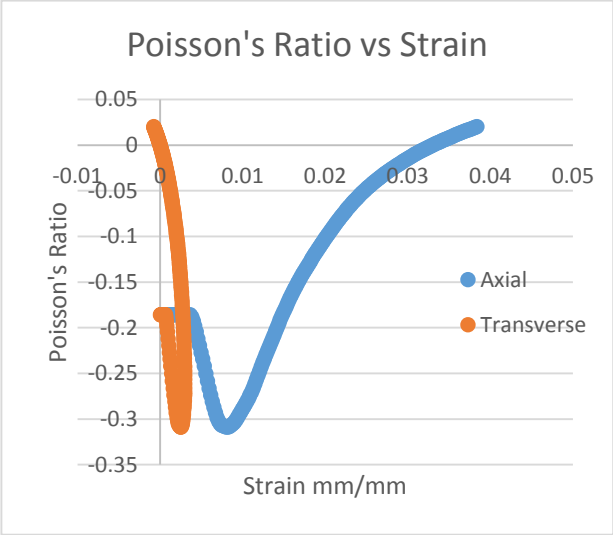

Mechanical Property	Value
Poisson's Ratio	-0.186
Young's Modulus (MPa)	1260
Ultimate Tensile Strength (MPa)	17
0.2% Yield Strength (MPa)	13

Model 2

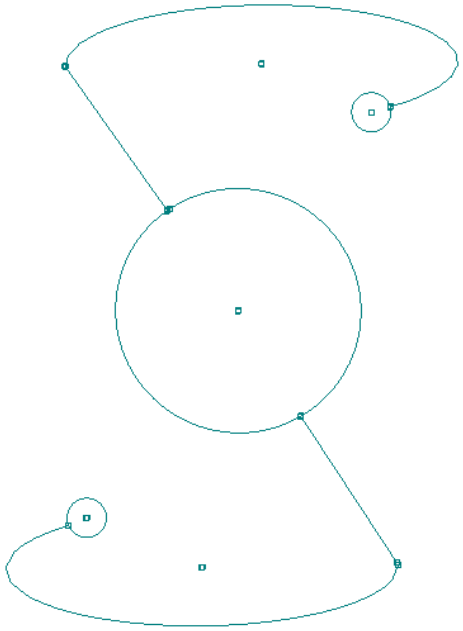

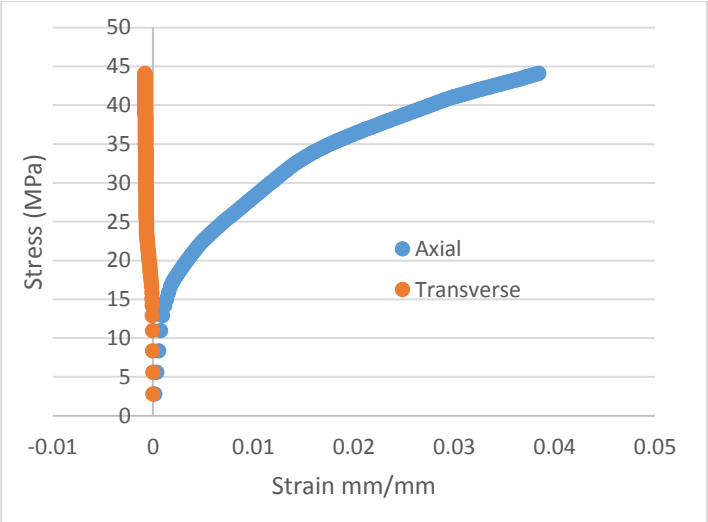

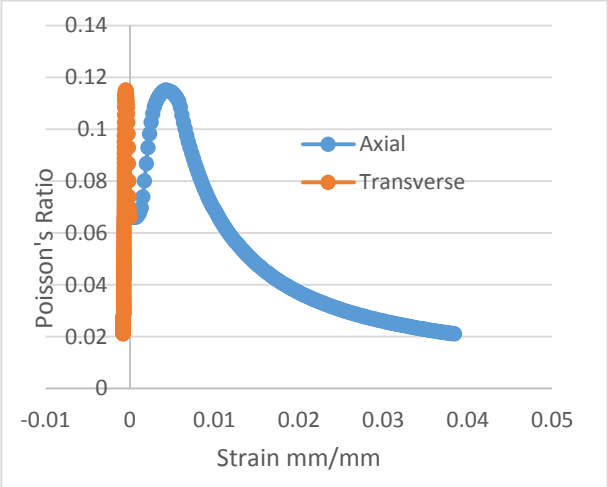

Mechanical Property	Value
Poisson's Ratio	0.066
Young's Modulus (MPa)	14503
Ultimate Tensile Strength (MPa)	44
0.2% Yield Strength (MPa)	18.5

Model 3

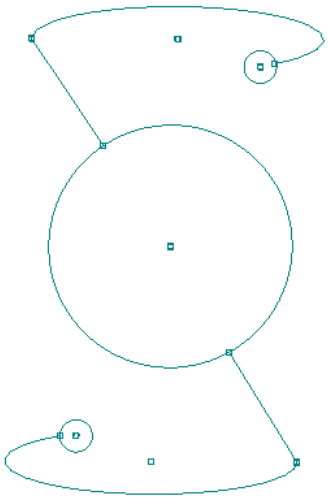

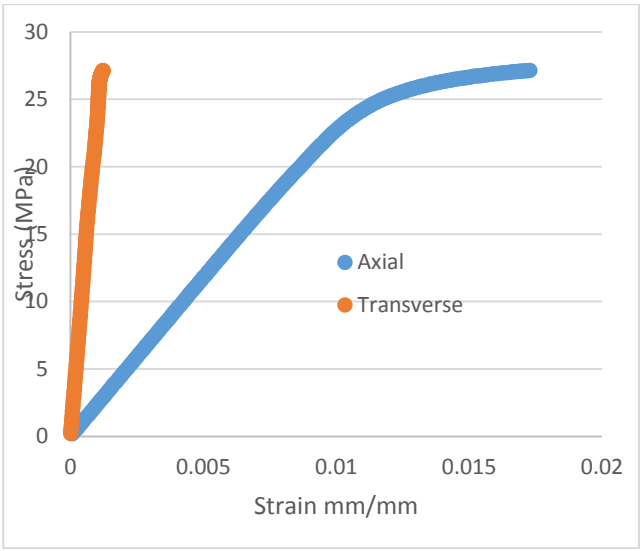

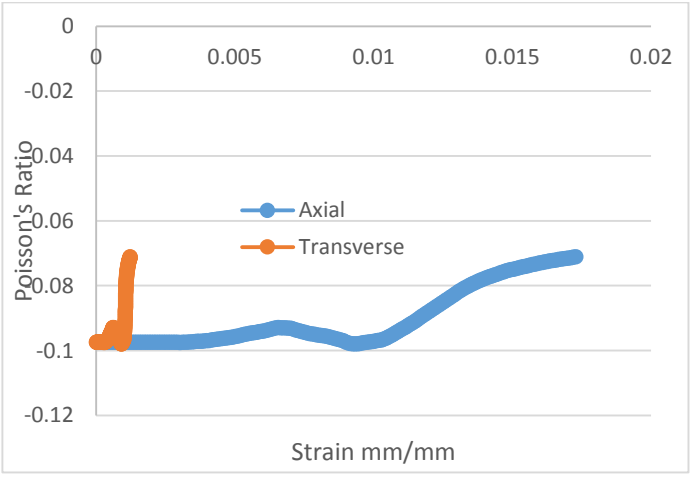

Mechanical Property	Value
Poisson's Ratio	-0.095
Young's Modulus (MPa)	2435
Ultimate Tensile Strength (MPa)	26
0.2% Yield Strength (MPa)	22.2

Model 4

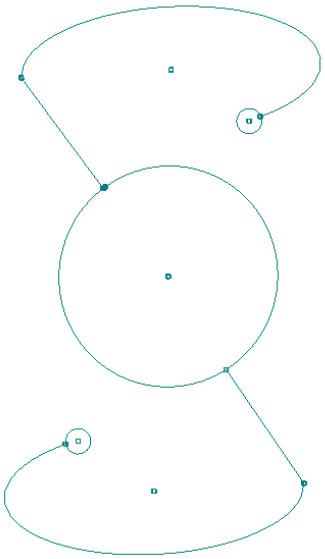

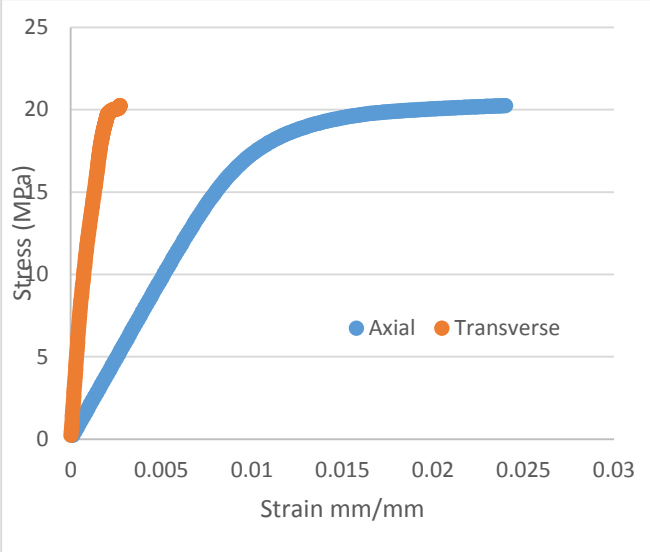

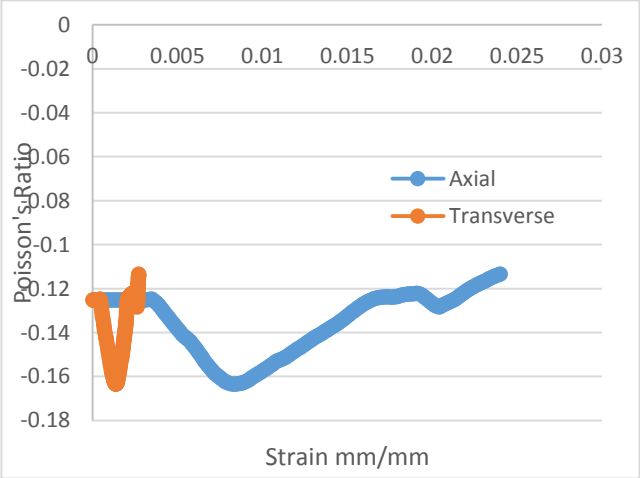

Mechanical Property	Value
Poisson's Ratio	-0.125
Young's Modulus (MPa)	1968
Ultimate Tensile Strength (MPa)	20
0.2% Yield Strength (MPa)	18

Model 5

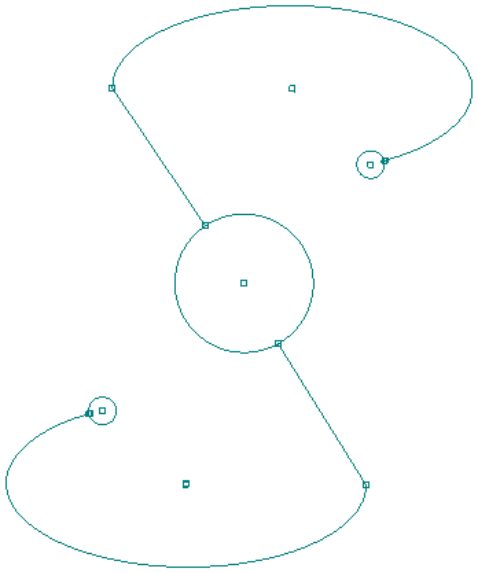

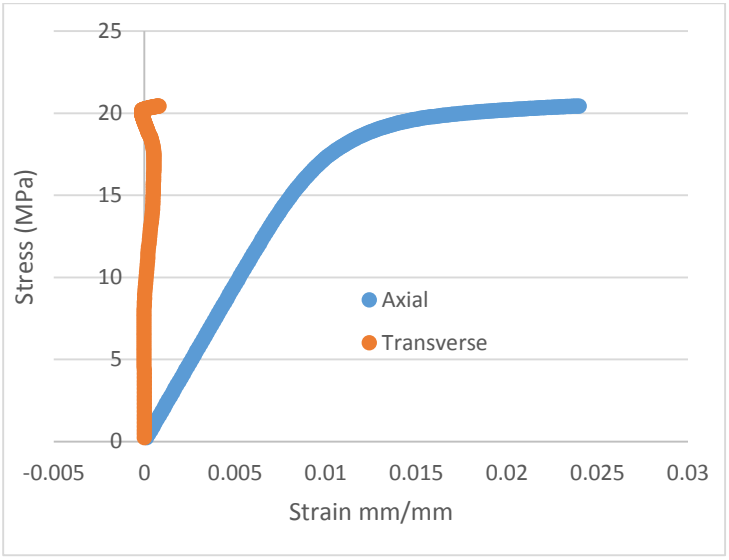

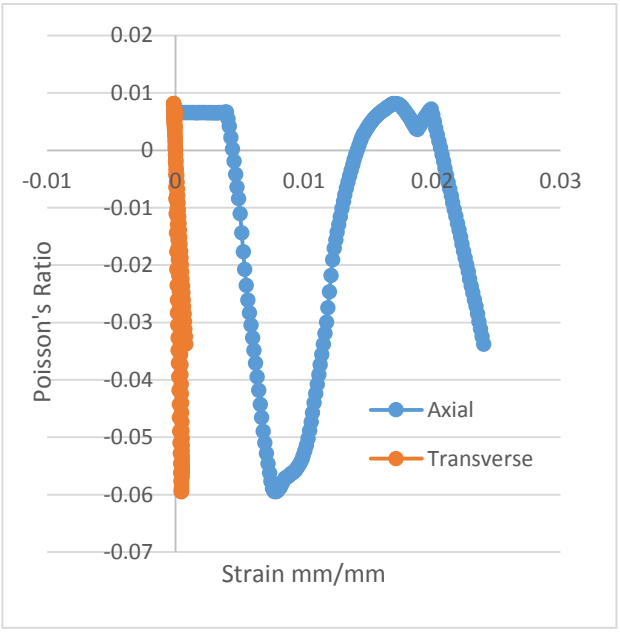

Mechanical Property	Value
Poisson's Ratio	0.0065
Young's Modulus (MPa)	1911
Ultimate Tensile Strength (MPa)	20.4
0.2% Yield Strength (MPa)	19.5

Model 6

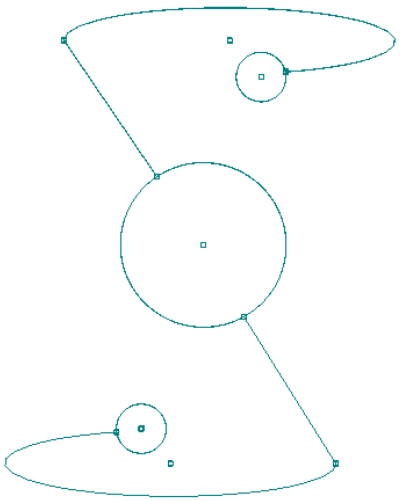

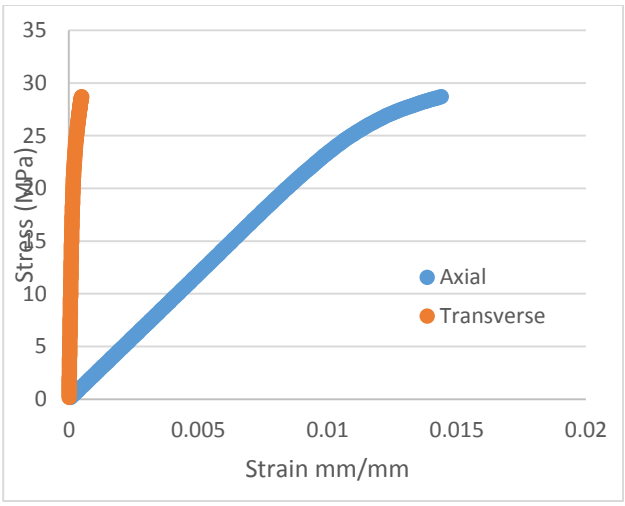

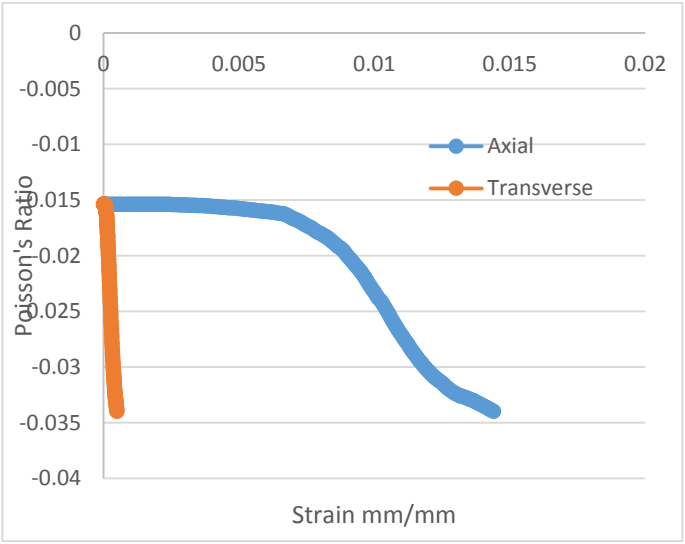

Mechanical Property	Value
Poisson's Ratio	-0.015
Young's Modulus (MPa)	2371
Ultimate Tensile Strength (MPa)	29
0.2% Yield Strength (MPa)	28.4

Model 7

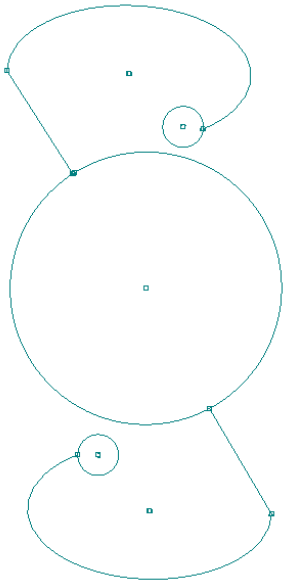

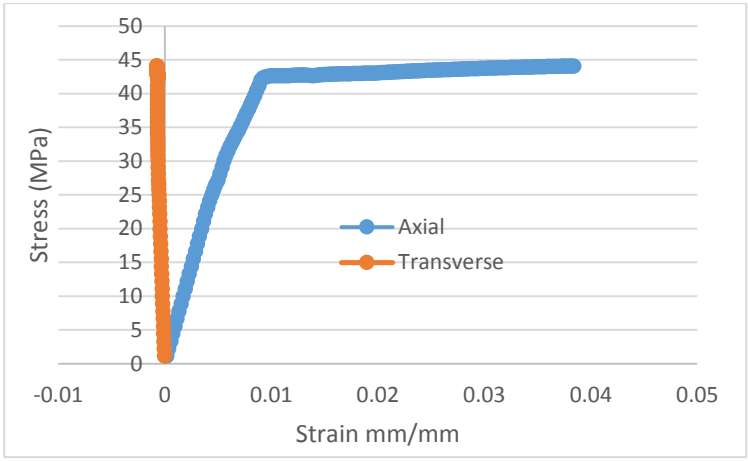

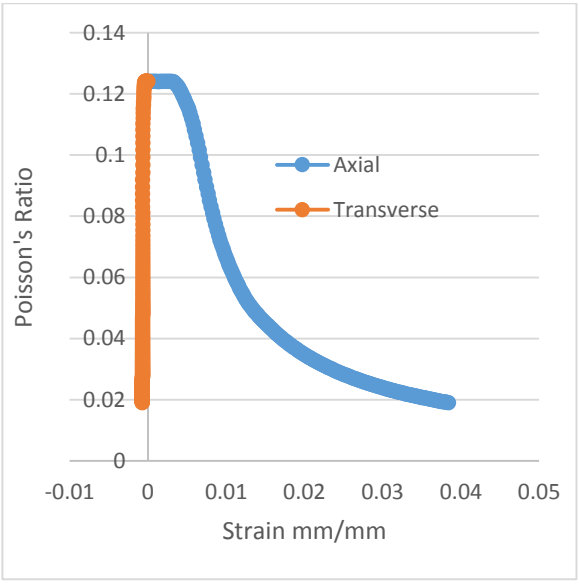

Mechanical Property	Value
Poisson's Ratio	0.124
Young's Modulus (MPa)	5777
Ultimate Tensile Strength (MPa)	44
0.2% Yield Strength (MPa)	42.35

Model 8

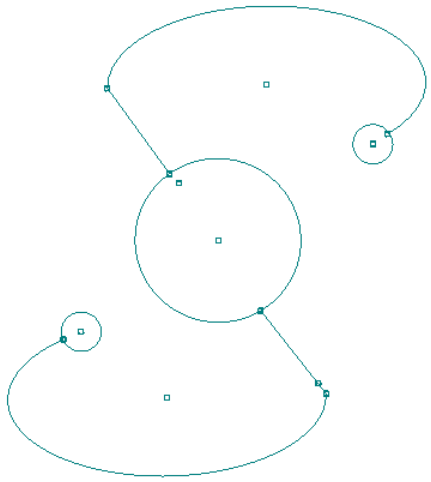

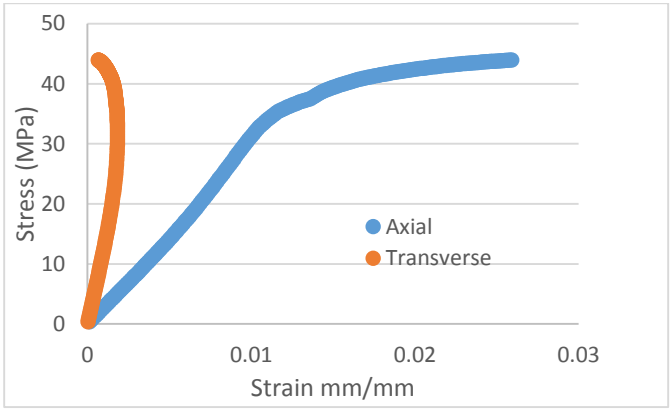

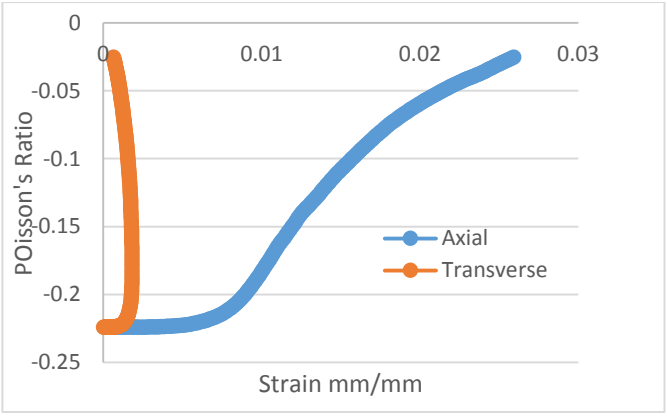

Mechanical Property	Value
Poisson's Ratio	-0.224
Young's Modulus (MPa)	2766
Ultimate Tensile Strength (MPa)	44
0.2% Yield Strength (MPa)	40.78

Model 9

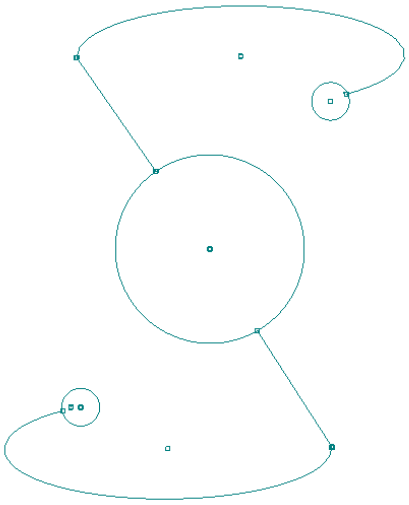

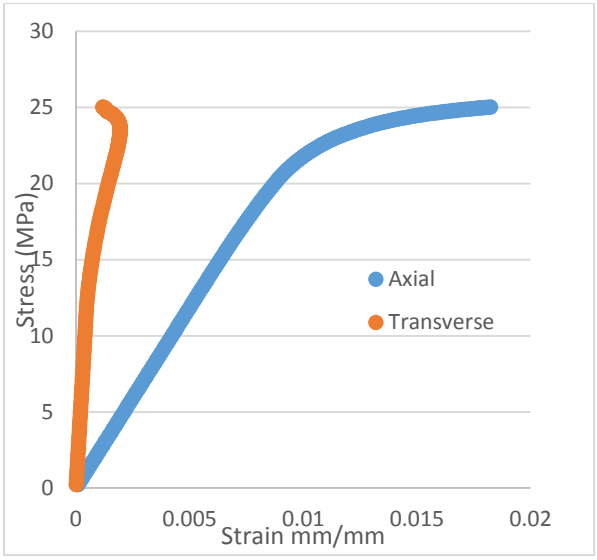

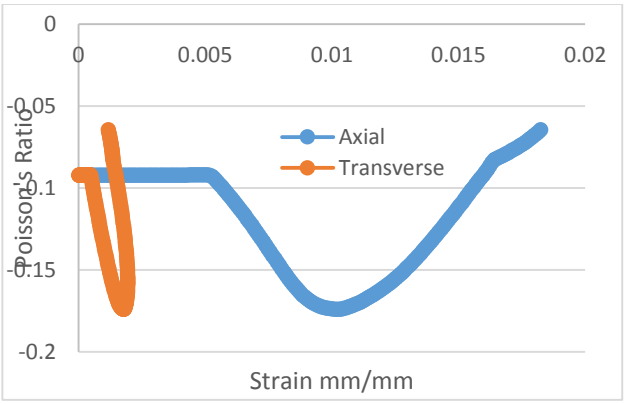

Mechanical Property	Value
Poisson's Ratio	-0.092
Young's Modulus (MPa)	2369
Ultimate Tensile Strength (MPa)	25
0.2% Yield Strength (MPa)	23.2

Model 10

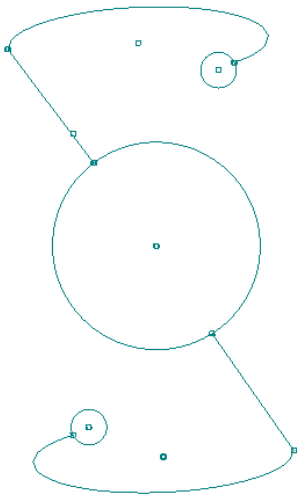

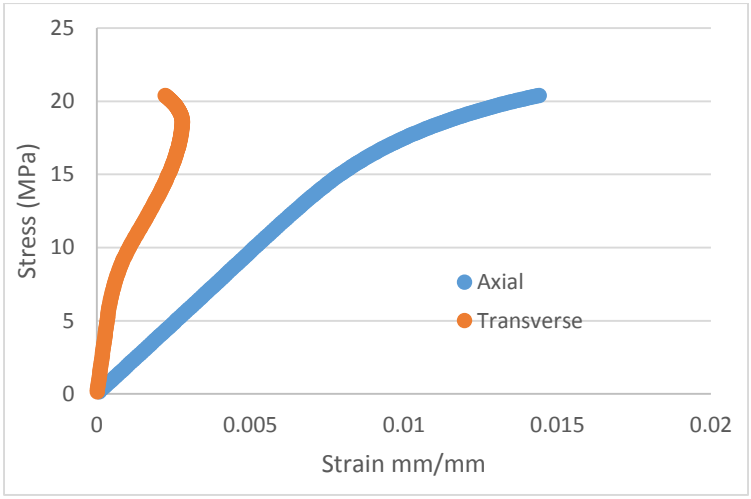

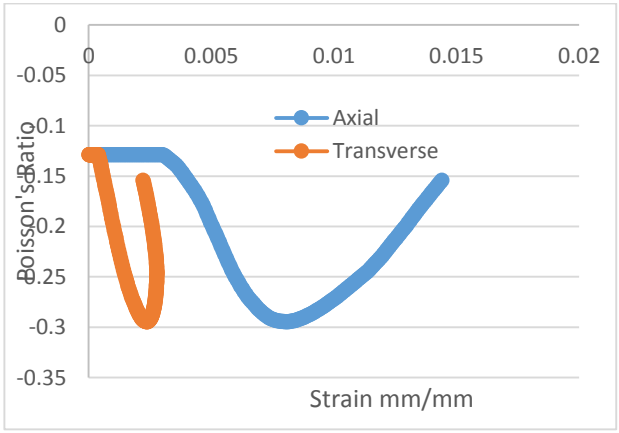

Mechanical Property	Value
Poisson's Ratio	-0.129
Young's Modulus (MPa)	1938
Ultimate Tensile Strength (MPa)	20.5
0.2% Yield Strength (MPa)	18.92

Model 11

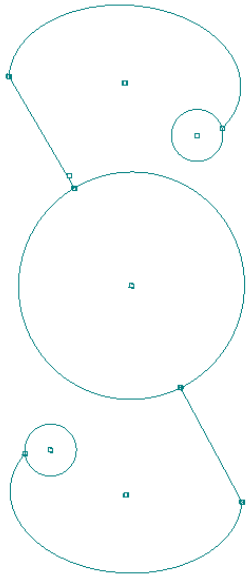

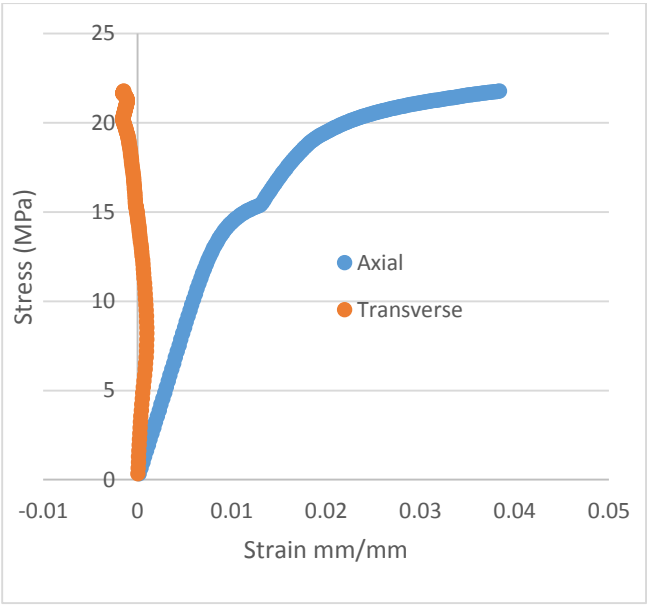

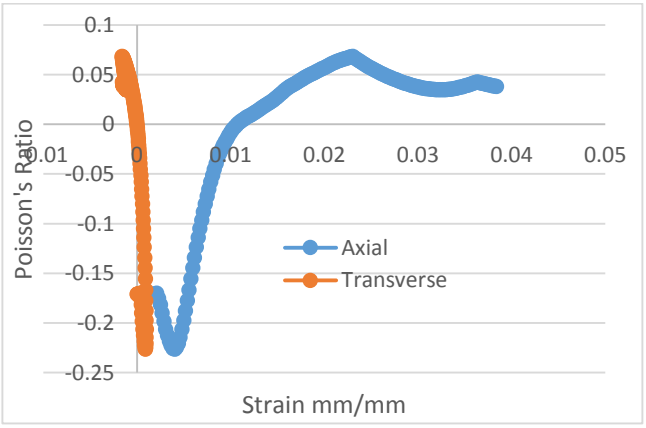

Mechanical Property	Value
Poisson's Ratio	-0.171
Young's Modulus (MPa)	1684
Ultimate Tensile Strength (MPa)	21.8
0.2% Yield Strength (MPa)	14.8

Model 12

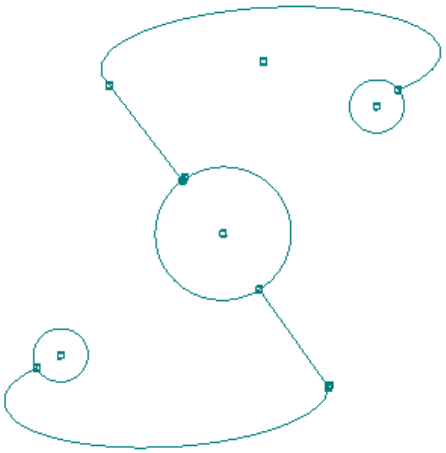

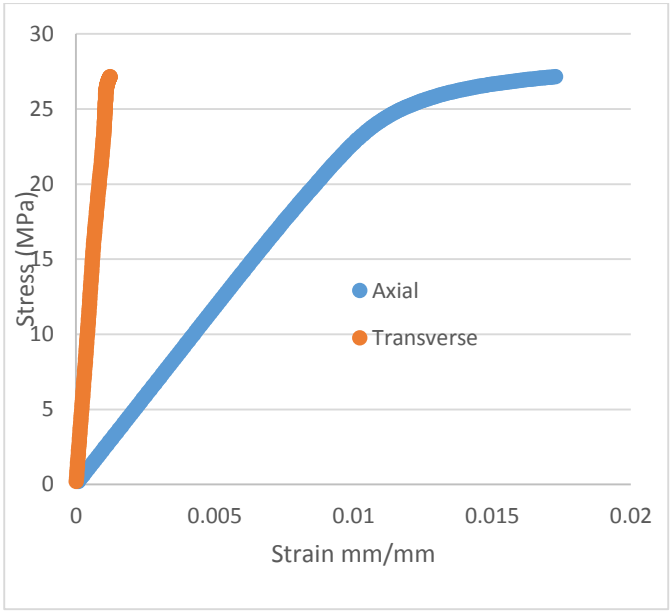

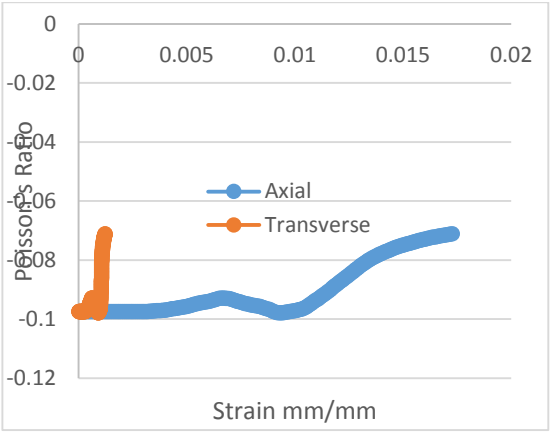

Mechanical Property	Value
Poisson's Ratio	-0.097
Young's Modulus (MPa)	2357
Ultimate Tensile Strength (MPa)	27.15
0.2% Yield Strength (MPa)	25.8

Model 13

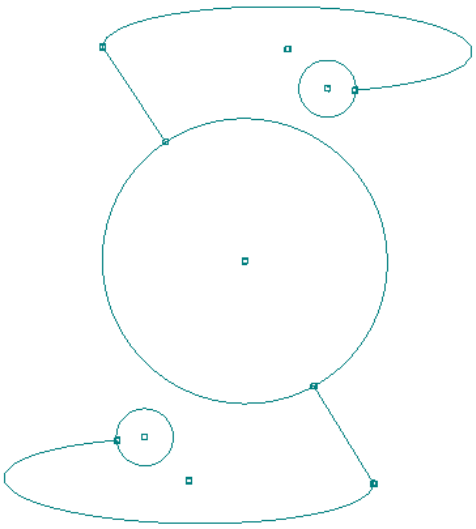

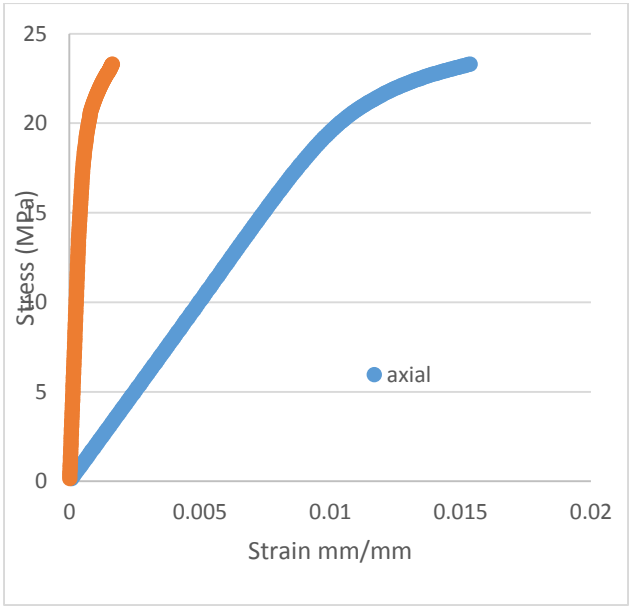

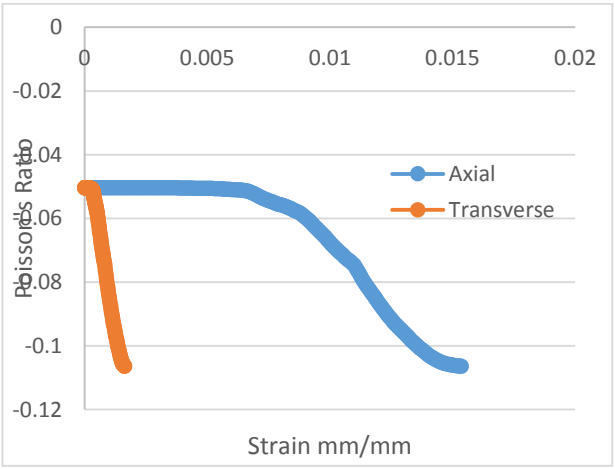

Mechanical Property	Value
Poisson's Ratio	-0.05
Young's Modulus (MPa)	2005
Ultimate Tensile Strength (MPa)	23.05
0.2% Yield Strength (MPa)	22.32

Model 14

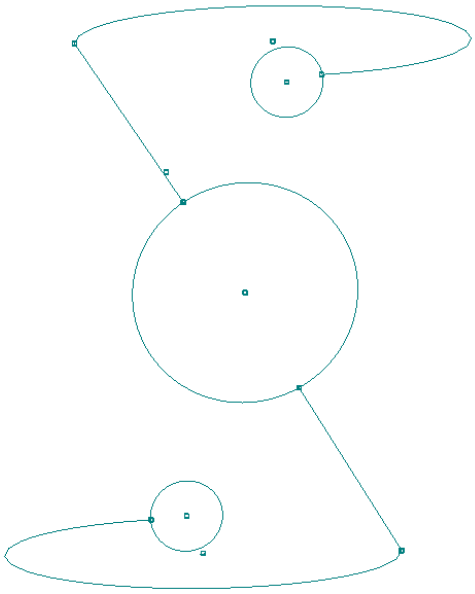

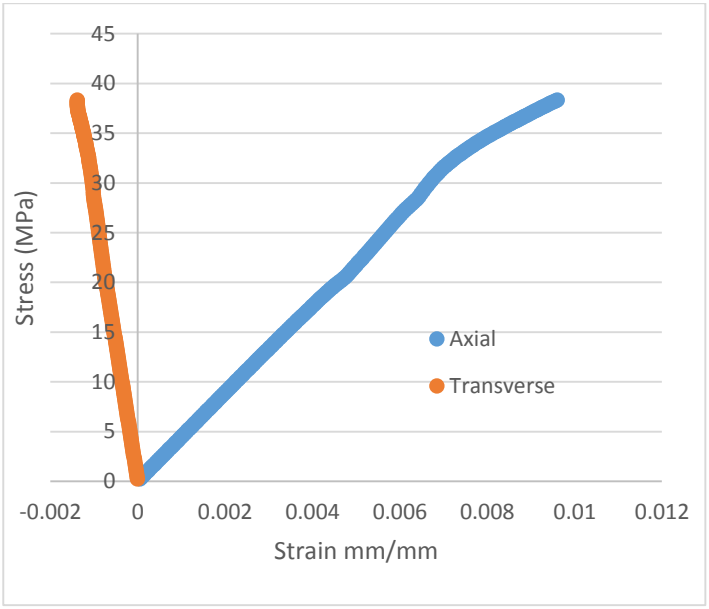

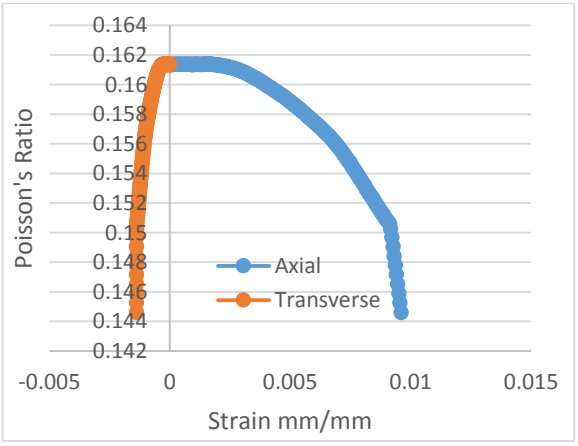

Mechanical Property	Value
Poisson's Ratio	0.161
Young's Modulus (MPa)	4460
Ultimate Tensile Strength (MPa)	41
0.2% Yield Strength (MPa)	40

Model 15

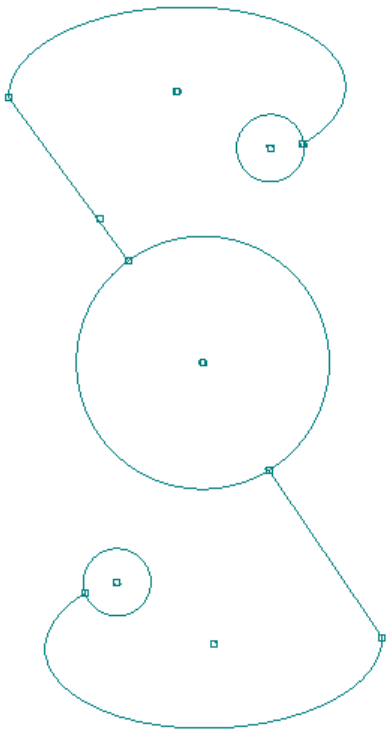

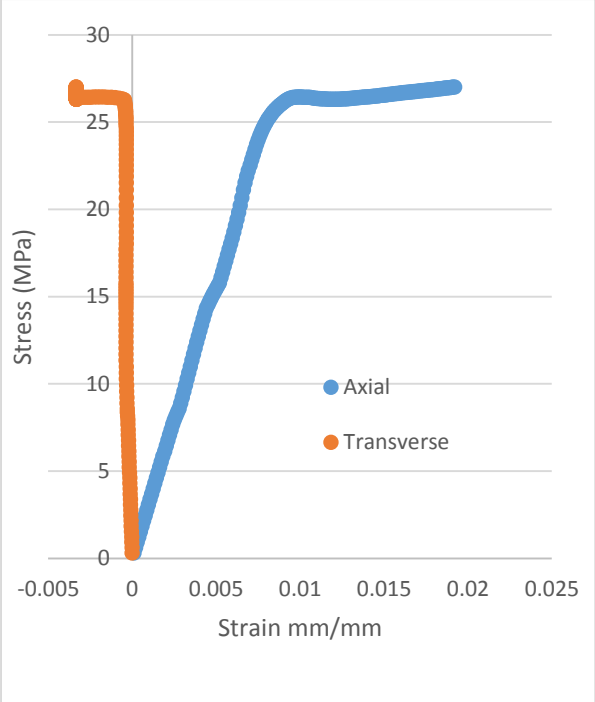

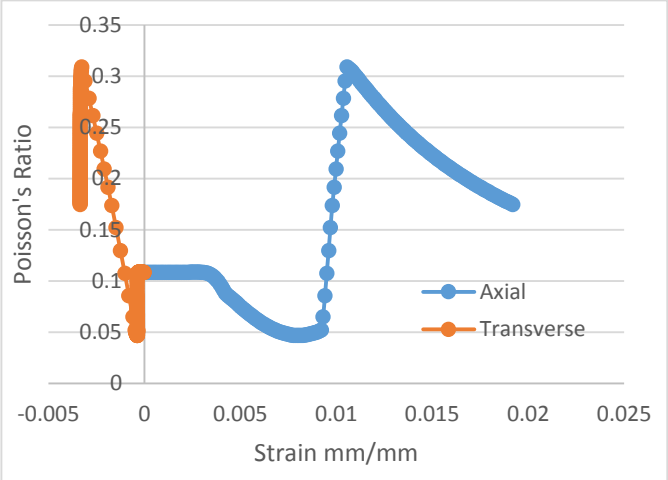

Mechanical Property	Value
Poisson's Ratio	0.108
Young's Modulus (MPa)	3198
Ultimate Tensile Strength (MPa)	27
0.2% Yield Strength (MPa)	26.42

Model 16

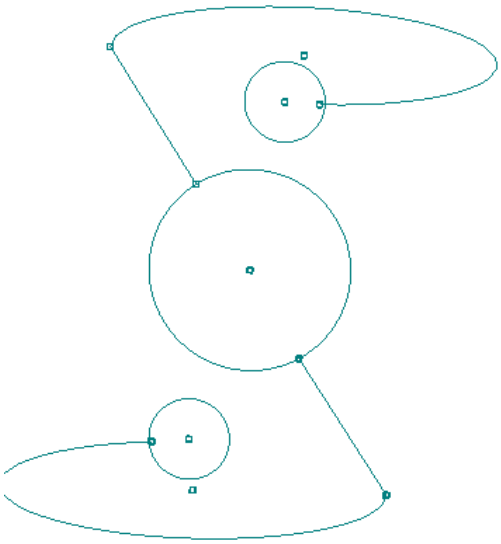

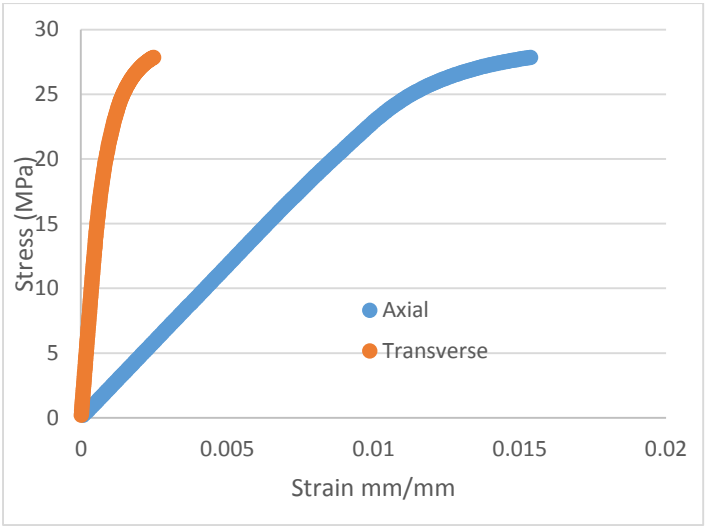

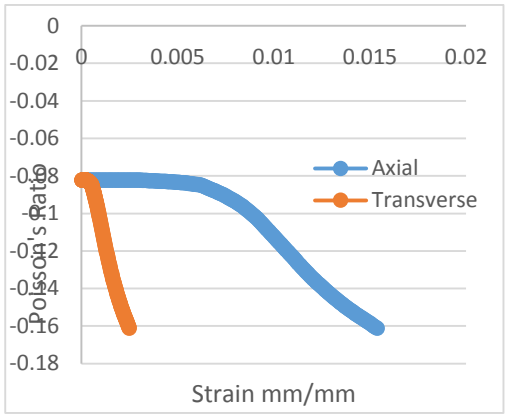

Mechanical Property	Value
Poisson's Ratio	-0.082
Young's Modulus (MPa)	2352
Ultimate Tensile Strength (MPa)	28
0.2% Yield Strength (MPa)	26.97

Model 17

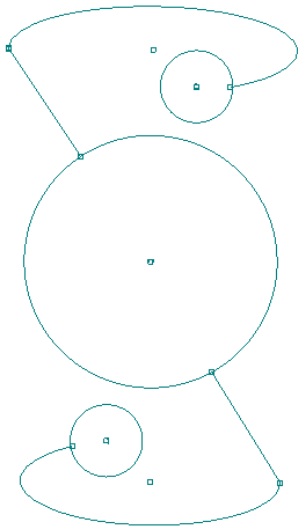

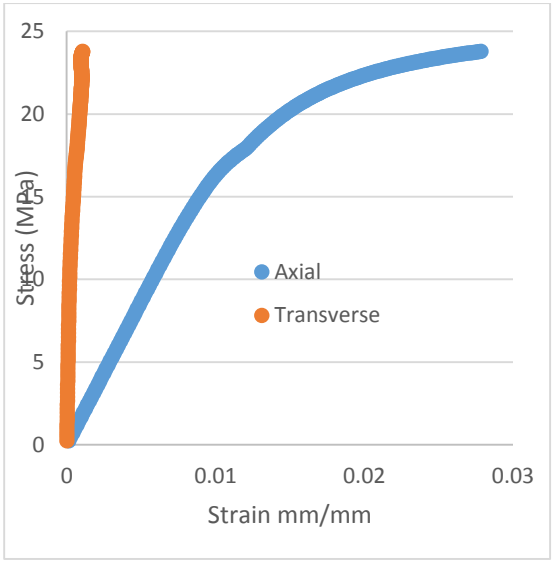

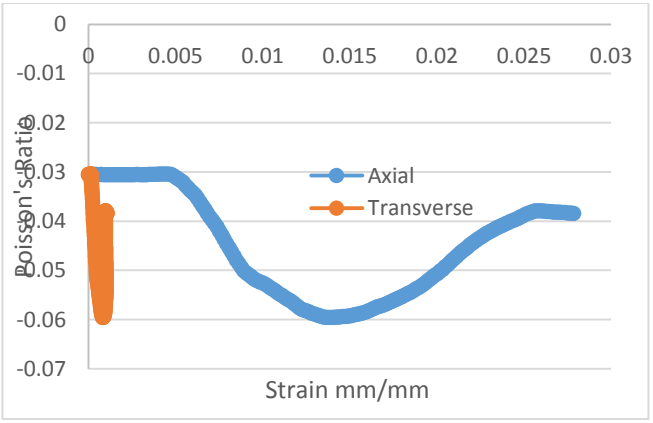

Mechanical Property	Value
Poisson's Ratio	-0.03
Young's Modulus (MPa)	1731
Ultimate Tensile Strength (MPa)	24
0.2% Yield Strength (MPa)	18.5

Model 18

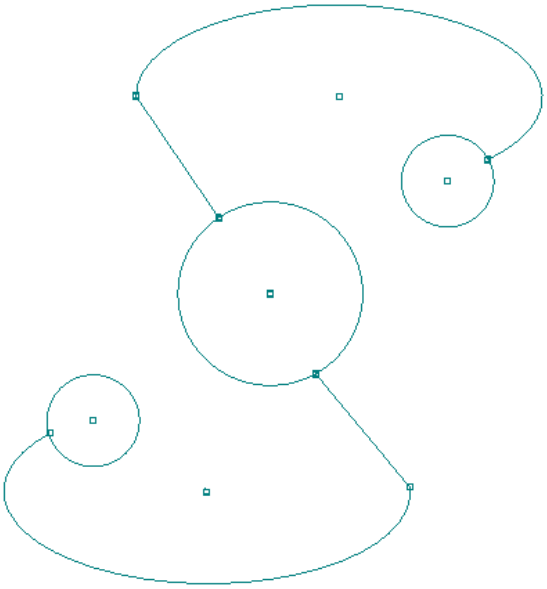

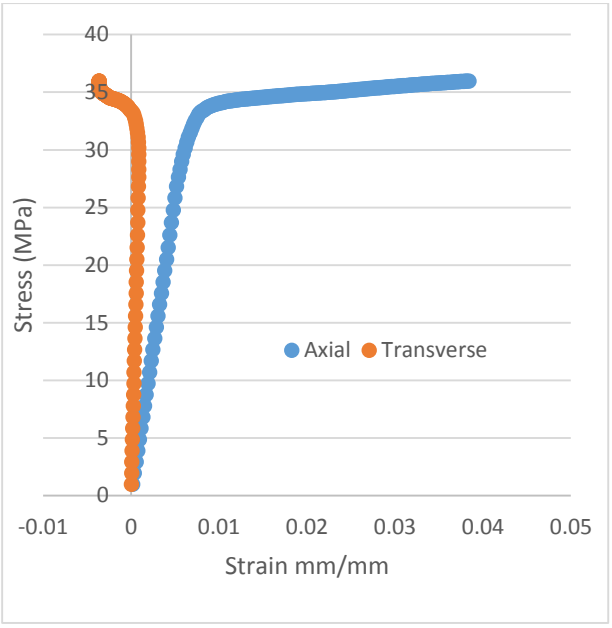

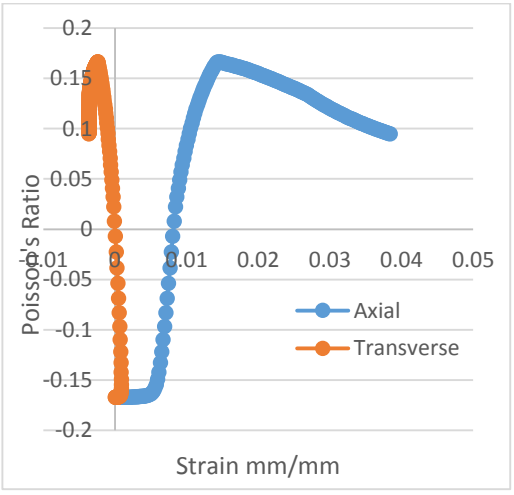

Mechanical Property	Value
Poisson's Ratio	-0.167
Young's Modulus (MPa)	5066
Ultimate Tensile Strength (MPa)	36
0.2% Yield Strength (MPa)	33.67

Model 19

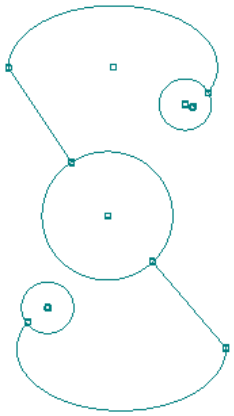

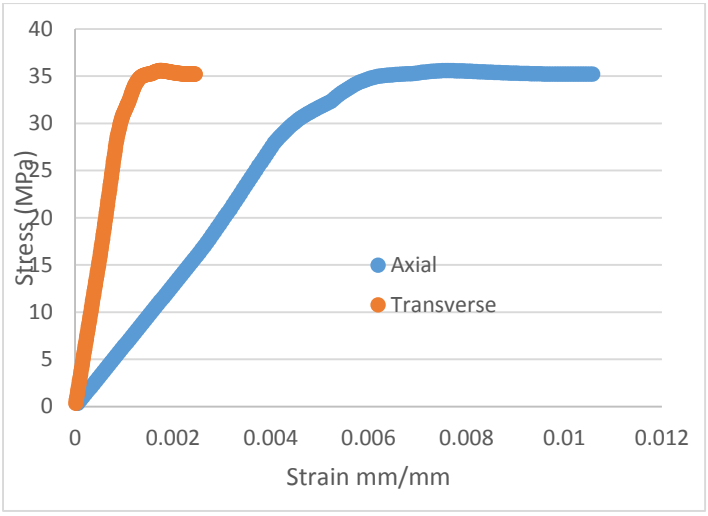

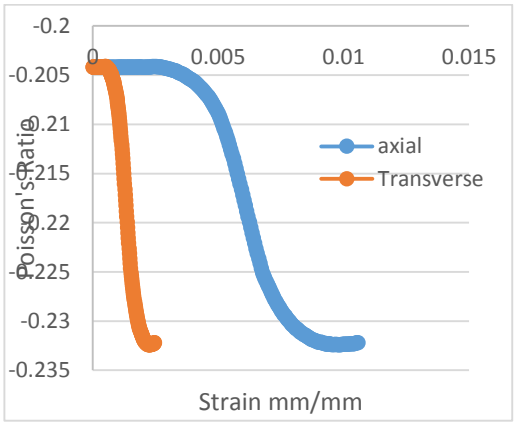

Mechanical Property	Value
Poisson's Ratio	-0.204
Young's Modulus (MPa)	6419
Ultimate Tensile Strength (MPa)	45.5
0.2% Yield Strength (MPa)	35.57

Model 20

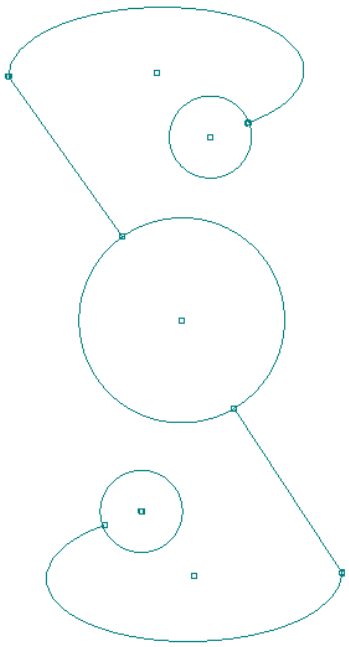

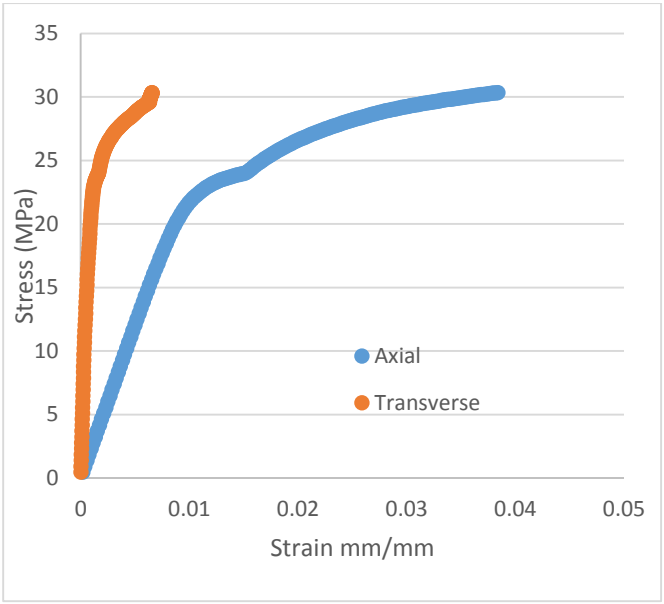

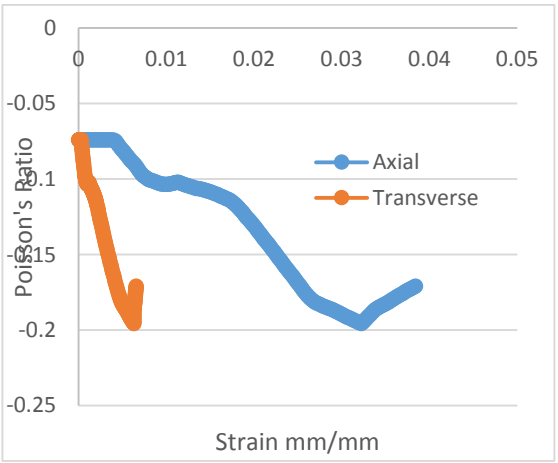

Mechanical Property	Value
Poisson's Ratio	-0.0754
Young's Modulus (MPa)	2413
Ultimate Tensile Strength (MPa)	30.4
0.2% Yield Strength (MPa)	22.8

Model 21

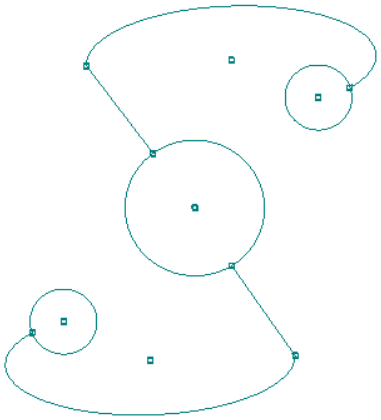

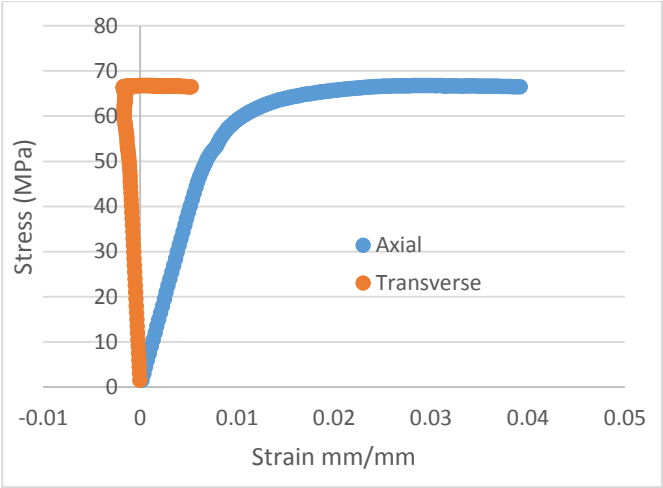

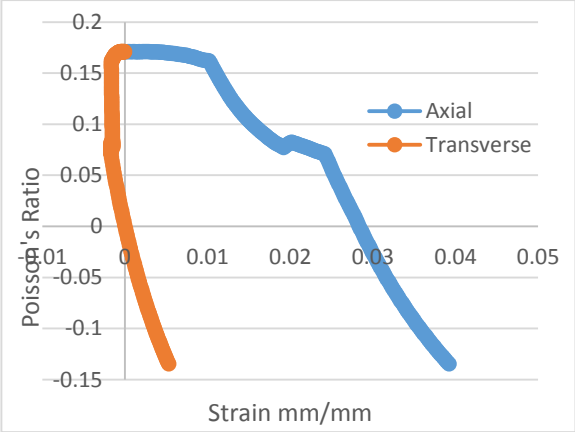

Mechanical Property	Value
Poisson's Ratio	0.171
Young's Modulus (MPa)	7798
Ultimate Tensile Strength (MPa)	66.7
0.2% Yield Strength (MPa)	58

Model 22

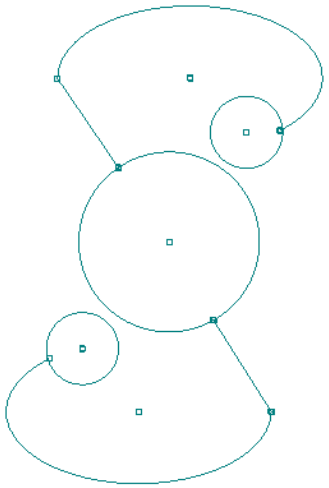

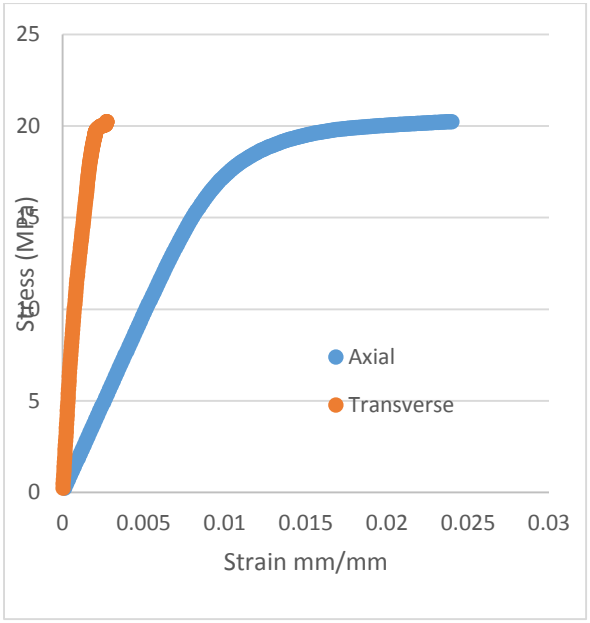

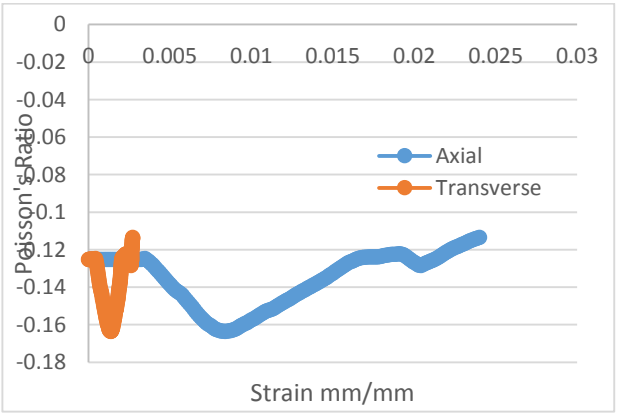

Mechanical Property	Value
Poisson's Ratio	-0.125
Young's Modulus (MPa)	1950
Ultimate Tensile Strength (MPa)	20.25
0.2% Yield Strength (MPa)	18.23

Model 23

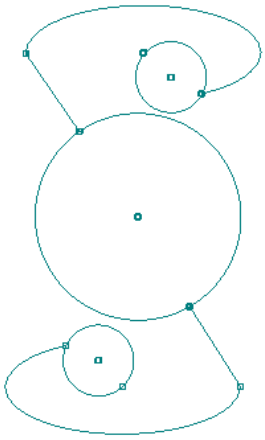

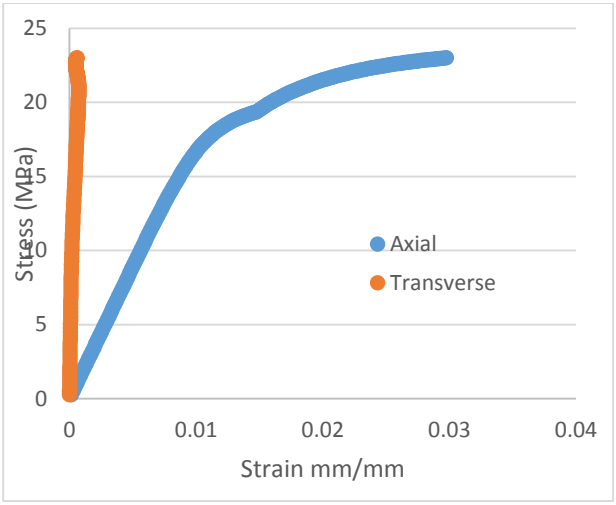

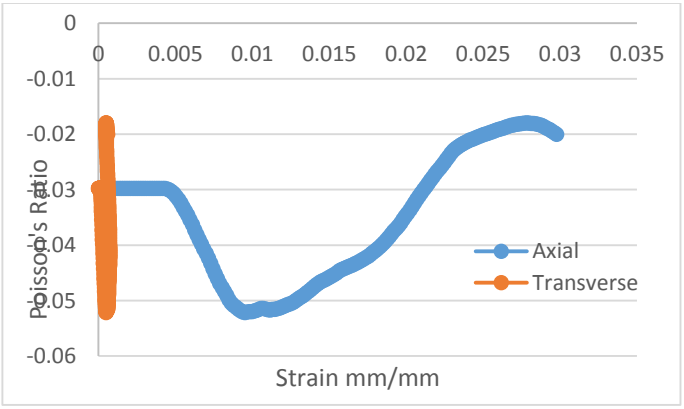

Mechanical Property	Value
Poisson's Ratio	-0.029
Young's Modulus (MPa)	1780
Ultimate Tensile Strength (MPa)	23
0.2% Yield Strength (MPa)	21.9

Model 24

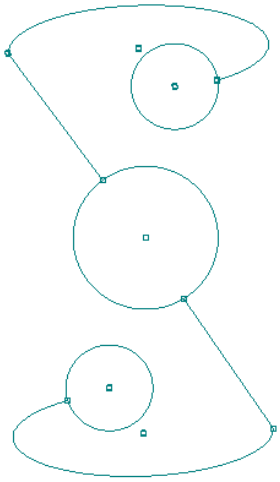

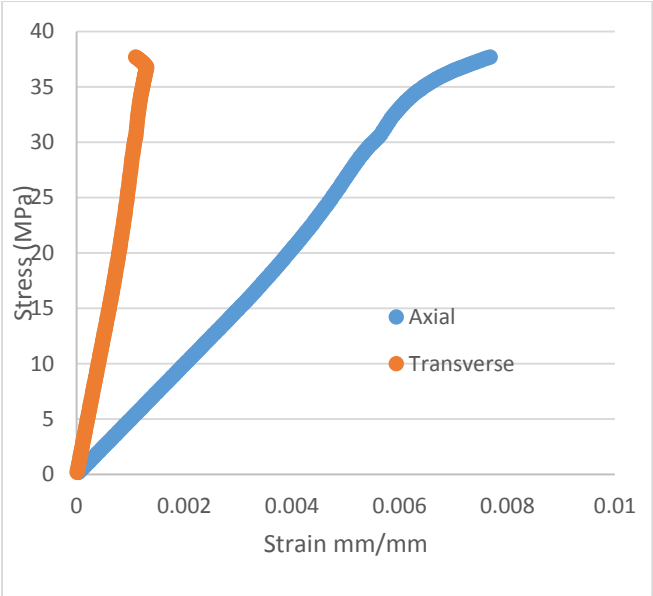

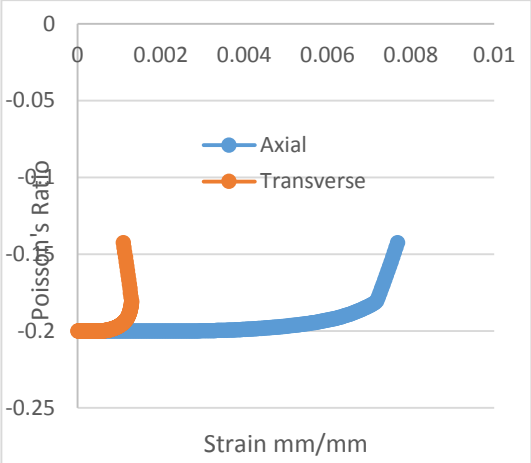

Mechanical Property	Value
Poisson's Ratio	-0.199
Young's Modulus (MPa)	4969
Ultimate Tensile Strength (MPa)	39
0.2% Yield Strength (MPa)	38.5

Model 25

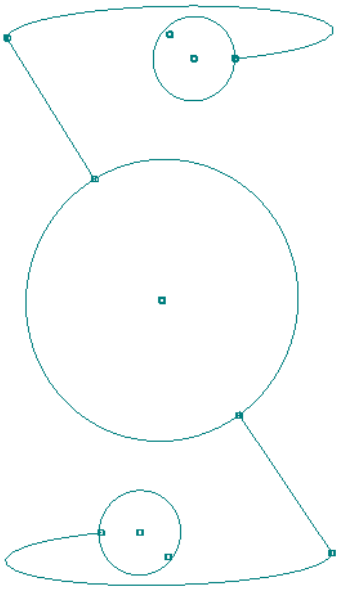

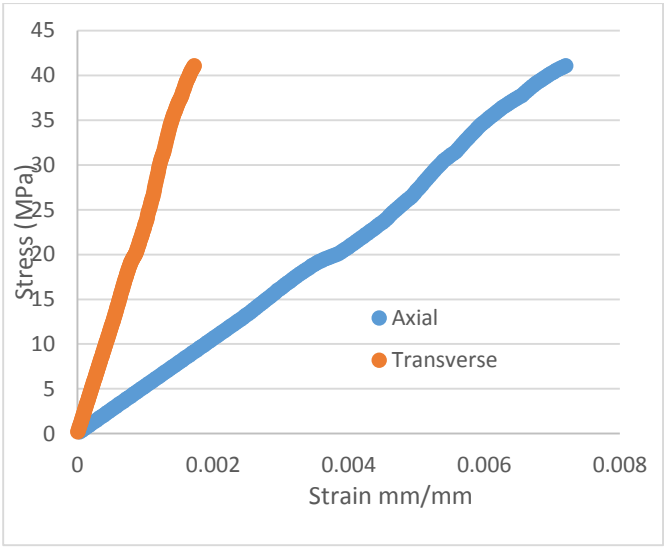

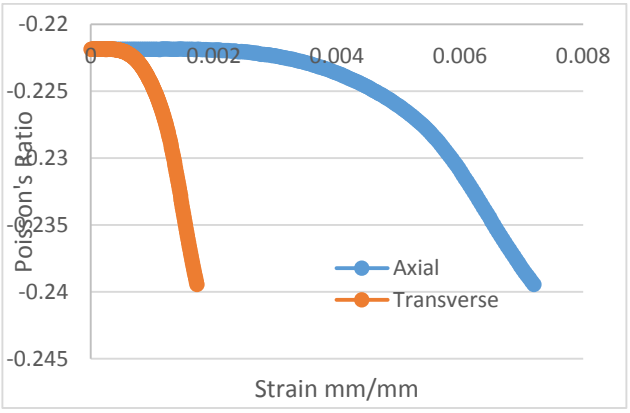

Mechanical Property	Value
Poisson's Ratio	-0.222
Young's Modulus (MPa)	5304
Ultimate Tensile Strength (MPa)	53
0.2% Yield Strength (MPa)	50

Model 26

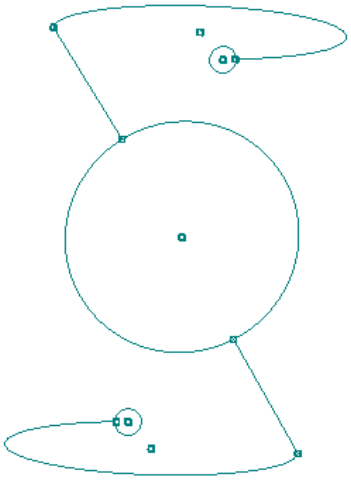

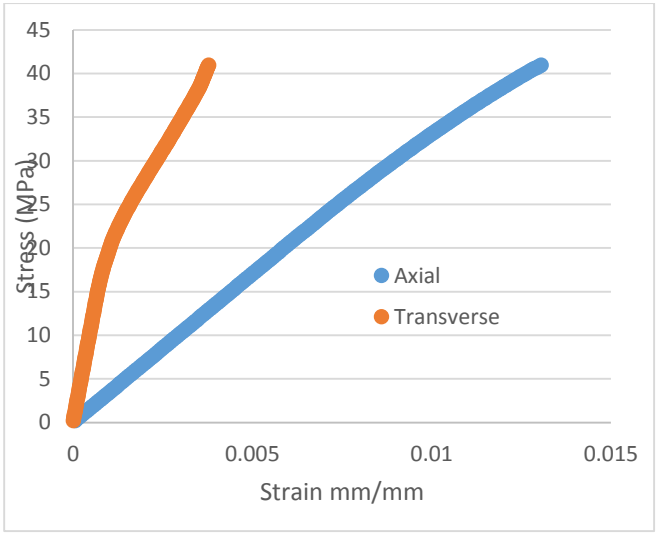

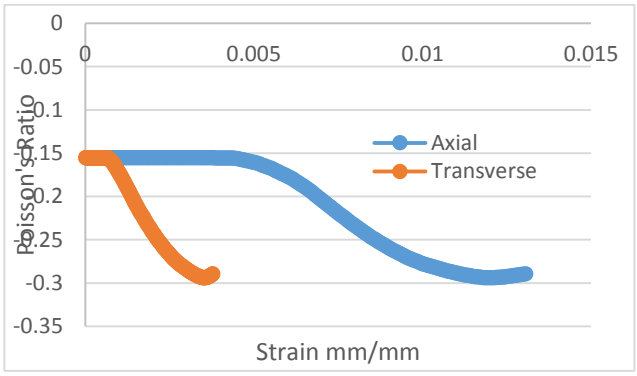

Mechanical Property	Value
Poisson's Ratio	-0.155
Young's Modulus (MPa)	3402
Ultimate Tensile Strength (MPa)	42.5
0.2% Yield Strength (MPa)	42

Model 27

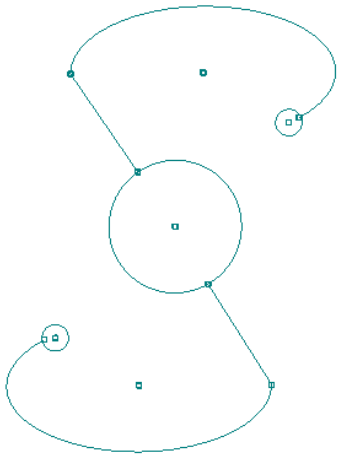

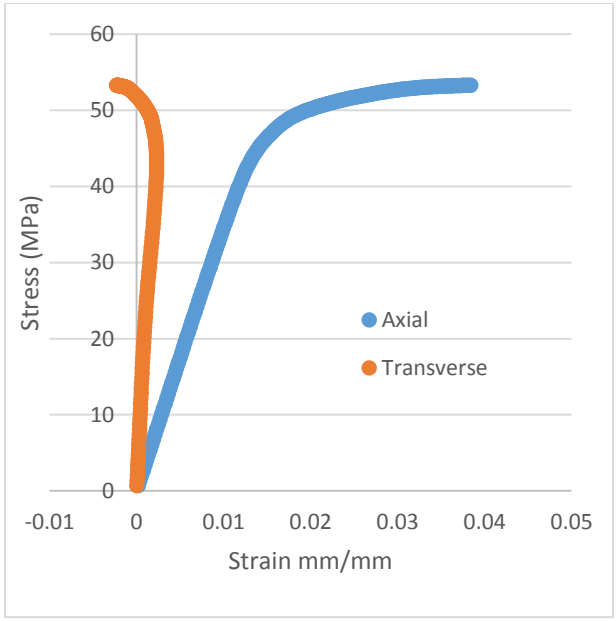

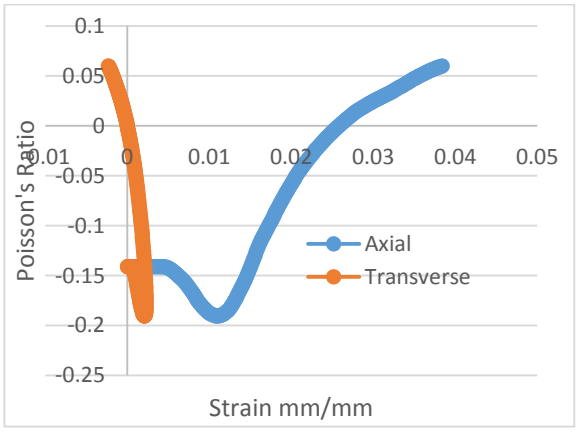

Mechanical Property	Value
Poisson's Ratio	-0.141
Young's Modulus (MPa)	3503
Ultimate Tensile Strength (MPa)	53.5
0.2% Yield Strength (MPa)	36.9

Model 28

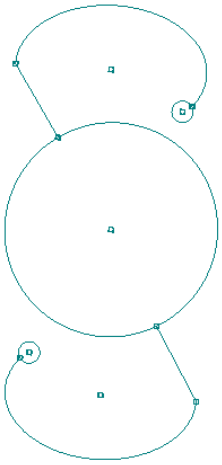

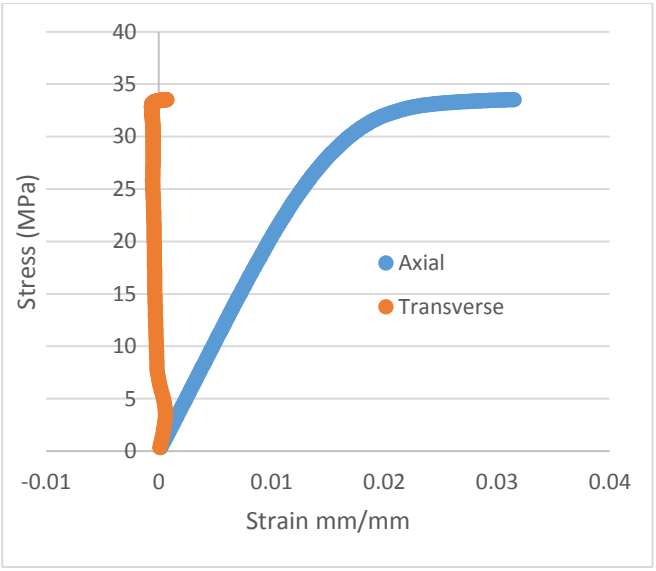

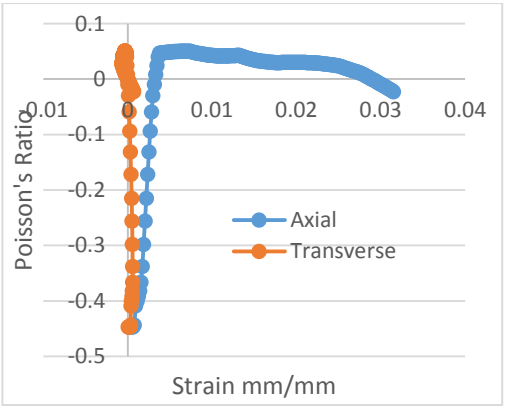

Mechanical Property	Value
Poisson's Ratio	-0.447
Young's Modulus (MPa)	2068
Ultimate Tensile Strength (MPa)	33.5
0.2% Yield Strength (MPa)	29.4

Model 29

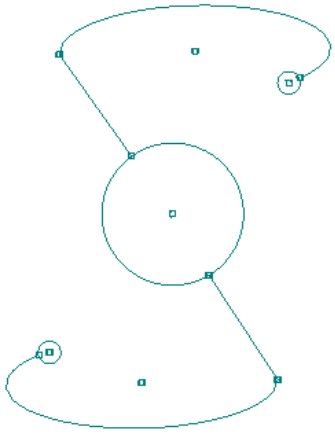

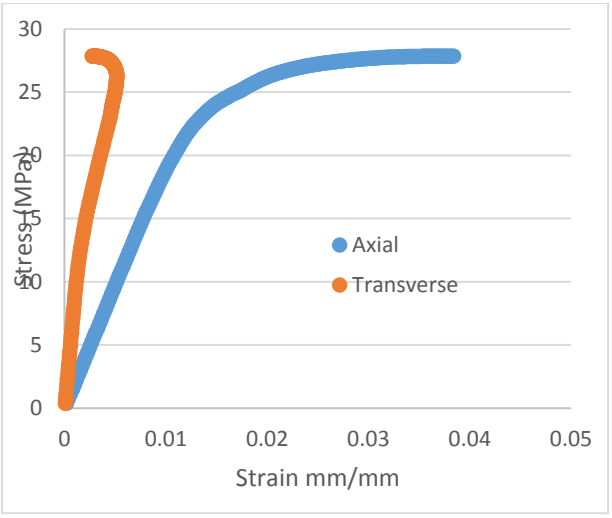

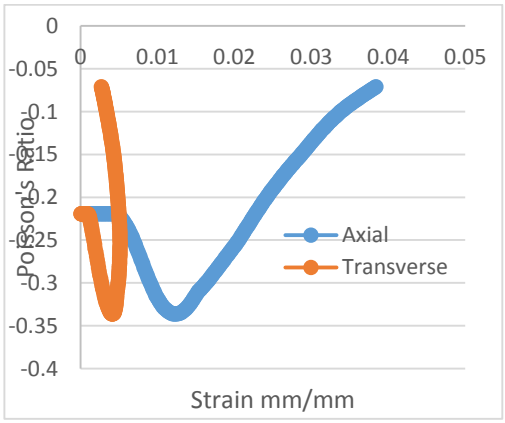

Mechanical Property	Value
Poisson's Ratio	-0.219
Young's Modulus (MPa)	1947
Ultimate Tensile Strength (MPa)	27.85
0.2% Yield Strength (MPa)	23.5

Model 30

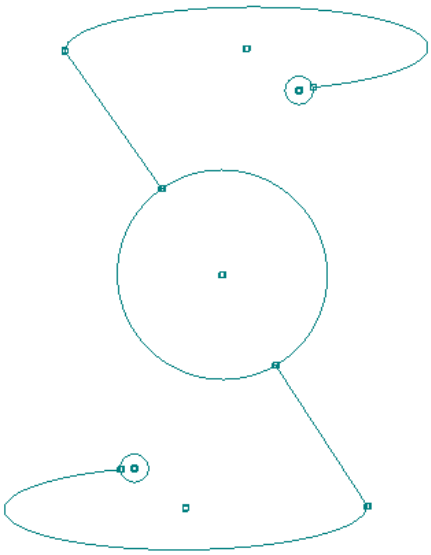

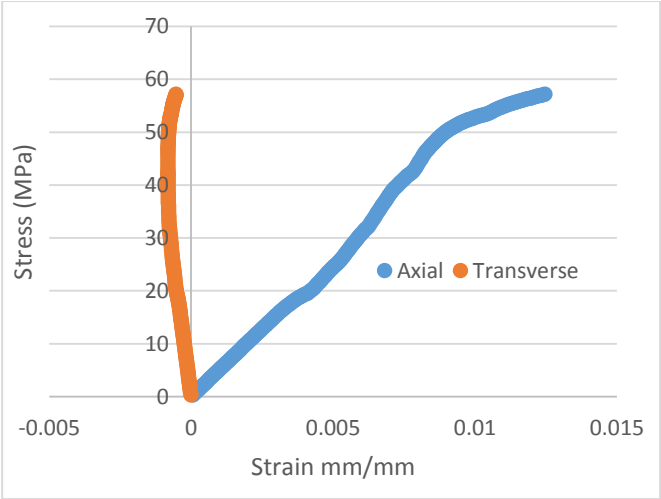

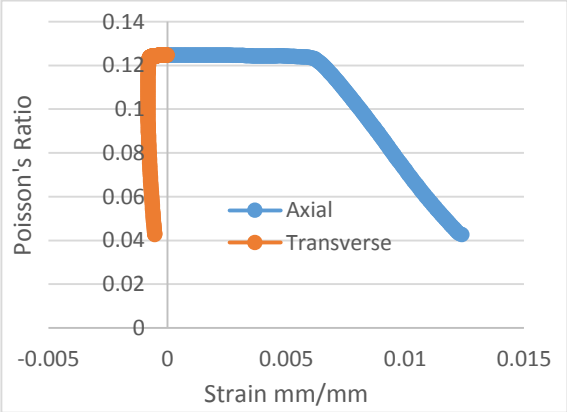

Mechanical Property	Value
Poisson's Ratio	0.124
Young's Modulus (MPa)	5135
Ultimate Tensile Strength (MPa)	57
0.2% Yield Strength (MPa)	56.5

Model 31

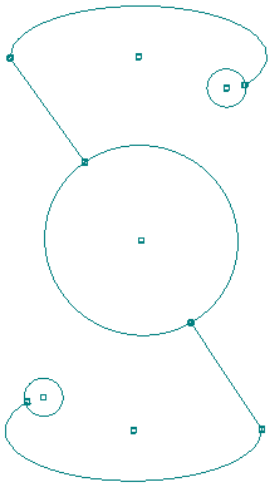

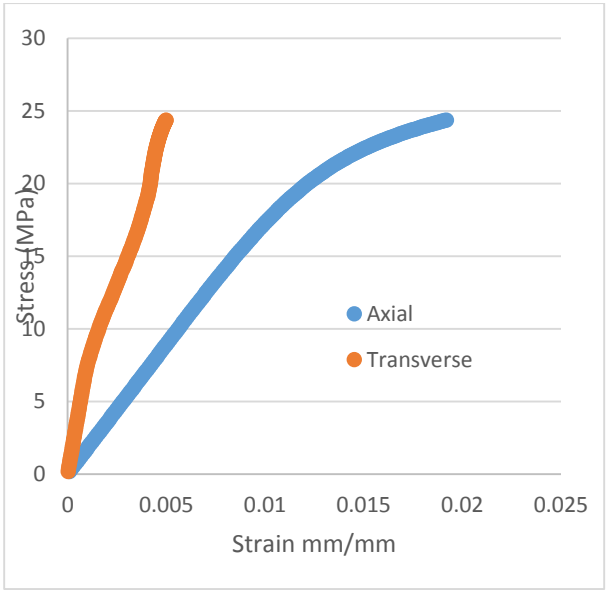

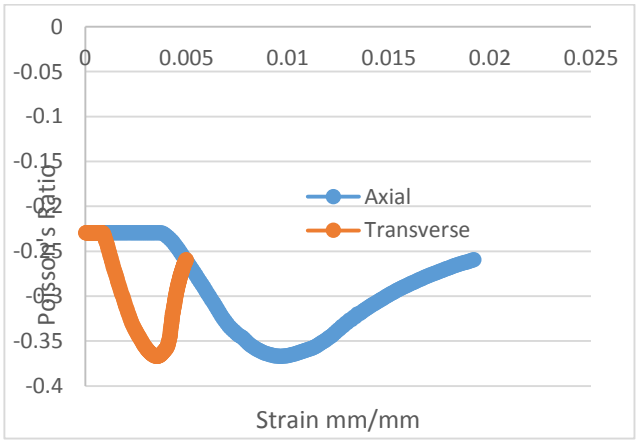

Mechanical Property	Value
Poisson's Ratio	-0.229
Young's Modulus (MPa)	1780
Ultimate Tensile Strength (MPa)	24.2
0.2% Yield Strength (MPa)	21.9

Model 32

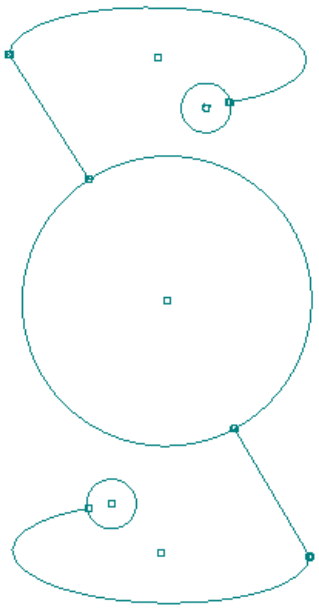

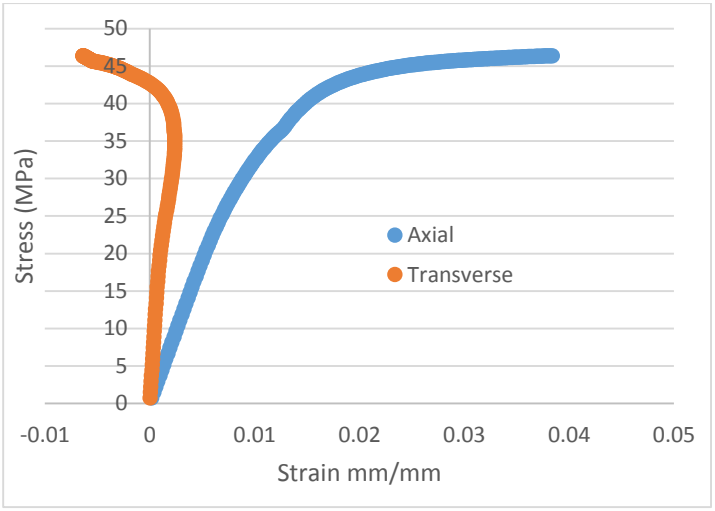

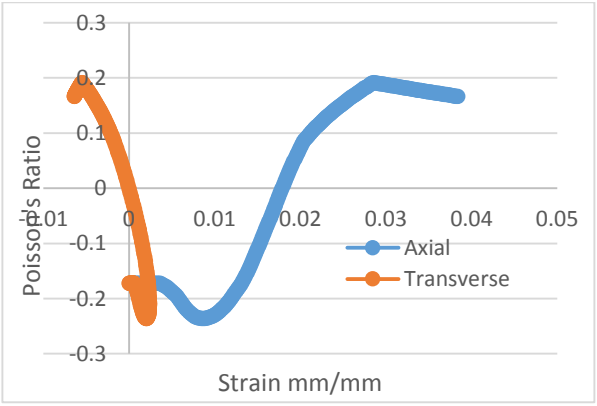

Mechanical Property	Value
Poisson's Ratio	-0.172
Young's Modulus (MPa)	3858
Ultimate Tensile Strength (MPa)	46.4
0.2% Yield Strength (MPa)	33.9

Model 33

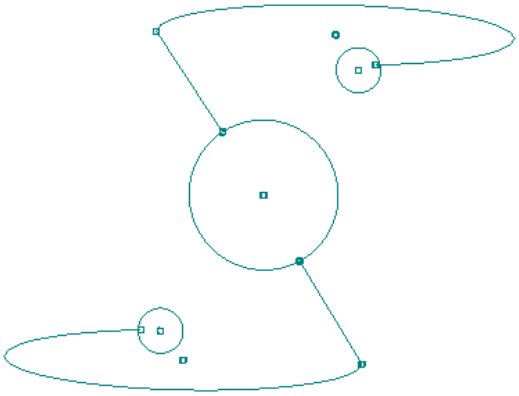

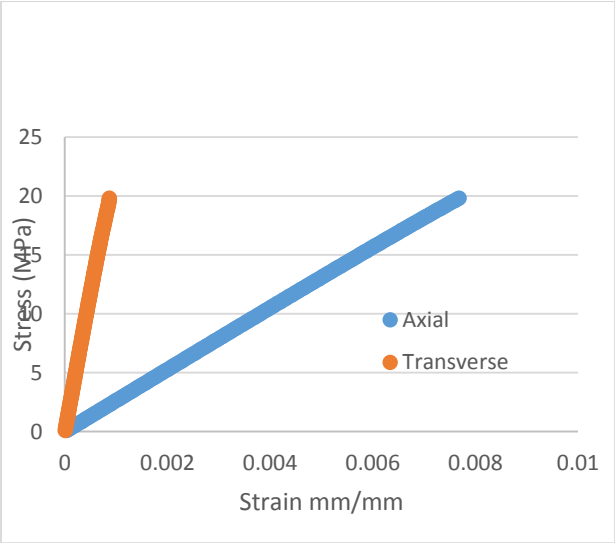

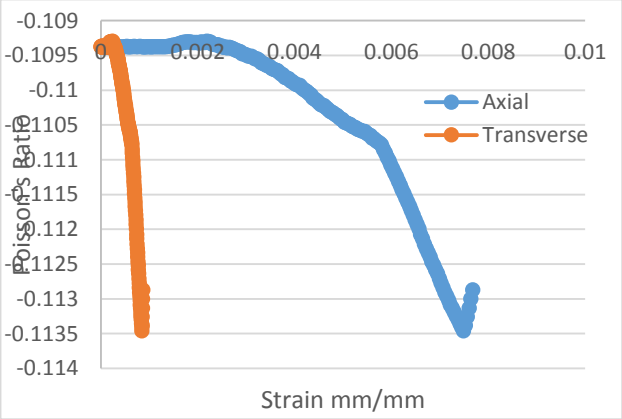

Mechanical Property	Value
Poisson's Ratio	-0.109
Young's Modulus (MPa)	2634
Ultimate Tensile Strength (MPa)	30
0.2% Yield Strength (MPa)	27

Model 34

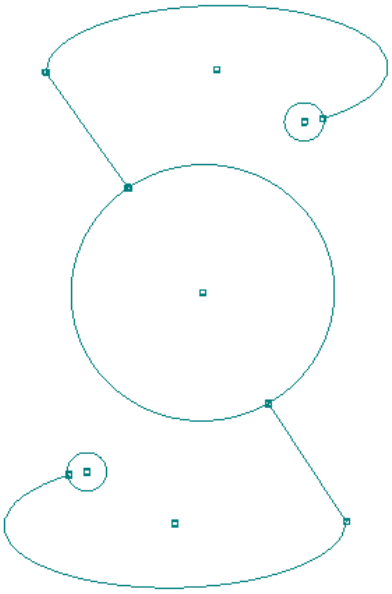

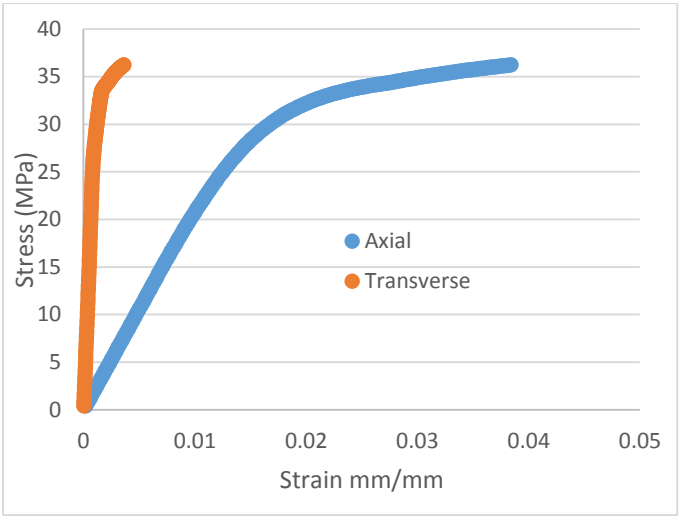

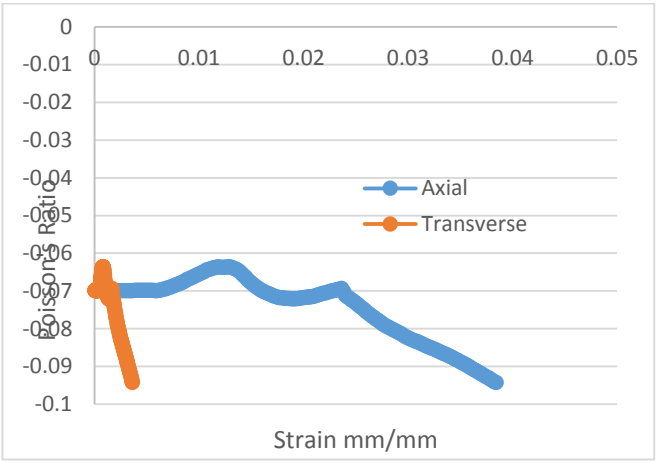

Mechanical Property	Value
Poisson's Ratio	-0.0698
Young's Modulus (MPa)	2118
Ultimate Tensile Strength (MPa)	36.5
0.2% Yield Strength (MPa)	28.8

Model 35

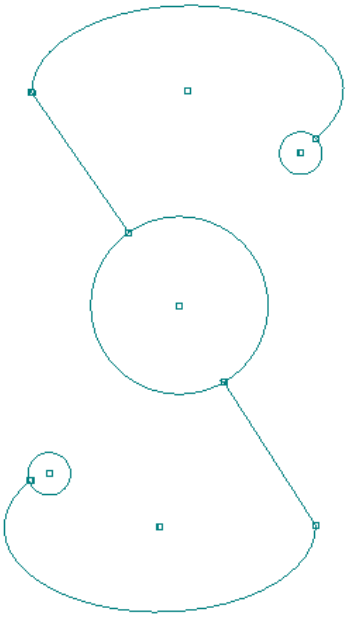

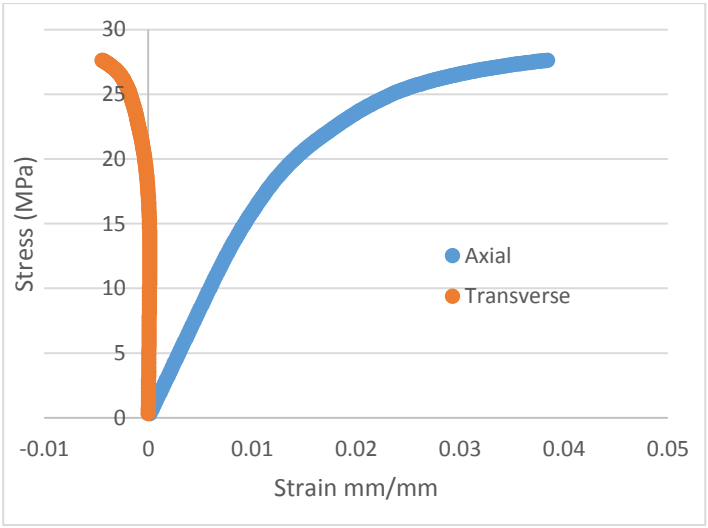

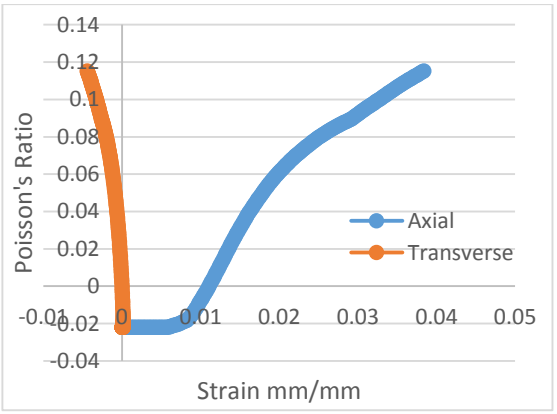

Mechanical Property	Value
Poisson's Ratio	-0.0219
Young's Modulus (MPa)	1687
Ultimate Tensile Strength (MPa)	28
0.2% Yield Strength (MPa)	19.7

Model 36

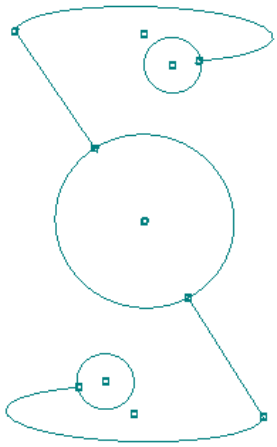

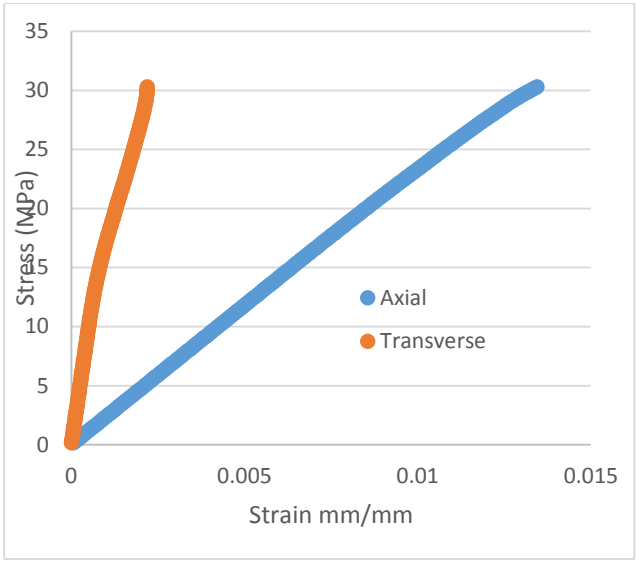

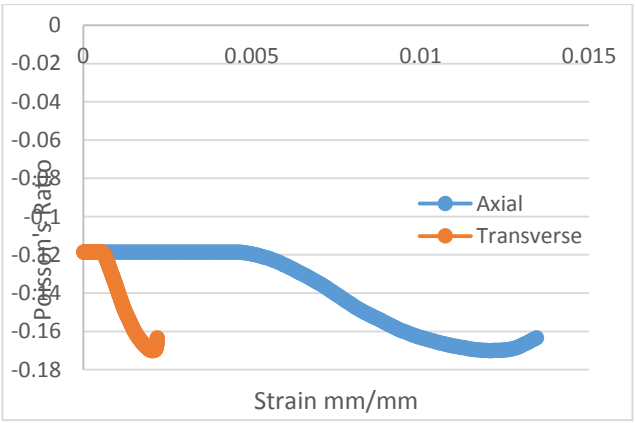

Mechanical Property	Value
Poisson's Ratio	-0.118
Young's Modulus (MPa)	2359
Ultimate Tensile Strength (MPa)	41
0.2% Yield Strength (MPa)	36.5

Model 37

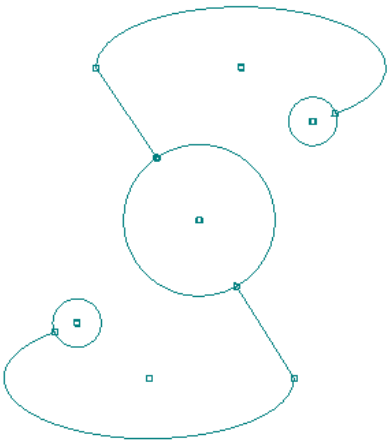

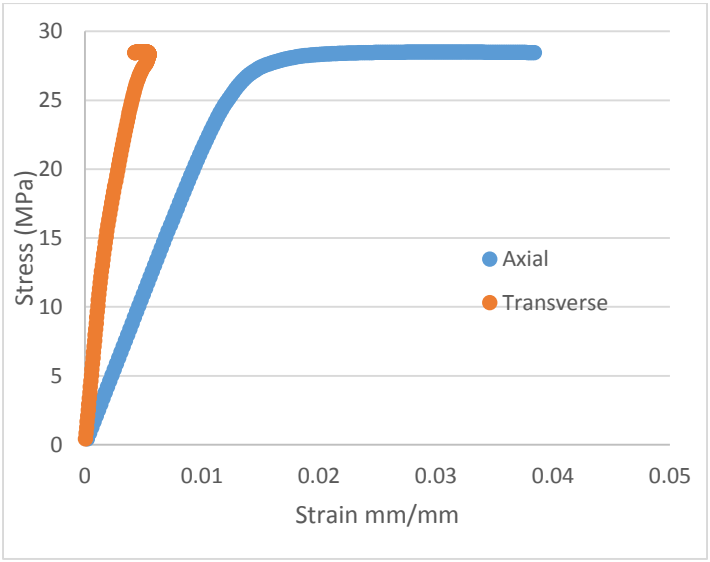

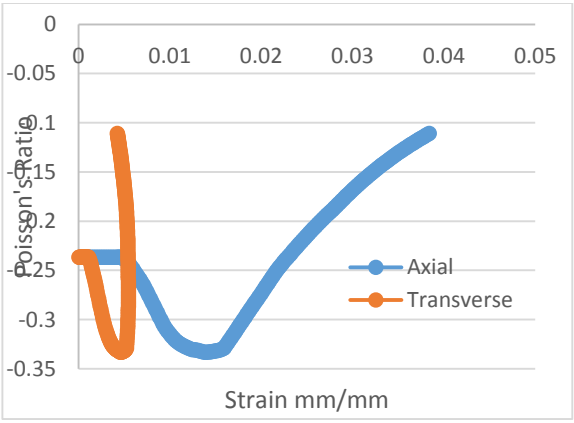

Mechanical Property	Value
Poisson's Ratio	-0.2366
Young's Modulus (MPa)	2185
Ultimate Tensile Strength (MPa)	28.5
0.2% Yield Strength (MPa)	27

Model 38

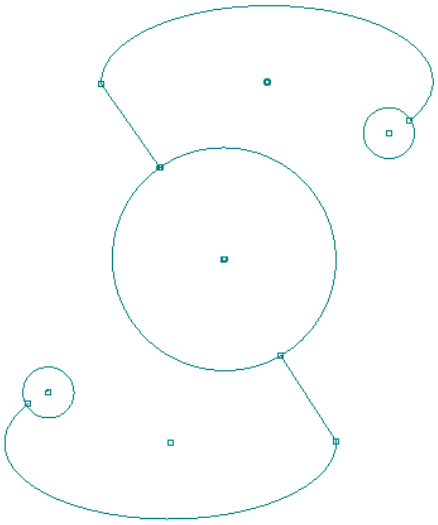

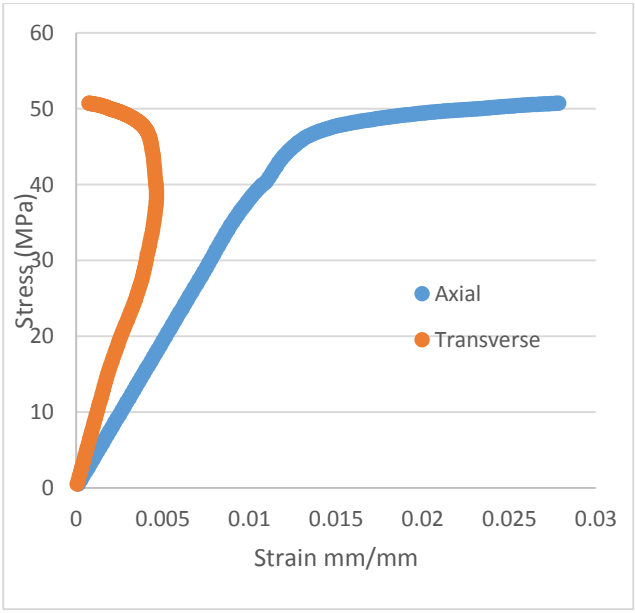

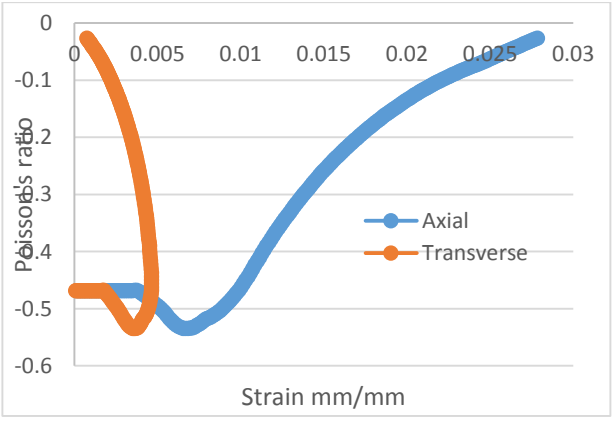

Mechanical Property	Value
Poisson's Ratio	-0.4685
Young's Modulus (MPa)	3868
Ultimate Tensile Strength (MPa)	51
0.2% Yield Strength (MPa)	47.17

Model 39

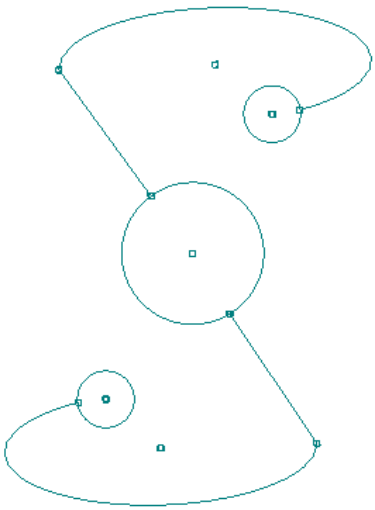

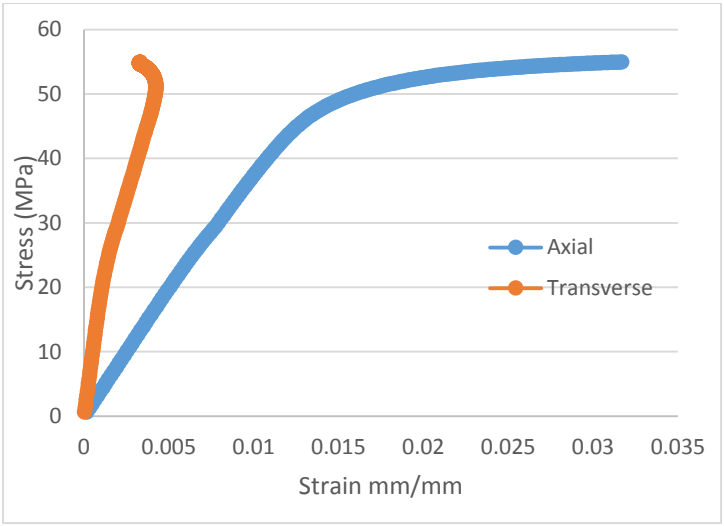

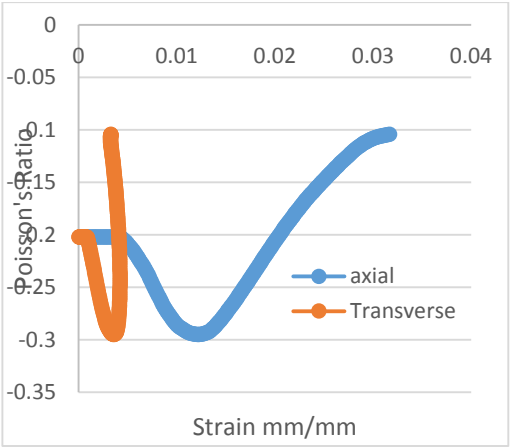

Mechanical Property	Value
Poisson's Ratio	-0.2022
Young's Modulus (MPa)	3988
Ultimate Tensile Strength (MPa)	55
0.2% Yield Strength (MPa)	47.65

Model 40

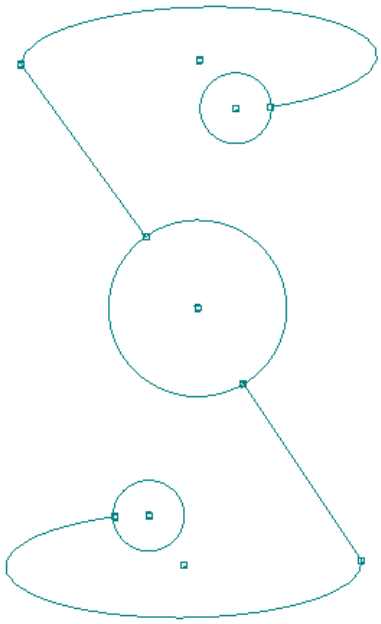

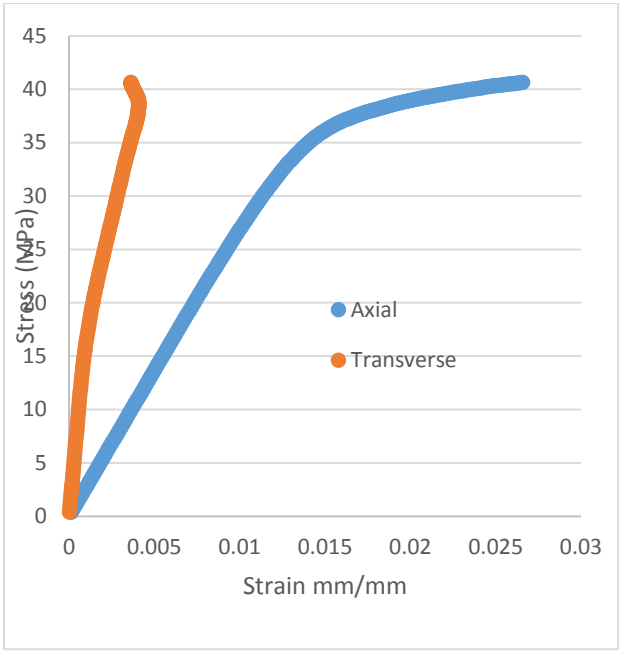

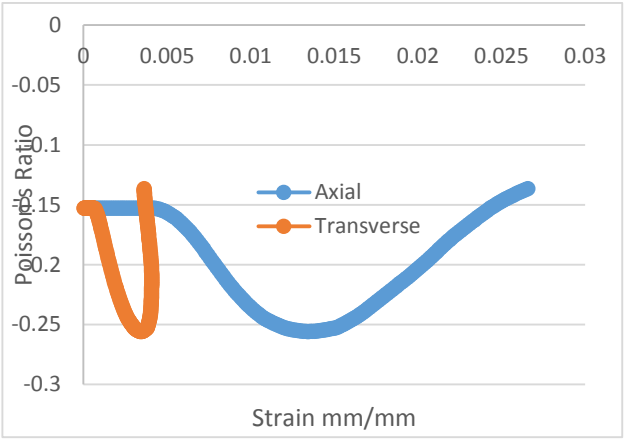

Mechanical Property	Value
Poisson's Ratio	-0.153
Young's Modulus (MPa)	2733
Ultimate Tensile Strength (MPa)	40.6
0.2% Yield Strength (MPa)	36.45

Model 41

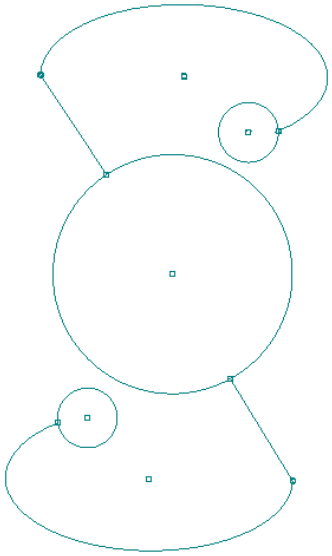

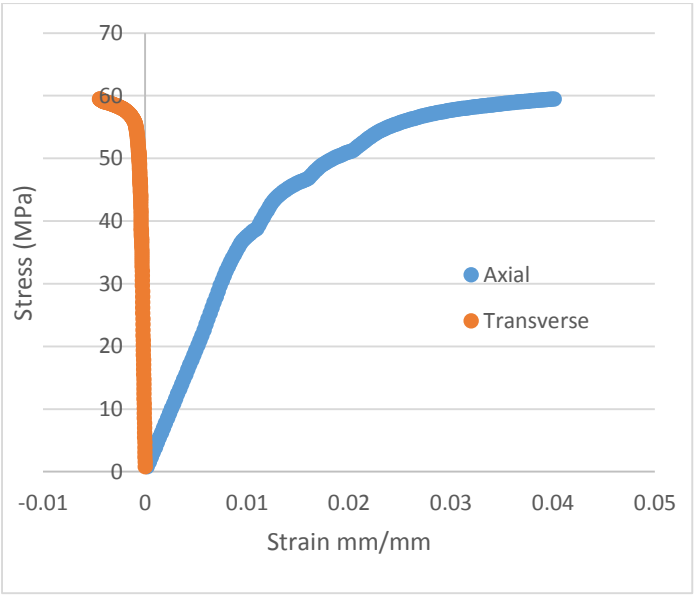

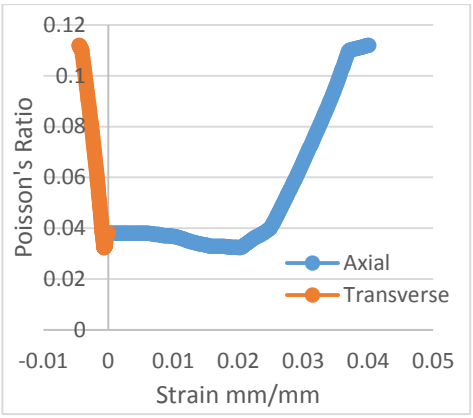

Mechanical Property	Value
Poisson's Ratio	0.0379
Young's Modulus (MPa)	4675
Ultimate Tensile Strength (MPa)	60
0.2% Yield Strength (MPa)	45.5

Model 42

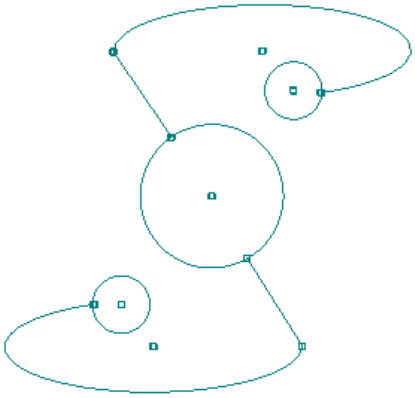

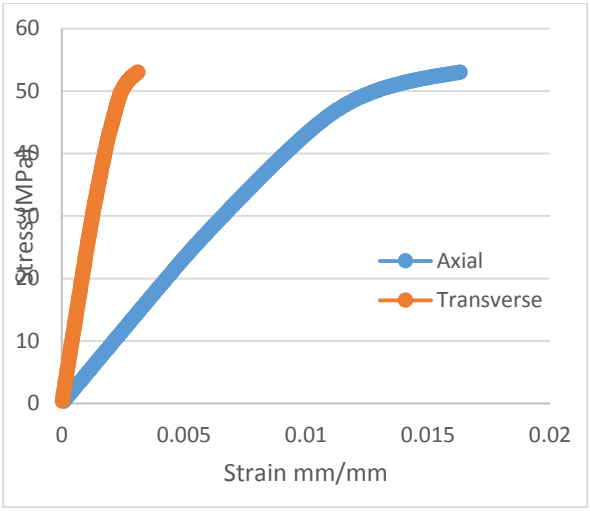

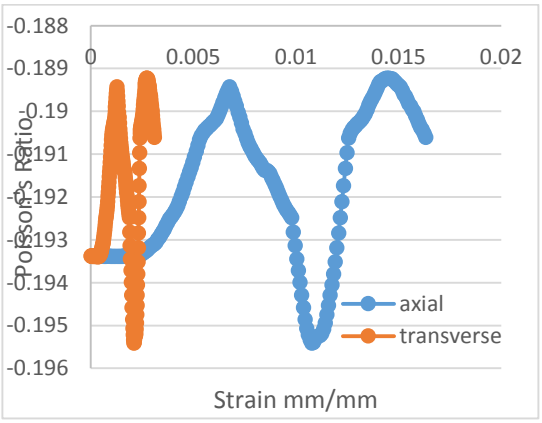

Mechanical Property	Value
Poisson's Ratio	-0.193
Young's Modulus (MPa)	4675
Ultimate Tensile Strength (MPa)	53
0.2% Yield Strength (MPa)	50

Model 43

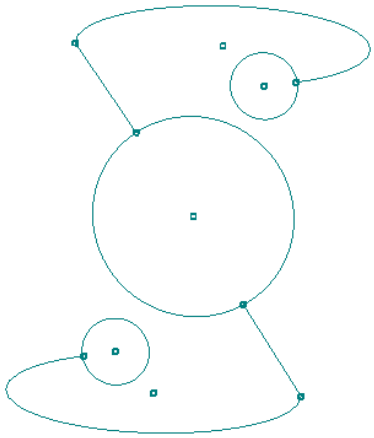

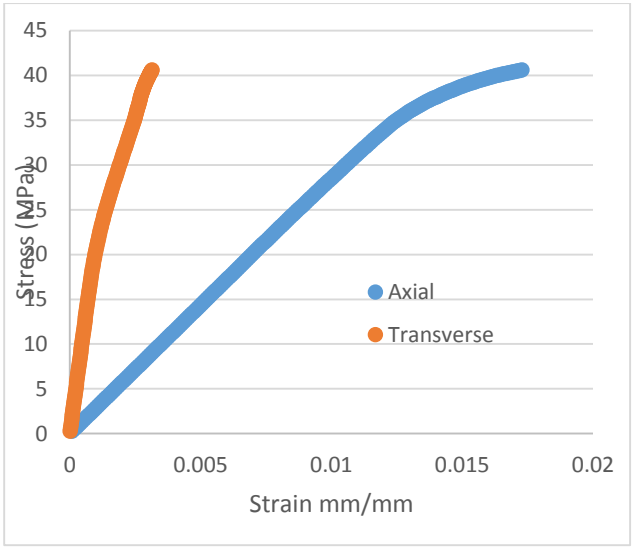

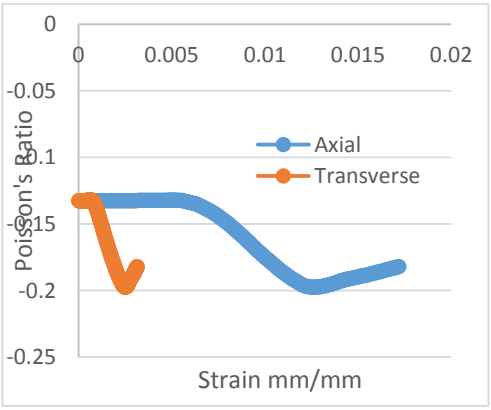

Mechanical Property	Value
Poisson's Ratio	-0.132
Young's Modulus (MPa)	2865
Ultimate Tensile Strength (MPa)	40.5
0.2% Yield Strength (MPa)	39.57

Model 44

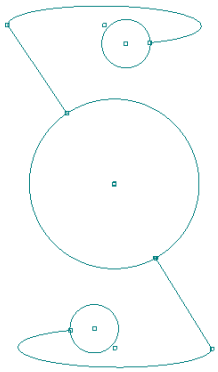

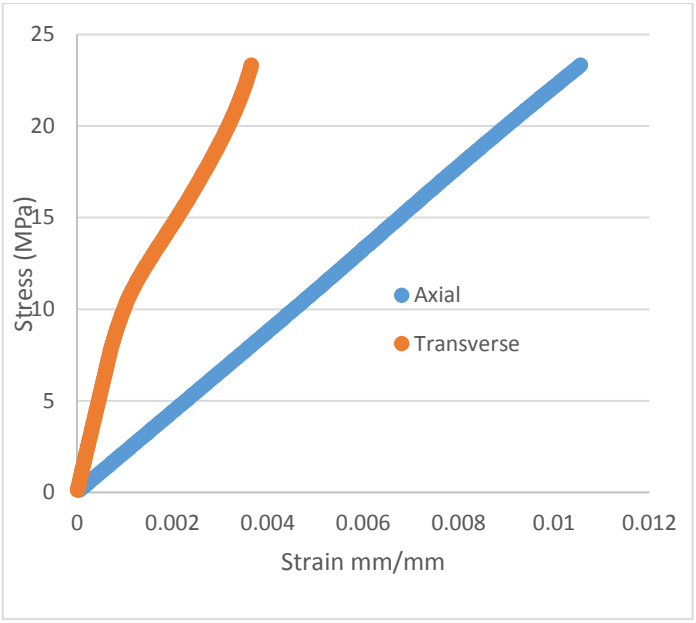

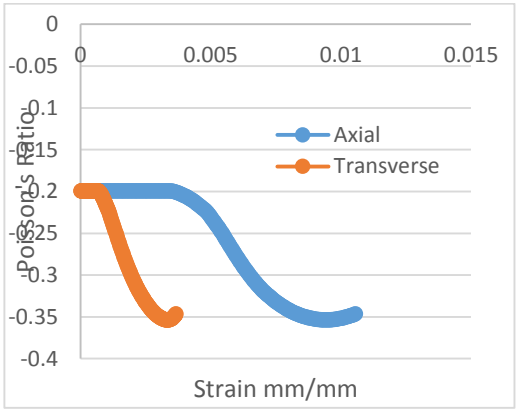

Mechanical Property	Value
Poisson's Ratio	-0.199
Young's Modulus (MPa)	2190
Ultimate Tensile Strength (MPa)	28
0.2% Yield Strength (MPa)	26.5

Model 45

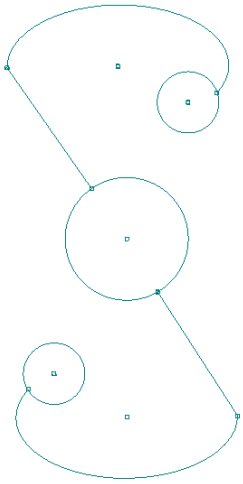

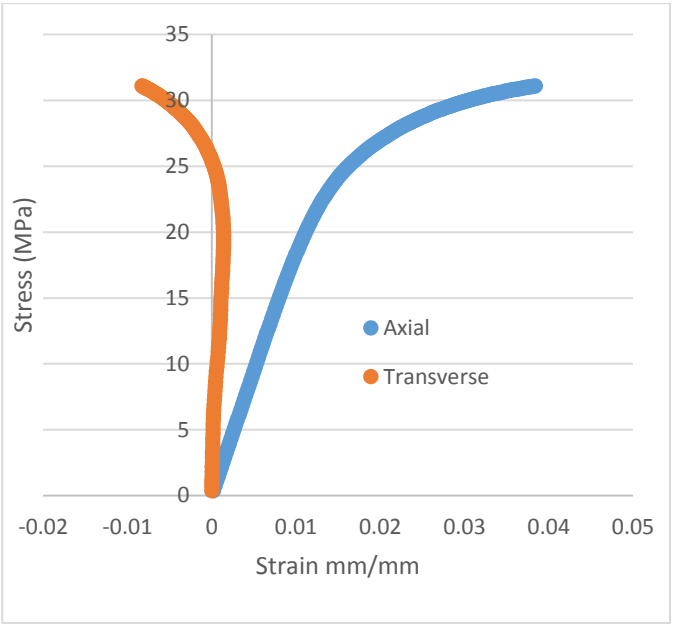

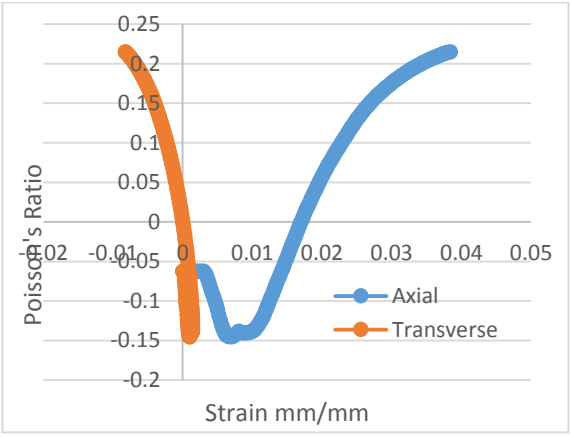

Mechanical Property	Value
Poisson's Ratio	-0.062
Young's Modulus (MPa)	1879
Ultimate Tensile Strength (MPa)	31.5
0.2% Yield Strength (MPa)	24

Model 46

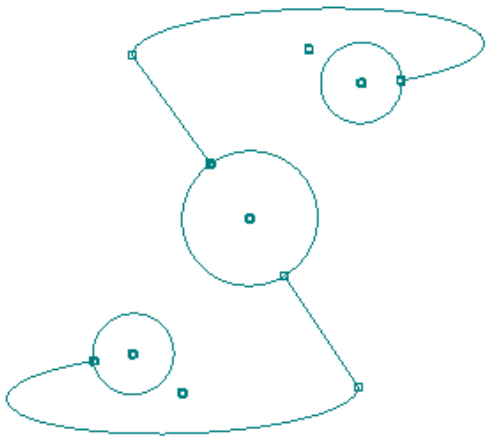

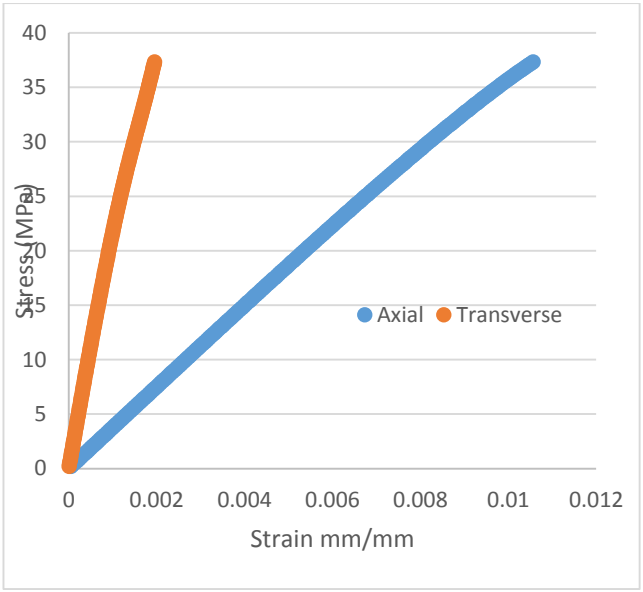

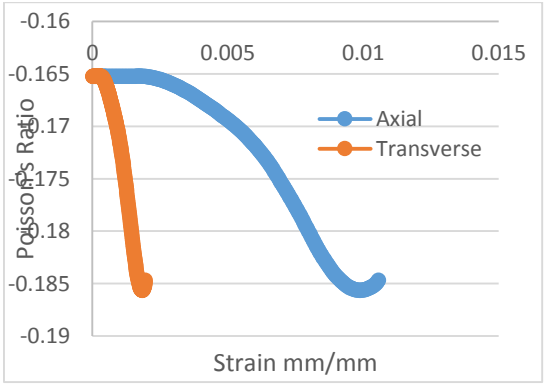

Mechanical Property	Value
Poisson's Ratio	-0.165
Young's Modulus (MPa)	3756
Ultimate Tensile Strength (MPa)	47
0.2% Yield Strength (MPa)	41.5

Model 47

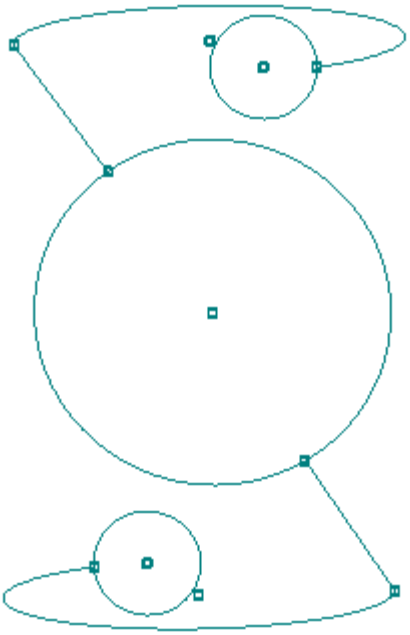

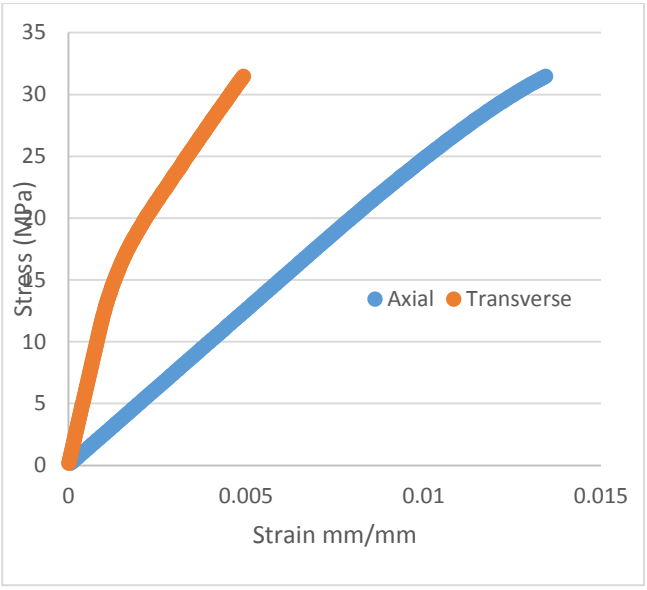

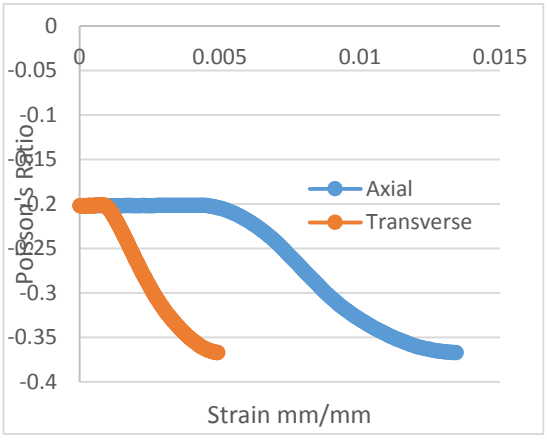

Mechanical Property	Value
Poisson's Ratio	-0.2016
Young's Modulus (MPa)	2512
Ultimate Tensile Strength (MPa)	38
0.2% Yield Strength (MPa)	32.5

Model 48

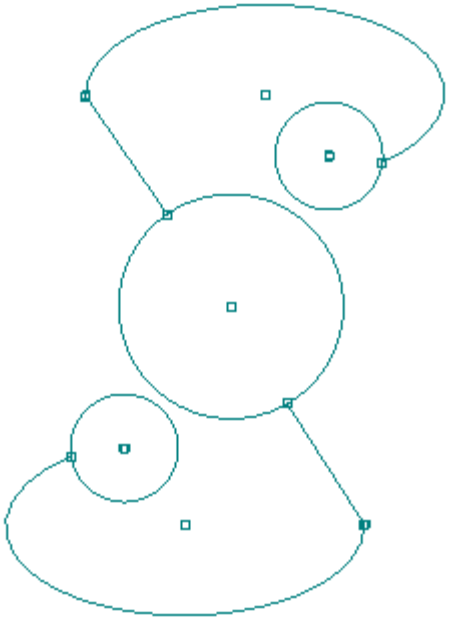

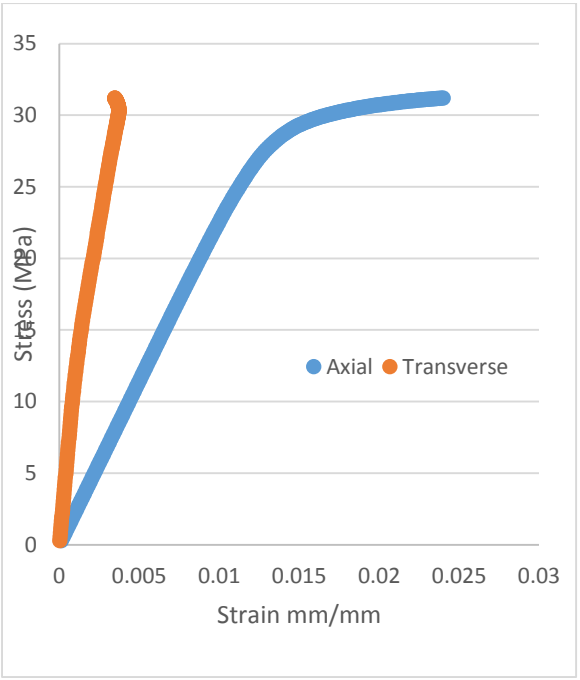

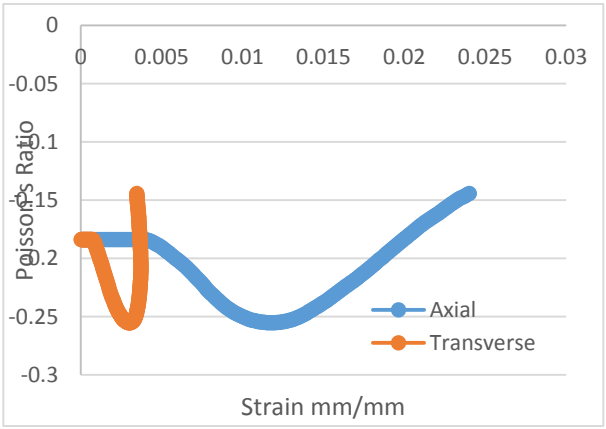

Mechanical Property	Value
Poisson's Ratio	-0.183
Young's Modulus (MPa)	2291
Ultimate Tensile Strength (MPa)	31.5
0.2% Yield Strength (MPa)	29.12

Model 49

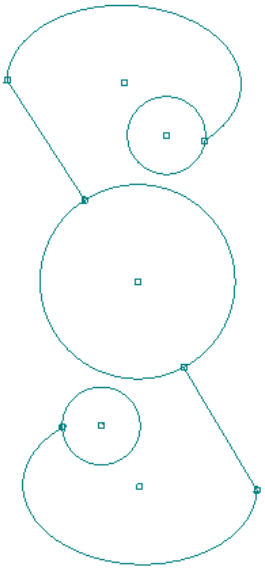

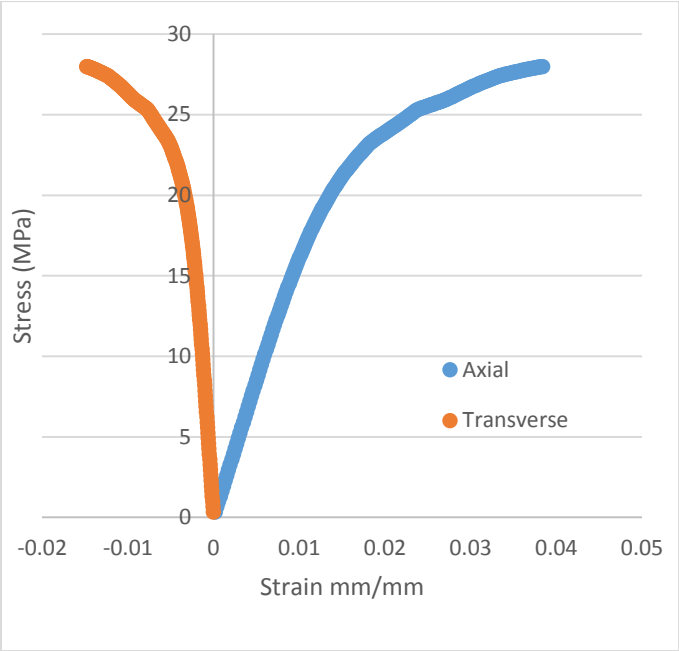

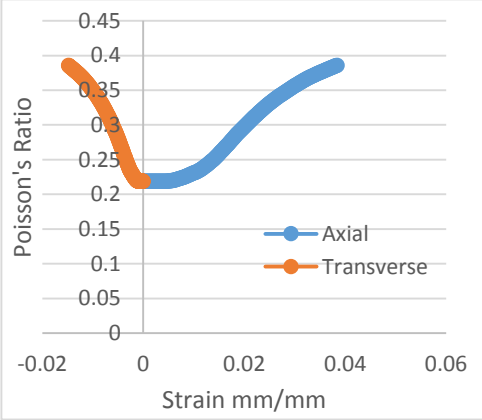

Mechanical Property	Value
Poisson's Ratio	0.219
Young's Modulus (MPa)	1705
Ultimate Tensile Strength (MPa)	28
0.2% Yield Strength (MPa)	20.3

Model 50

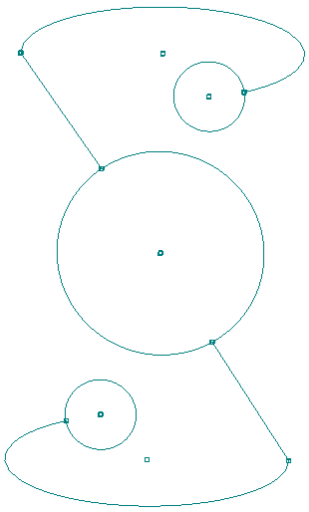

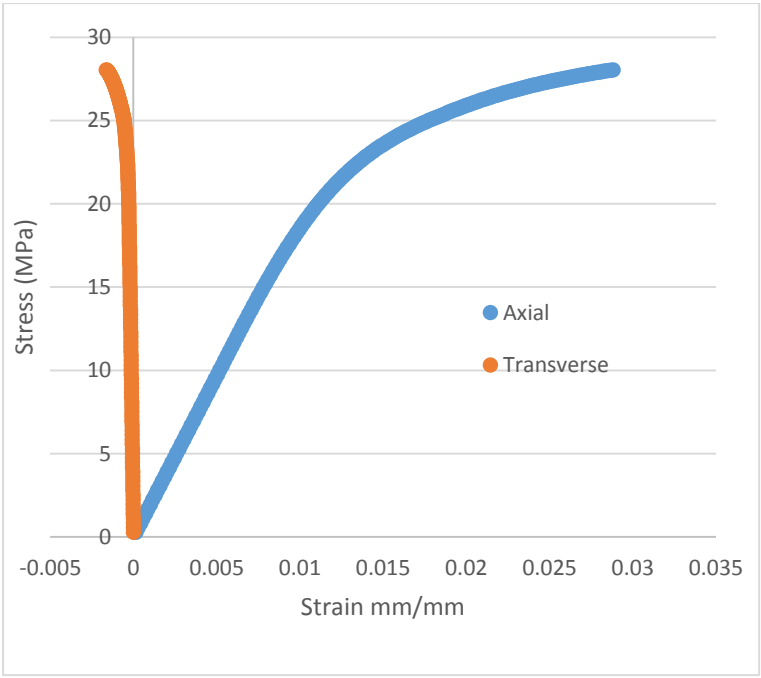

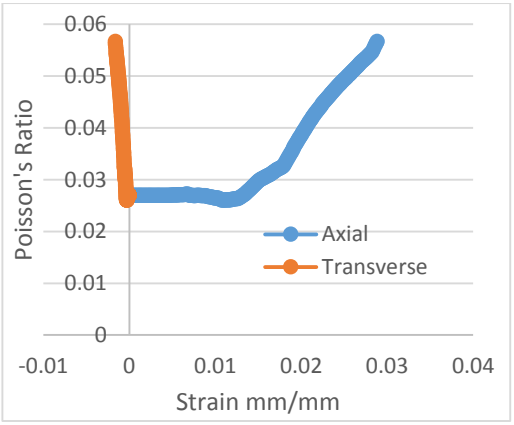

Mechanical Property	Value
Poisson's Ratio	0.0269
Young's Modulus (MPa)	1932
Ultimate Tensile Strength (MPa)	28.5
0.2% Yield Strength (MPa)	26.3

REFERENCES

[1] Yang, W., Li, Z., Shi, W., Xie, B., and Yang, M. (2004). Review on auxetic materials. *Journal of Materials Science*, 39: 3269-3279.

[2] Yang, L., Harrysson, O., West, H., & Cormier, D. (2015). Mechanical properties of 3D re-entrant honeycomb auxetic structures realized via additive manufacturing. *International Journal of Solids and Structures*, 69-70, 475-490.

[3] Prawoto, Y. (2012). Seeing auxetic materials from the mechanics point of view: A structural review on the negative Poisson's ratio. *Computational Materials Science*, 58, 140-153.

[4] Taylor, M., Francesconi, L., Gerendãs, M., Shanian, A., Carson, C., and Bertoldi, K. (2013). Low Porosity Metallic Periodic Structures with Negative Poisson's Ratio. *Adv. Mater.*, 26, 2365-2370.

[5] Liu, Y., Hu, Hong. (2010). A review on auxetic structures and polymeric materials. *Scientific Research and Essays*, 5, No. 10, 1052-1063.

[6] Peel, L. D., & Abdelrahman, M. (2012, June), "Studying the Physical Properties and Auxetic Behavior of 3D-printed Fasteners." Proceeding of 2012 ASEE Annual Conference, San Antonio, Texas. June 10-13, 2012.

[7] Lakes, R. (1987). Foam Structures with a Negative Poisson's Ratio. *Science*, 235, 1038-1040.

[8] Song, F., Zhou, J., Xu, X., Xu, Y., and Bai, Y. (2008). Effect of a Negative Poisson Ratio in the Tension of Ceramics. *Phys. Rev. Lett.*, 100, 245502, 1-4.

[9] Alderson, K., Alderson, A., and Evans, K. (1997). The interpretation of the strain-dependent Poisson's ratio in auxetic polyethylene. *The Journal of Strain Analysis for Engineering Design*, 32, No. 3, 201-212.

[10] Critchley, R., Corni, I., Wharton, J., Walsh, F., Wood, R., and Stokes, K. (2013). The Preparation of Auxetic Foams by Three-Dimensional Printing and Their Characteristics. *Advanced Engineering Materials*, 15, No. 10, 980-985.

[11] Mohsenizadeh, S., Alipour, R., Shokri Rad, M., Farokhi Nejad, A., and Ahmad, Z. (2015). Crashworthiness assessment of auxetic foam-filled tube under quasi-static axial loading. *Materials & Design*, 88, 258-268.

[12] Rockel, D., Weihard, S., Hachmann, A., Hupfer, A., and Kau, H. (2013). Numerical Investigation of an Additively Manufactured Compressor Casing: The Effect of Auxetic Structures on the Tip Clearances. Proceedings of 2013 ASME Turbo Expo, San Antonio, Texas. June 3-7, 2013.

[13] Sanami, M., Ravirala, N., Alderson, K., and Alderson, A. (2014). Auxetic Materials for Sports Applications. *Procedia Engineering*, 72, 453-458.

[14] Schwerdtfeger, J., Schury, F., Stingl, M., Wein, F., Singer, R., and Kãrner, C. (2011). Mechanical characterisation of a periodic auxetic structure produced by SEBM. *Phys. Status Solidi B*, 249, No. 7, 1347-1352.

[15] Wang, K., Chang, Y., Chen, Y., Zhang, C., and Wang, B. (2015). Designable dual-material auxetic metamaterials using three-dimensional printing, *Materials & Design*, 67, 159-164.

[16] Mizzi, L., Azzopardi, K., Attard, D., Grima, J., Gatt, R. (2015). Auxetic metamaterials exhibiting giant negative Poisson's ratios. *Phys. Status Solidi*, 9, No. 7, 425-430.

[17] Blumenfeld, R., Edwards, S. (2012). Theory of strains in auxetic materials. *Journal of Superconductivity and Novel Magnetism*, 25, 565-571.

[18] Torres, J., Cotelo, J., Karl, J., Gordon, A. (2015). Mechanical Property Optimization of FDM PLA in Shear with Multiple Objectives. *The Minerals, Metals, & Materials Society*, 67, No. 5, 1183-1193.